IOWA STATE UNIVERSITY
Digital Repository

1994

Anodic oxygen-transfer electrocatalysis at iron-doped lead dioxide electrodes

Jianren Feng
Iowa State University

Follow this and additional works at: https://lib.dr.iastate.edu/rtd

Part of the Analytical Chemistry Commons

IS-T 1713

Anodic Oxygen-transfer Electrocatalysis at Iron-doped Lead
Dioxide Electrodes

by

Feng, Jianren

MS   Thesis submitted to Iowa State University

Ames Laboratory, U.S. DOE

Iowa State University

Ames, Iowa 50011

Date Transmitted: July 27, 1994

MASTER

DISCLAIMER

DISCLAIMER

Portions of this document may be illegible in electronic image products. Images are produced from the best available original document.

Anodic oxygen-transfer electrocatalysis

at iron-doped lead dioxide electrodes

by

Jianren Feng

A Thesis Submitted to the

Graduate Faculty in Partial Fulfillment of the

Requirements for the Degree of

MASTER OF SCIENCE

Department: Chemistry
Major: Analytical Chemistry

Approved:

Iowa State University
Ames, Iowa

1994

TABLE OF CONTENTS

iii

ACKNOWLEDGEMENTS

It would be impossible to give just credit to all the people who have influenced my career at Iowa State University. The person most responsible for my development as a christian and a scientist is Dr. Dennis C. Johnson. I thank Dr. Johnson for everything he has done for me.

I am also grateful to all the teachers and committee members I have had the opportunity to learn from here at Iowa State Univeristy.

I would like to thank other members of the group with whom I have worked. Without their help and assistance, I could not complete my career as a graduate student.

I gratefully acknowledge the assistance of Jerry Amenson in obtaining scanning electron micrographs, and to Robert Z. Bachman, Robert J. Hofer, Robert J. Conzemius and Cheryl Bradly for elemental analysis. Assistance is greatly appreciated from the people in the Main Office, the Machine Shop, the Glass Shop and the Storeroom of the Chemistry Department.

This research was supported by Ames Laboratory of the U. S. Department of Energy and Eastman Kodak Company.

Finally, I want to thank my family for their constant support to my career and life.

1

CHAPTER 1

GENERAL INTRODUCTION

Thesis organization. - The four main chapters of this thesis include papers that

have been or will be submitted for publication in *Journal of the Electrochemical Society.*

These papers are written following the format requirements of this journal. These papers

are preceded by a general introduction and followed by a general conclusion. References

for the general introduction will be presented following the conclusion.

The research illustrated in this thesis was performed under the guidance of

Professor Dennis C. Johnson beginning in March 1987. Chapter 2 concentrates on the

development and electrocatalytic properties of iron-doped β-PbO$_2$ films on noble-metal

substrates. Chapter 3 focuses attention on the preparation and characterization of iron-

doped β-PbO$_2$ films on titanium substrates (Fe-PbO$_2$/Ti). Chapter 4 discusses anodic

evolution of ozone at Fe-PbO$_2$/Ti electrodes. Chapter 5 describes electrochemical

incineration of *p*-benzoquinone (BQ) at Fe-PbO$_2$/Ti electrodes. In addition, the Appendix

includes another published paper which is a detailed study of α-PbO$_2$ films deposited on

various types of stainless steel substrates.

Anodic oxygen-transfer electrocatalysis at iron-doped lead dioxide electrodes. -

The ultimate goal of this research is to incinerate chemical waste solutions

electrochemically. Electrochemical incineration is the oxidative degradation of chemical

waste by direct or indirect anodic reactions in which oxygen is transferred from H$_2$O in

the solvent phase to the oxidation product. For example, the partial and complete

degradation of the carcinogen benzene, as represented by:

$$C_6H_6 + 2H_2O \rightarrow C_6H_4O_2 + 6H^+ + 6e^-$$

(Benzene)   (Quinone)

$$C_6H_6 + 12H_2O \rightarrow 6CO_2 + 30H^+ + 30e^-$$

(Benzene)   (Carbon dioxide)

are of great interest and significance. Oxitative degradation of highly toxic inorganic

species is also of interest, as represented by:

$$CN^- + H_2O \rightarrow CNO^- + 2H^+ + 2e^-$$

(Cyanide)   (Cyanate)

These reactions which involve the transfer of oxygen from the solvent (H_2O) to the

oxidation product are defined as oxygen-transfer reactions and can be exemplified by the

general reaction in Eqn. 1.

$$R + xH_2O \rightarrow RO_x + 2xH^+ + 2xe^- \qquad (1)$$
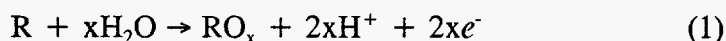
where R is the reactant and RO_x is the oxidation product [1]. Virtually all toxic organic

compounds can be predicted from thermodynamic calculations based on $E°$ values to be

spontaneously oxidized by a variety of O-transfer reactions. The general observation,

however, is that relatively few of these anodic O-transfer reactions occur at appreciable

rates at the common anode materials, *e.g.*, Pt, Au, graphite, and PbO_2. As a speculation,

in order to oxidize R to RO_x, it is necessary to first produce the required oxygen species,

surface adsorbed hydroxyl radicals $\cdot OH_{ads}$, by the discharge of water at the electrode

surface.

In this laboratory, attempts have been made to incorporate numerous metallic and nonmetallic ions into PbO_2-film electrodes [2-12]. These results support the premise that activation of PbO_2 electrodes for anodic O-transfer reactions can result from generation of surface defects at which hydroxyl radicals are absorbed. The strategies for activating PbO_2 electrodes can be expressed schematically in Fig. 1. The anodic formation of $\cdot OH_{ads}$ has been proposed as the rate limiting step in the anodic evolution of O_2 on metal oxide electrodes [13], as suggested by Eqn. 2-4. Hence, O_2 evolution is considered to be an inevitable but undesirable competing process.

$$S[\ ] + H_2O \rightarrow S[\cdot OH] + H^+ + e^- \qquad (2)$$

$$S[\cdot OH] + H_2O \rightarrow S[\ ] + O_2 + 3H^+ + 3e^- \qquad (3)$$

$$\text{net:} \quad 2H_2O \rightarrow O_2 + 4H^+ + 4e^- \qquad (4)$$
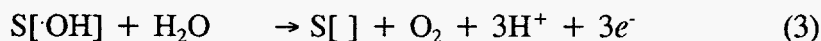
Yeo $et\ al.$ reported observing a positive correlation between increases in the rates of O_2 evolution and Mn(II) at Bi-PbO_2 electrodes as the ratio Bi/Pb is increased [5]. This supported as being in agreement with the conclusion that Bi(V) sites in the PbO_2 surface lattice can absorb $\cdot OH$ (case B in Fig. 1). It is also likely that some M(III) ions, $e.g.$, Fe(III) (case C in Fig. 1), might be good candidates for the activation. The result is that the increased surface activity of $\cdot OH$ promotes both the oxidation of Mn(II) as well as O_2 evolution (Eqn. 2-4).

Not all doped PbO_2 films are catalytically active for the same reactants. In addition to surface sites for adsorption of $\cdot OH$, it is now expected that adsorption of the reactant also can be a prerequisite for successful O-transfer reactions [8,14]. This

expectation is rationalized by the presumed necessity of pre-desolvation of the reaction site on the reactant. Desolvation is suspected to be a necessity because oxygen from $\cdot OH_{ads}$ cannot transfer to the reactant by a tunneling mechanism analogous to an electron-tunneling process. Such a synergism between two distinct but adjacent adsorption sites in the electrode surface is indicated by the generic mechanism shown in Eqn. 5-8. In Eqn. 5-8, S[ ] and S'[ ] represent the distinct vacant surface sites for adsorption of $\cdot OH$ and the reactant (R), respectively.

$$S[\ ] + H_2O \rightarrow S[\cdot OH] + H^+ + e^- \qquad (5)$$

$$S'[\ ] + R \rightarrow S'[R] \qquad (6)$$

$$S[\cdot OH] + S'[R] \rightarrow S[\ ] + S'[\ ] + RO + H^+ + e^- \qquad (7)$$

$$\text{net:} \quad R + H_2O \rightarrow RO + 2H^+ + 2e^- \qquad (8)$$
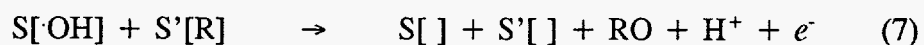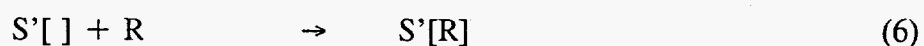
In view of the proposed importance of two types of surface sites, it is conceivable that doping with a single species whose presence creates sites for reactant adsorption only can result in a net decrease in the density of sites for $\cdot OH$ formation. Hence, a net decrease in the overall rate of O_2 evolution would correlate with an overall increase in the rate of a selected anodic O-transfer reaction. It is well known that many catalysts in industrially important reactions are usually transition metals (*e.g.*, Fe and V) or transition-metal compounds (*e.g.*, Fe_2O_3, V_2O_5). The transition-metal atoms in catalysts act as sites for holding the reacting species in a conformation favorable for reaction. In addition, electrons in the transition metal *d* orbitals can become involved in the bonding and permit the formation of complexes with a wide variety of negative or polar ligands.

Based on the concepts disscussed above, it is reasonable to chose transition metals as the candidates for incorporation into PbO_2. This research has emphasized the usage of iron as catalytic doping agents in PbO_2 films for various anodic O-transfer reactions. Furthermore, to achieve the application of electrochemical incineration in large scale, special endeavors have been made to search some less expensive materials , *e.g.*, titanium and stainless steel,as substrates, for supporting physically stable and catalytic $Fe-PbO_2$ films.
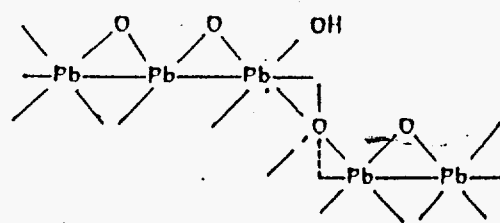
A. Surface "steps"
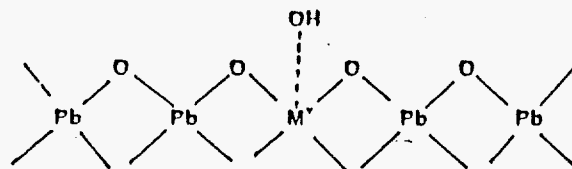
B. M (V) sites
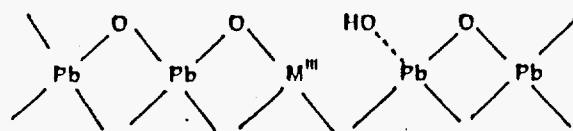
C. M (III) sites
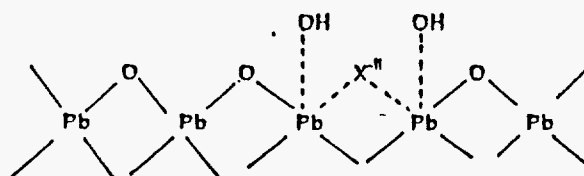
D. Anion doping

Fig. 1.   Strategies for activating PbO_2 electrodes.

CHAPTER 2

PREPARATION AND CHARACTERIZATION OF IRON-DOPED LEAD DIOXIDE FILM ELECTRODES DEPOSITED ON NOBLE-METAL SUBSTRATES

J. Feng[2] and D. C. Johnson[2,3]

ABSTRACT

Films of Fe(III)-doped β-PbO_2 were electrodeposited from solutions containing Pb(II) and Fe(II) onto noble metal substrates. Scanning electron micrographs indicated the films consisted of a densely packed array of small crystallites. The Fe-PbO_2 film electrodes were determined to be substantially more active than pure PbO_2 film electrodes for several anodic oxygen-transfer reactions, including the oxidations of Mn(II) and CN^-.

---

[2] Graduate student and Professor, respectively, Department of Chemistry, Iowa State University.

[3] Author for correspondence.

Introduction

The chief goal of this and related research in this laboratory is the electrocatalysis of anodic reactions which require transfer of oxygen from H_2O to the oxidation products. Applications of such electrocatalytic electrodes are anticipated for electrosynthesis, as electroanalytical sensors, and in anodic degradation of toxic chemical wastes ("electrochemical incineration"). Most anodic O-transfer reactions are mechanistically inhibited at the popular anode materials (*e,g.*, Pt, Au, PbO_2, and glassy carbon). In fact for PbO_2, the large overpotential for O_2 evolution, has been a contributing factor in the popularity of this metal oxide as an anode material [7]. It is a premise of this research that hydroxyl radicals (·OH) generated at an electrode surface (S) by anodic discharge of H_2O can be adsorbed at specific surface sites (*i.e.*, S[OH]). Furthermore, it is proposed that the adsorbed ·OH can be transferred to oxidation products within electrocatalytic O-transfer mechanisms. These processes are illustrated below for oxidation of a generic reactant (R) to the corresponding product (RO)

$$+ H_2O, - H^+, - e^-$$

$$R \rightarrow S[\ ] + RO + H^+ + e^-$$

$$S[OH] +$$

$$H_2O \rightarrow S[\ ] + O_2 + 3H^+ + 3e^-$$

$$+ H_2O, - H^+, - e^-$$
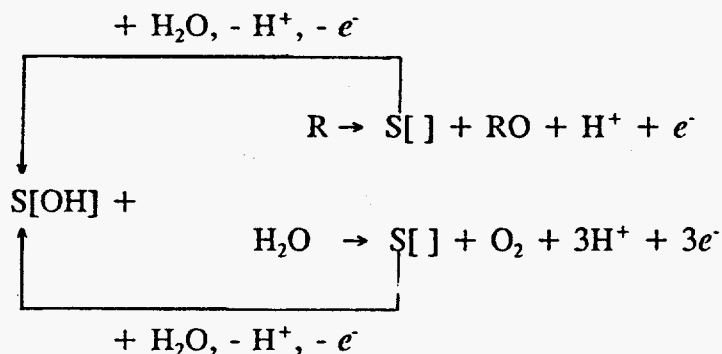
As proposed above, O-transfer reactions can be electrocatalyzed by increasing the surface concentration (density) of adsorption sites (S[OH]). However, the rate of O_2 evolution also is enhanced by increasing the coverage by S[OH], and it is surmised that there is an optimal low density of surface sites for which the desired O-transfer process can occur at near mass transport-limited rates without an unduly high background signal for O_2 evolution.

The O-transfer activity of electrodes consisting of electro-deposited β-PbO_2 on noble substrates has been determined to be increased substantially when group (VA) metals [2,3] and some anions [4] are incorporated into the oxide film. The structure of the doped oxides has been determined to be virtually unchanged from that of the pure β-PbO_2 (slightly distorted rutile), which is electrodeposited from acidic solutions of Pb(II) in the absence of the doping ions. Because the oxides of several transition metals (*e.g.*, Fe and V) are known to function effectively as catalysts in gas phase oxidations [5], these metals are also candidates for incorporation into PbO_2 films. Reported here is a portion of work focused on the use of transition metals as catalytic doping agents in PbO_2 films on various substrates.

Experimental

All reagents were of analytical reagent grade quality. Water was distilled, followed by purification in a NANO-pure-II system (Barnstead). Current-time (I-t) curves for electrochemical stripping of the oxide films were recorded on a Model 4510BF strip-

chart recorder (Houston Instrument Company). A small mirror was placed under the electrolysis cell for observing the variation of color at the electrode. All other instrumentation has been described [3]. All potential values are given *vs.* the standard calomel electrode (SCE) reference. Cathodic currents are positive in the current-potential (I-E) curves shown. Elemental analysis was performed using a Model 5000 atomic absorption spectrometer (Perkin-Elmer) with a HGA-5000 graphite furnace.

Most of the experimental arrangements and procedures have been described [2,3]. Films of Fe(III)-doped β-PbO$_2$ were electrodeposited on a Au rotated disk electrode (RDE; 1600 rev min^{-1}) at potentials in the range 1.60 - 1.80 V *vs.* SCE in solutions of 1.0 M HClO$_4$ containing 1-10 mM Pb(NO$_3$)$_2$. Dissolved O$_2$ was removed from working solutions by dispersed N$_2$. Iron (II) was added to the deaerated solutions as Fe(NH$_4$)$_2$(SO$_4$)$_2 \cdot$ 6H$_2$O.

Results and Discussion

Electrodeposition of Fe(III)-doped β-PbO$_2$ films. - Current-potential (I-E) curves are shown in Fig. 1 obtained at the Au RDE in 1.0 M HClO$_4$. For the absence of Pb(II) (curve a), formation of surface oxide (AuO) occured during the positive scan at *ca.* 1.2 V and the oxide was cathodically dissolved on the negative scan to produce the peak at *ca.* 0.9 V. Evolution of O$_2$ was very evident for E > *ca.* 1.7 V by the rapid increase in anodic current on the positive scan. Addition of Pb(II) (curve b) resulted in the anodic deposition of PbO$_2$ at E > *ca.* 1.4 V with cathodic stripping of the PbO$_2$ on the negative

scan at *ca.* 1.3 V. The nucleation process for deposition of bulk PbO_2 requires simultaneous evolution of O_2 on the Au substrate and therefore occurred simultaneously with the rapid increase in anodic current for E $>$ *ca.* 1.7 V [6,7]. The anodic peak observed on the positive scan at *ca.* 1.25 V in the presence of Pb(II) has been concluded [6] to correspond to the oxidation back to PbO_2 of an ultra-thin layer of PbO which remains at the electrode following the cathodic stripping of bulk PbO_2. The quantity of AuO formed during the positive scan was decreased slightly by the formation of PbO_2, as determined by the decreased cathodic peak for AuO at 0.9 V (compare curve a and b). Addition of SO_4^{2-} to the Pb(II) solution (curve c) caused an apparent increase in the AuO peak at 0.9 V.

Addition of Fe(II) as $Fe(NH_4)_2(SO_4)_2 \cdot 6H_2O$ to the deposition solution of Pb(II), following the recording of curves a - c, produced a large reproducible anodic wave for E $>$ *ca.* 0.5 V, corresponding to the reaction Fe(II) $\rightarrow$ Fe(III) + e^- (curve d). Furthermore, a very large and broad cathodic peak was obtained at *ca.* 0.9 V superimposed on the cathodic peak for AuO. This is concluded to correspond to the reduction of a mixed-oxide phase, designated $Fe\text{-}PbO_2$. The shape of curve d did not change by an appreciable extent with increasing cycle number. The anodic current for Fe(II) in the range 0.9 - 1.1 V was determined to be virtually the transport-limited value and therefore, the form of iron in the mixed oxide is tentatively concluded to be Fe(III). The deposition of PbO_2 in this acidic medium has been shown to be under kinetic rather than transport control [7]. Hence, it is interesting to note that the anodic current for Pb(II) (5 mM, n = 2 eq mol^{-1}) was very much smaller than the transport-limited current for Fe(II)

(8 mM, n $=$ 1 eq mol^{-1}). The color of the Fe-PbO$_2$ films was dark purple, even for deposition times extended to 80 min, whereas the color of pure PbO$_2$ was dark brown to black.

Scanning electron microscopy (SEM). - An SEM micrograph of the Fe-PbO$_2$ film is shown in Fig. 2. The film appears to correspond to a densely packed aggregation of small crystallites (0.5 - 1 μm), which is similar to the appearance of an electrodeposited film of pure β-PbO$_2$. The film thickness was estimated to be 10-25 μm, from the micrograph of a cross section of the film (not shown). No EDS (X-ray energy dispersive spectroscopy) signal for Fe was detected for the top view of the oxide (Fig. 2), whereas some Fe was detected in the edge view. Since the EDS technique samples only to a depth of approximately 1-2 μm, it was concluded tentatively that the Fe(III) in the film was not distributed homogeneously, with a low concentration near the surface. Nevertheless, as noted above, a definite purple coloration was observed for the film, which is attributed to the Fe-doped PbO$_2$.

A thick deposit of Fe-PbO$_2$ was analyzed quantitatively by atomic absorption spetroscopy. The mole ratio of Fe-Pb was determined to be 0.052, which corresponds to the average value for the thick film. Hence, only a small fraction of the Fe(II) transported to the electrode is actually incorporated into the Fe-PbO$_2$ film.

The absence of an anodic peak on the positive scan in curve d shown in Fig. 1 might be attributed to oxidation of an Fe(II) species does not remain on the electrode surface after the cathodic stripping process on the preceding negative scan. Furthermore,

there is no evidence of the incorporation of Fe(II) into the ultra-thin PbO film remaining on the electrode after cathodic stripping. This probably can be attributed to the fact that the ultra-thin film was formed prior to addition of Fe(II) in the experiment, producing Fig. 1.

Anodic oxidation of Mn(II) in acidic media. - The oxidation of Mn(II) has been used as a model O-transfer reaction in several studies because of the large number of oxygens (four) transferred in the anodic process and because of the possible use of electrogenerated MnO_4^- for air and water purification. It has been demonstrated that some $MnO_2(s)$ is produced at pure β-PbO_2 films, indicating low O-transfer catalytic activity. However, MnO_4^- is produced with very high efficiencies at the more catalytically active Bi-doped and Cl-doped PbO_2 film electrodes. Current-potential curves are shown in Fig. 3A-E for oxidation of Mn(II) at several electrodes. A relatively small net current was obtained for Mn(II) at the pure PbO_2 film (Fig. 3A). Response for Mn(II) obtained for films deposited from the Pb(II) solution following addition of $Fe(NO_3)_2$ (Fig. 3B) and $Fe(NO_3)_2$ with Na_2SO_4(Fig. 3C) was only slightly improved over the response at the pure PbO_2 film. Addition of Fe(II) to the deposition solution as $Fe(NH_4)_2(SO_4)_2 \cdot 6H_2O$ resulted in an Fe-PbO_2 film with a significantly higher activity for Mn(II) oxidation (Fig. 3D). The residual current in Fig. 3D was small and we conclude this is the result of a low degree of surface roughness for the corresponding Fe-PbO_2 in comparison to the other electrodes.

The catalytic activities of various film electrodes were compared on the basis of

so-called "Koutecky-Levich plots" of $1/J$ vs. $1/\omega^{1/2}$, shown in Fig. 4, where J is the normalized current density (I/AC^b) for rotation speeds (ω) in the range of 400-4900 rev min^{-1} (rpm). The significance of these plots has been discussed [8]. Values of the apparent heterogeneous rate constant (k_{app}) were calculated from the intercepts in Fig. 4 and are summarized in Table I. It is readily confirmed that the O-transfer activity of the Fe-PbO$_2$ film deposited from 1.0 M HClO$_4$ containing 5 mM Pb(NO$_3$)$_2$ and 10 mM Fe(NH$_4$)$_2$(SO$_4$)$_2$ was superior to that for the other electrodes. The response of Mn(II) at this electrode adhered closely to the Levich equation for a mass transport controlled reaction.

Table 1.   Rate constants for anodic oxidation of 1.0 mM Mn(II) at

1.7 V in 1.0 M HClO$_4$ at several PbO$_2$-film electrodes.

Electrode	Deposition solution[a]	$10^3 k_{app}$ [b] (cm s^{-1})
Au	- no deposition film -	5 $\pm$ 1
PbO$_2$	5 mM Pb(NO$_3$)$_2$/1 M HClO$_4$	13 $\pm$ 1
PbO$_2$	5 mM Pb(NO$_3$)$_2$/20 mM Na$_2$SO$_4$/1 M HClO$_4$	15 $\pm$ 1
Fe-doped PbO$_2$	5 mM Pb(NO$_3$)$_2$/2 mM Fe(NH$_4$)$_2$(SO$_4$)$_2$/1 M HClO$_4$	16 $\pm$ 2
Fe-doped PbO$_2$	5 mM Pb(NO$_3$)$_2$/4 mM Fe(NH$_4$)$_2$(SO$_4$)$_2$/1 M HClO$_4$	130 $\pm$ 3
Fe-doped PbO$_2$	5 mM Pb(NO$_3$)$_2$/10 mM Fe(NH$_4$)$_2$(SO$_4$)/1 M HClO$_4$	883 $\pm$ 10

[a]   Deposition conditions: 1.8 V vs. SCE, 10 min, 1600 rpm.

[b]   Value of $n_{eff} = n_{tot} = 5.0 \pm 0.1$ eq mol^{-1}, by exhaustive

electrolysis.

Oxidation of cyanide in alkaline solutions. - A possible application of anodes which have high catalytic activity for O-transfer reactions is the oxidative degradation of toxic chemical wastes, including cyanide from metal plating industries. Previously, the author had noted a high activity for CN^- oxidation at PbO_2 films deposited on a stainless steel substrate [3] and speculated that the higher activity might be the result of a small quantity of Fe(III) in the oxide as a result of dissolution of the substrate during deposition. The voltammetric response of CN^- is shown in Fig. 5 for PbO_2, $Bi-PbO_2$, and $Fe-PbO_2$ film electrodes in alkaline solutions (pH 10). Very little activity for CN^- oxidation was obtained for the pure $\beta-PbO_2$ electrode. At 3600 rpm, the value of $E_{1/2}$ for the $Fe-PbO_2$ electrode (1.20 V) was only *ca.* 50 mV more negative than that for the $Bi-PbO_2$ electrode; however, a plateau current was obtained at that rotation speed only for the $Fe-PbO_2$ electrode. The product of the anodic reaction is cyanate, as given by Eqn. (2)

$$CN^- + H_2O \rightarrow CNO^- + 2H^+ + 2e^- \qquad (2)$$
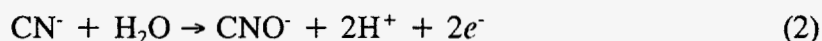
The formal reduction potential ($E^{o'}$) is -0.19 V *vs* SCE at this pH. The large disparity between the observed $E_{1/2}$ and $E^{o'}$ is a consequence of the significance of the electrocatalytic mechanism in this O-transer process.

Plots of $1/J$ *vs.* $1/\omega^{1/2}$ are shown in Fig. 6 for data at 1.40 V in Fig. 5. The values of k_{app} (cm s^{-1}) calculated from the intercepts of the plots are: $(2.2 \pm 0.5) \times 10^{-3}$ for PbO_2, $(15 \pm 1) \times 10^{-3}$ for $Bi-PbO_2$, and $(410 \pm 10) \times 10^{-3}$ for $Fe-PbO_2$. The higher catalytic activity of the $Fe-PbO_2$ films is clearly evident.

16

Conclusions

The catalytic coupling of anodic O-transfer reactions to the mechanism of O_2 evolution, as described by Eqn. (1), requires surface sites for adsorption of hydroxyl radicals. It is also concluded that surface oxygen cannot tunnel in electrocatalytic O-transfer reactions and, therefore, surface sites are required for adsorption of reactants. Furthermore, it is concluded that these sites can be generated either by creation of defects in the PbO_2 surface lattice or by incorporating dissimilar metal cations into the PbO_2 which can offer unfilled p- and/d-orbitals which function for adsorption of ·OH and the reactants. Accordingly, O-transfer electrocatalysis has been achieved by incorporation of anions, *e.g.*, Cl⁻ and AcO⁻ [4], group VA metals, *e.g.*, As (V) and Bi(III/V) [2] and, now, a transition metal. Gottesfeld [9] has used a similar argument to predict that d-orbitals at Ru(IV) sites in the surface of RuO_2 can function as very efficient ·OH adsorbers in the evolution of O_2.

Acknowledgments
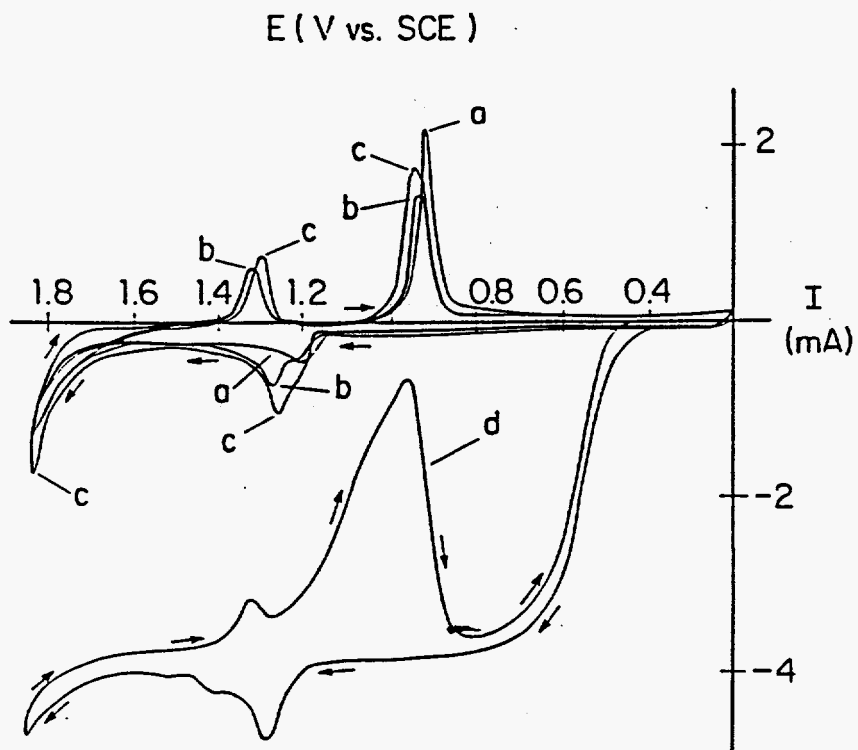
Fig. 1.   Current-potential response for film deposition at Au RDE.
Conditions: 6.0 V min^{-1}, 1600 rev min^{-1}. Curves: (a) 1.0 M HClO$_4$
(blank); (b) 5 mM Pb(NO$_3$)$_2$/1 M HClO$_4$; (c) 5 mM Pb(NO$_3$)$_2$/16 mM
Na$_2$SO$_4$/1 M HClO$_4$;
and (d) 5 mM Pb(NO$_3$)$_2$/8mM Fe(NH$_4$)$_2$(SO$_4$)$_2$·6H$_2$O/1 M HClO$_4$.
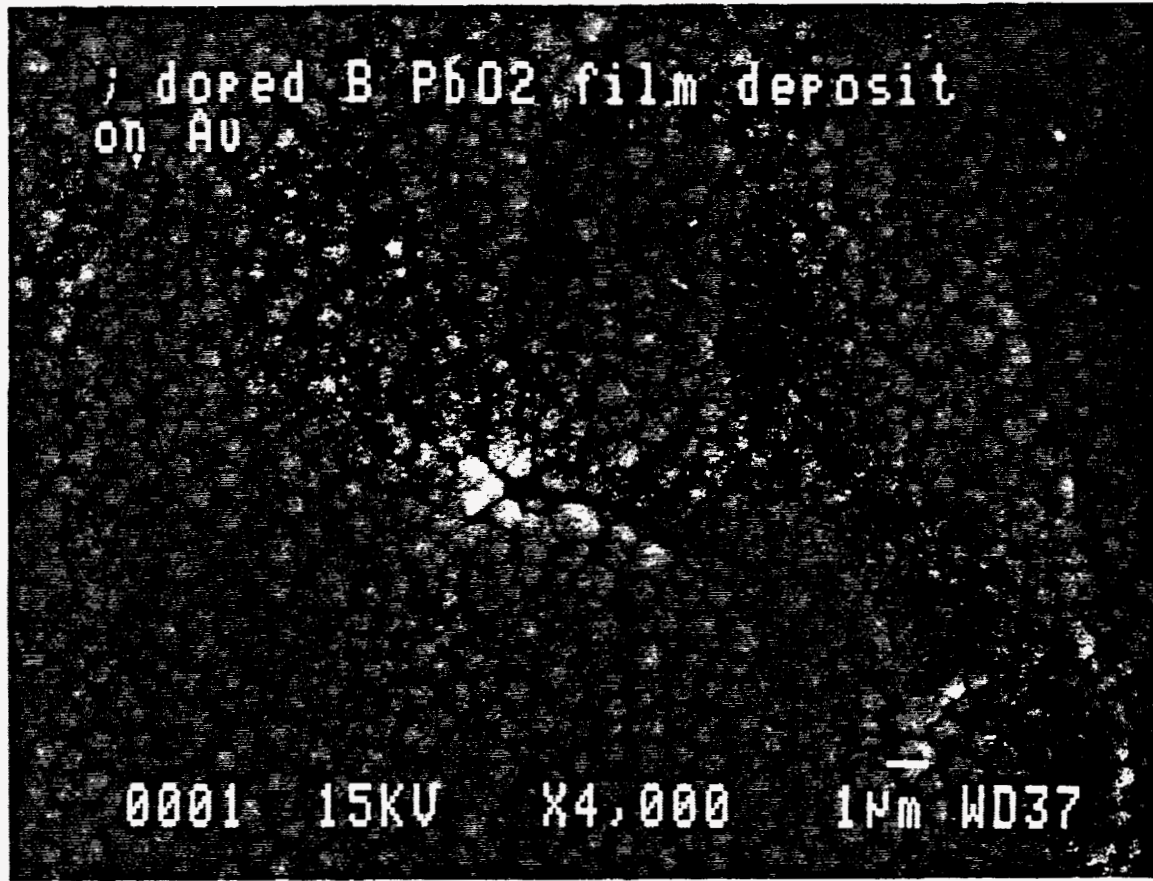
Fig. 2.   Scanning electron micrograph of Fe-PbO$_2$ film.
Deposition conditions: 1.8 V, 20 min, 1600 rpm; 5 mM Pb(NO$_3$)$_2$/8 mM
Fe(NH$_4$)$_2$(SO$_4$)$_2 \cdot$6H$_2$O.
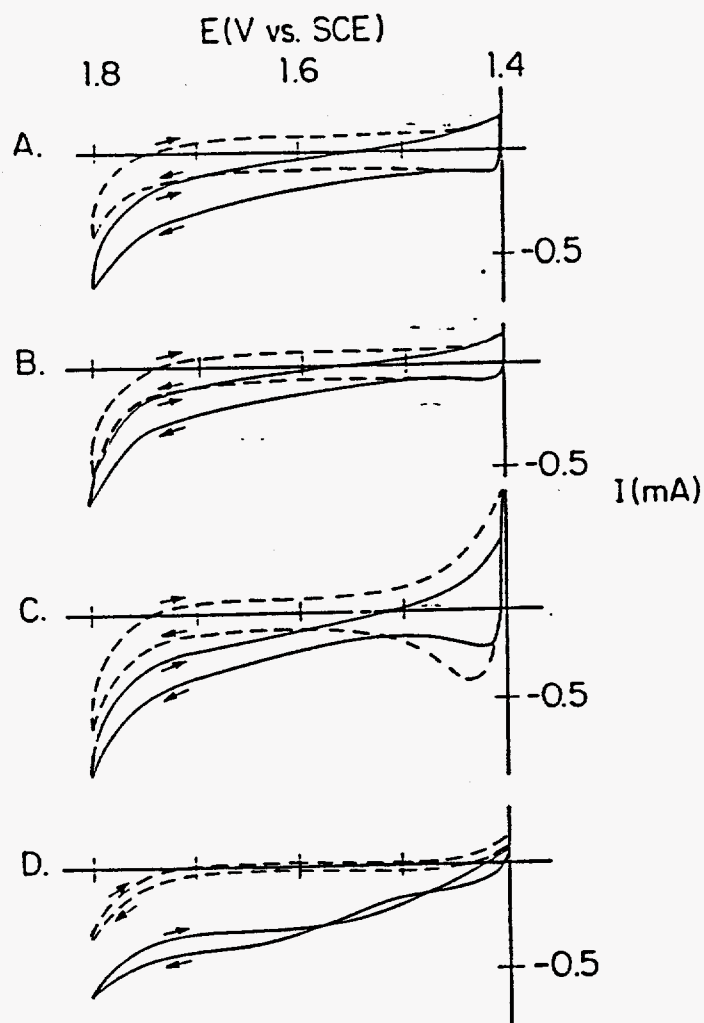
Fig. 3.   Voltammetric response of Mn(II) at various film electrodes.
Test conditions: 1.0 mM Mn(II)/1 M HClO$_4$, 0.6 V min^{-1}, 1600 rpm.
Deposition conditions: 1.8 V, 20 min, 1600 rpm; (A) 5 mM Pb(NO$_3$)$_2$/1 M
HClO$_4$; (B) 5 mM Pb(NO$_3$)$_2$/8 mM Fe(NO$_3$)$_3$/1 M HClO$_4$; (C) 5 mM
Pb(NO$_3$)$_2$/8 mM Fe(NO$_3$)$_3$/16 mM Na$_2$SO$_4$/1 M HClO$_4$; and
(D) 5 mM Pb(NO$_3$)$_2$/8 mM Fe(NH$_4$)$_2$(SO$_4$)$_2 \cdot$6H$_2$O/1 M HClO$_4$.
Curves: (...) residual for 1 M HClO$_4$, (—) for Mn(II).
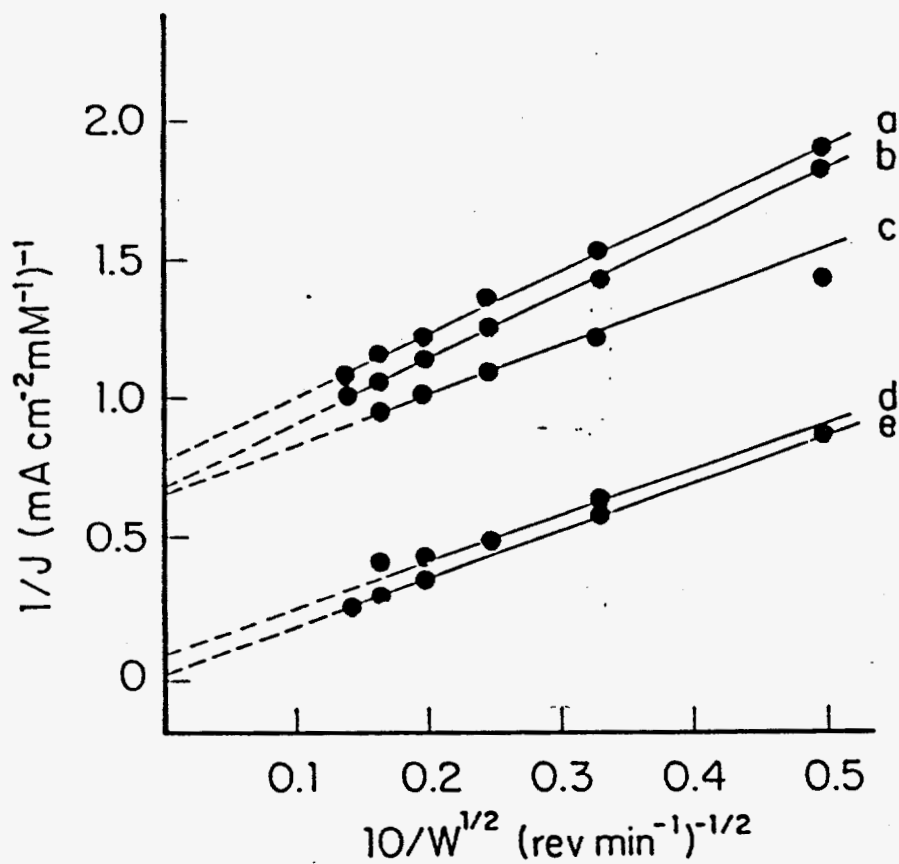
Fig. 4.   Plots of $1/J$ *vs.* $1/\omega^{1/2}$ for the oxidation of Mn(II) at various film electrodes.
Test consitions: 1 mM Mn(II)/1 M HClO$_4$, 1.7 V. Deposition conditions:
1.8 V, 20 min, 1600 rpm; (a) 5 mM Pb(NO$_3$)$_2$/1 M HClO$_4$; (b) 5 mM
Pb(NO$_3$)$_2$/20 mM Na$_2$SO$_4$/1 M HClO$_4$; (c) 5 mM Pb(NO$_3$)$_2$/2 mM
Fe(NH$_4$)$_2$(SO$_4$)$_2$·6H$_2$O/1 M HClO$_4$; (d) 5 mM Pb(NO$_3$)$_2$/4 mM
Fe(NH$_4$)$_2$(SO$_4$)$_2$·6H$_2$O/1 M HClO$_4$; (e) 5 mM Pb(NO$_3$)$_2$/10 mM
Fe(NH$_4$)$_2$(SO$_4$)$_2$·6H$_2$O/1 M HClO$_4$.
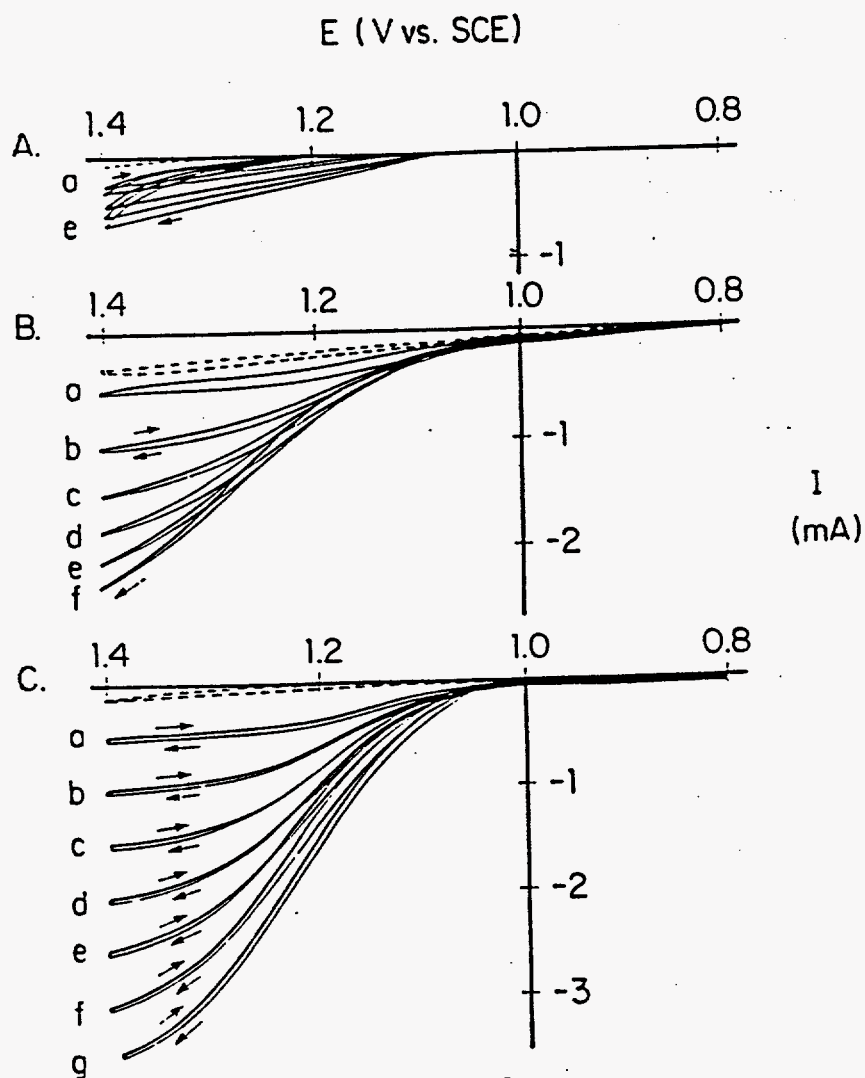
Fig. 5.   Current-potential response for cyanide at various film electrodes in alkaline solution.
Test conditions: 5 mM NaCN in $NaHCO_3/Na_2CO_3$ (pH 10.0).
Deposition conditions: 1.8 V, 20 min, 1600 rpm; (A) 1 mM $Pb(NO_3)_2$ / 1 M $HClO_4$; (B) 1 mM $Pb(NO_3)_2/0.7$ mM $Bi(NO_3)_3 \cdot 5H_2O/1$ M $HClO_4$; (C) 5 mM $Pb(NO_3)_2/8$ mM $Fe(NH_4)_2(SO_4)_2 \cdot 6H_2O/1$ M $HClO_4$. Rotation speed (rpm): (a) 100, (b) 400, (c) 900, (d) 1600, (e) 2500, (f) 3600, (g) 4900.
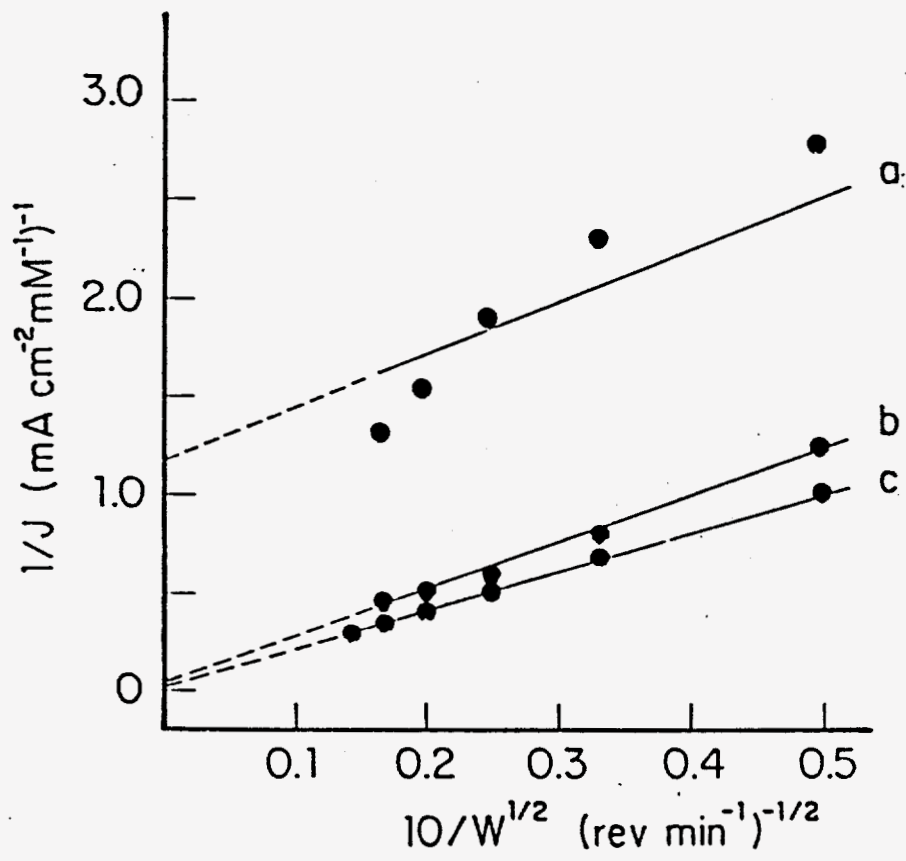
Fig. 6.   Plots of 1/J *vs.* $1/\omega^{1/2}$ for data at 1.4 V in Fig. 5.

REFERENCES

[1]   "The Electrochemistry of Lead," A. T. Kuhn, Editor, pp. 217-251, Academic Press, London (1979).

[2]   I.-H. Yeo and D. C. Johnson, *J. Electrochem. Soc.*, **134**, 1973 (1987).

[3]   J. Feng and D. C. Johnson, *J. Appl. Electrochem.*, **20**, 116 (1990).

[4]   Y.L. Hsiao and D. C. Johnson, *J. Electrochem. Soc.*, **136**, 3704 (1989).

[5]   C. N. Satterfield, "Heterogeneous Catalysis in Ptractice," pp. 183-186, 301-304, McGraw-Hill Book Co., New York (1980).

[6]   H. Chang, Ph. D. Dissertation, Iowa State University, Ames, IA (1989).

[7]   H. Chang and D. C. Johnson, *J. Electrochem. Soc.*, **136**, 17 (1989).

[8]   Yu. V. Pleskov and V. Yu. Filinovskii, "The Rotating Disk Electrode," pp. 89-90. Consultants Bureau, New York (1976).

[9]   S. Gottesfeld, J. Rishpon, and S. Srinivasan, in "Electrocatalysis," W. E. O'Grady *et al.*, Editors, p. 155, The Electrochemical Society Softbound Proceedings Series, Vol. 82-2, Pennington, NJ (1982).

CHAPTER 3

PREPARATION AND CHARACTERIZATION OF

IRON-DOPED LEAD DIOXIDE

FILM ELECTRODES DEPOSITED ON TITANIUM SUBSTRATES

A paper published in the *Journal of the Electrochemical Society*[1]

J. Feng and D. C. Johnson

ABSTRACT

Voltammetric and kinetic results are described for the electrocatalytic oxidation of various compounds at doped PbO_2 film electrodes on Ti substrates. Compounds tested include dimethyl sulfoxide and several thiophene derivatives. Results are emphasized for PbO_2 films doped with Fe(III)(Fe-PbO_2), and with Ag(I) and Bi(V) (Ag-Bi-PbO_2), that were electrolytically deposited on Ti substrates with the presence of an interlayer of PbO_2 deposited from acidic solution of Pb(II) and NaF. These "laminar" film electrodes are quite stable and offer significantly improved catalytic activity for various anodic oxygen-transfer reactions in comparison to pure PbO_2-film electrodes.

Introduction

Previous research in this laboratory has demonstrated that the activity of PbO_2-film electrodes, anodically deposited on noble metal substrates, can be increased substantially for numerous anodic oxygen-transfer reactions by the incorporation of various cationic and anionic dopants within the deposited films [1-6]. The catalytic effect of the dopants has generally been interpreted on the basis of the generation of surface defect sites with enhanced rates for anodic discharge of H_2O to produce adsorbed hydroxyl radicals ($\cdot OH_{ads}$) that are believed to be the requisite intermediate state of oxygen from H_2O in the anodic oxygen-transfer processes. Application of electrocatalytically activated PbO_2-film electrodes is suggested for anodic degradation of toxic chemical wastes, *i.e.*, so-called "electrochemical incineration." However, prior to extensive demonstrations of such applications, it is desirable to examine alternative and less expensive substrates for the catalytic film electrodes. Stainless steel was investigated as an alternate substrate; however, the resulting electrodes cannot withstand highly acidic conditions [4].

Titanium has been used successfully as a substrate for pure PbO_2-film electrodes (PbO_2/Ti) [7-10]. Clean Ti surfaces are very reactive in the presence of O_2, and passive oxide films (TiO_2) are quickly developed. Whereas TiO_2 is a nonconductor, the oxide film is destroyed, and, therefore, the metal slowly dissolves under anodic polarization at large applied potentials in aqueous media, *e.g.*, $\geqslant$ 2 V *vs.* SCE at pH 1 [7]. Because the passive oxide is formed virtually instantaneously upon anodic polarization in aqueous

media, anodic electrodeposition of PbO_2 on Ti from solutions of Pb(II) is not as easily achieved as for Au or Pt substrates. Successful deposition can be achieved from solutions of high Pb(II) concentration and relatively low acidity. Furthermore, etching agents, *e.g.*, sodium fluoride and sodium oxalate, can be added to dissolve any TiO_2 that forms. In a typical successful procedure, the deposition solution contains 200 g l^{-1} $Pb(NO_3)_2$ and 6.5 g l^{-1} $Cu(NO_3)_2$ at pH 4.2 to 4.5 [10]. These conditions are not satisfactory for anodic deposition of Bi(V)-doped PbO_2 films (Bi-PbO_2), however, because Bi(III) is hydrolyzed at these pH values.

Fukasawa has described the preparation of laminar PbO_2-film anodes composed of alternate layers of α-PbO_2, deposited from alkaline media, and β-PbO_2, deposited from acidic media [11]. This successful preparation of laminar film electrodes led us to consider the deposition of doped PbO_2 films on Ti substrates previously coated by very adherent PbO_2 films deposited from solutions of Pb^{2+} containing NaF. Accordingly, conditions can then be optimized independently for deposition of the respective layers on the Ti substrates.

Experimental

Chemicals. - All chemicals were analytical reagent grade from Fisher Scientific, Alfa Products, or Aldrich Chemicals. Water was distilled and purified in a NANOpure-II system (Barnstead).

Instrumentation. - Procedures for obtaining voltammetric and kinetic data have been described [4,5]. Titanium disk electrodes (A = 0.196 cm^2) were made from a Ti rod (99.99%; Johnson Matthey, Inc.) and were mounted on the ends of stainless steel rods machined to appropriate dimensions for rotation in a MSR rotator with speed controller (Pine Instrument Co.). Only the end-surface of the rotated disk electrode (RDE) was allowed to contact the solutions used for deposition and kinetic testing. A Ti-coil electrode (*ca.* 26 cm^2) was made from Ti wire (99.7%, 0.83 mm diam, Johnson Matthey, Inc.). A saturated calomel electrode (SCE) reference was used for all voltammetric work and potentials are given as V *vs.* SCE. The scanning electron microscope (SEM) was a Model-200 Stereoscan (Cambridge Instruments).

Elemental analysis of films. - Analysis of Fe-doped PbO_2 films for Fe content was performed with a Model 5000 atomic absorption spectrometer (Perkin-Elmer) using a HGA-500 graphite furnace. Films were dissolved by treatment with 10 drops of a 1:1 (v/v) mixture of glacial acetic acid and 32% hydrogen peroxide, and the resulting solutions were washed into volumetric containers.

Pretreatment of Ti. - End-surfaces of Ti-disk electrodes were polished on 320-grit paper strips (Carbimet), using H_2O as the lubricant, followed by 1 μm diamond paste (Buehler). The Ti-coil electrode was degreased in 40% NaOH and then cleaned in a hot 1:1 mixture of HNO_3 and H_2SO_4, followed by thorough washing with water. The treated surfaces were immersed in boiling aqueous solutions of oxalic acid (15%) until the TiO_2

dissolved; a reddish-brown Ti(III) oxalate was produced. The Ti surfaces were washed again and then boiled in a solution containing 0.2 M Ti(IV) oxalate and 1.25 M oxalic acid. The deposition of PbO_2 proceeded immediately to minimize formation of TiO_2.

Electrodeposition of PbO_2-films. - Deposition of PbO_2 from acidic media on clean Ti disks was achieved at constant potential (1.6 to 1.8 V, 5 to 20 min) or constant anodic current (-1.0 to -2.0 mA, 5 to 20 min) from 0.1 M HNO_3 containing 0.5 M $Pb(NO_3)_2$ and 40 mM NaF [9]. These films are suspected to contain low levels of F^-, although no analysis was performed to determine F^- content. The voltammetric character of these film differs from that of pure PbO_2 on Ti and, hence, they are designated as "F-PbO_2/Ti". Films of Fe(III)-doped PbO_2 on F-doped PbO_2/Ti (Fe-PbO_2/F-PbO_2/Ti) were electrodeposited (1.8 V, 10 to 20 min) from 1 M $HClO_4$ containing 10 mM $Pb(NO_3)_2$ and 10 mM Fe^{2+} formed by room-temperature dissolution of Fe powder (99.99%) in the acidic media. Fe-PbO_2/F-PbO_2/Ti films were also electrodeposited (1.8 V, 10 to 20 min) from 1 M $HClO_4$ containing 8 mM $Fe(NH_4)_2(SO_4)_2 \cdot 6H_2O$.

Postdeposition treatment of films. - According to the description of Wabner and Fritz [14], two similar approaches were applied in this research for the postdeposition treatment of some PbO_2 films to produce beneficial changes in surface morphology.

Method A. —— The potential of the film electrode in 0.5 M H_2SO_4 was cycled ($0.0 \leq E \leq 1.8$ V, 6 V min^{-1}) until successive *i-E* curves were identical.

Method B. —— The film electrode was polarized in 0.5 M H_2SO_4

by a constant cathodic current (+0.1 mA, 10 min) to convert PbO_2 to $PbSO_4$. Then the electrode was polarized at a constant anodic current (-0.1 mA, 10 min) to oxidize $PbSO_4$ back to PbO_2. The resulting PbO_2 films are believed to have been doped with SO_4^{2-} and/or HSO_4^- [10].

Measurement of rate constants. Values of an apparent heterogeneous rate constant (k_{app}) for reactions at the RDEs were calculated from the intercepts of plots of $1/J$ *vs.* $1/\omega^{1/2}$ as indicated by Eqn. 1 [11]. In Eqn. 1, $J = I/AC^b$ is the normalized electrode

$$\frac{1}{I/AC^b} = \frac{1}{J} = \frac{1}{nFk_{app}} + \frac{1}{0.62nFD^{2/3}v^{-1/6}}\left(\frac{1}{\omega^{1/2}}\right) \tag{1}$$

response, where I is current (C s⁻¹), A is the geometric disk area (cm²), and C^b is the bulk concentration of reactant (mol cm⁻³). Also, ω is the rotational velocity (rad s⁻¹), γ is the kinematic viscosity (cm² s⁻¹) of the solution, and n, F and D have their usual significance.

Results and Discussion

Electrodeposition of PbO_2 films on Ti substrates. - Successive current-potential (*i-E*) curves are shown in Fig. 1 obtained at a Ti disk electrode in various solutions. Scan numbers are indicated in the figure. Formation of surface oxide (TiO_2) in 1 M $HClO_4$

(Fig. 1A) occurs during the first positive scan (...) from *ca.* 0.0 V, and the anodic current remains nearly constant until scan reversal at 1.8 V. No cathodic current is observed on the subsequent negative scan, and it is apparent that cathodic dissolution of the oxide film does not occur. Virtually no anodic current is observed for subsequent positive scans 2 to 4 (——), and it is concluded that the Ti surface is virtually passivated by the oxide formed during the first scan to 1.8 V. Addition of 10 mM Pb(II) and 10 mM Fe(II) to this solution after the fourth scan does not produce a visible change in *i-E* response at the oxide-covered Ti electrode (data not shown). Furthermore, there is no visible evidence for deposition of a PbO_2 film.

Voltammetric deposition and stripping of PbO_2 is observed to occur at the oxide-free Ti RDE during the first positive scan in 1 M $HClO_4$ containing 0.5 M $Pb(NO_3)_2$ (Fig.1B), and in 0.1 M HNO_3 containing 0.5 M $Pb(NO_3)_2$ and 40 mM NaF (Fig. 1C). In both cases, voltammetric scans are initiated from 0.0 V to minimize formation of surface oxide prior to onset of the first scans. During the first positive scan, the deposition process requires transfer of oxygen from H_2O to the oxide film, *i.e.*, $Pb^{2+} + 2H_2O \rightarrow PbO_2 + 4H^+ + 2e^-$. It has been concluded that the process requires the simultaneous anodic discharge of some H_2O to produce adsorbed hydroxyl radicals ($\cdot OH_{ads}$). which are consumed in the deposition process [12]. Hence initiation of the deposition process (*i.e.*, nucleation) during the first positive scan occurs at *ca.* 1.6 V, which is characteristic of H_2O discharge at TiO_2, *i.e.*, E > *ca.* 1.7 V (Fig. 1B). Deposition during the subsequent negative scan persists to *ca.* 1.6 V, which is characteristic of the more favorable anodic discharge of H_2O on PbO_2. After several cyclic scans, onset of PbO_2 deposition during

the positive scan occurs at *ca.*1.6 V, as compared to 1.7 V for the first scan. This is the evidence for retention of a residual film of PbO_2 following cathodic stripping of the majority of the PbO_2 in the range 1.2 V to 0.8 V during the negative scans. This phenomenon has been reported also for Au substrates [16]. The PbO_2 residue apparently nucleates the anodic deposition on the succeeding positive scan with the result of a less positive scan with the results of a less positive potential for onset of deposition (*i.e.*, change from *ca.* 1.7 V to 1.6 V).

Voltammetric data (*i-E*) shown in Fig. 1C for Pb(II) in the presence of NaF and HNO_3 indicate a more favorable condition for the deposition process, as indicated by a negative shift in the onset potential for oxide deposition. Furthermore, the voltammetric stability of these $F-PbO_2$ films appears to be greater than that in Fig. 1B, as indicated by the negative shift in the peak potential for cathodic dissolution. No effort was made to determine whether these effects were caused primarily by the presence of F or a slight change in acidity caused by addition of NaF.

The major beneficial effect of adding NaF to the deposition medium is not apparent from the *i-E* curves in Fig. 1B and C. That benefit is the significantly greater adhesive qualities of the $F-PbO_2$ films on Ti. Films of PbO_2/Ti deposited from the NaF-free media (Fig. 1B) have a granular appearance and are easily removed by gentle scraping with a fingernail, or by application and quick removal of a piece of adhesive "transparent" tape (Scotch, 3M). The $F-PbO_2$ films deposited from NaF media (Fig. 1C) are visibly smooth and cannot be removed either by intense scraping with a fingernail or with the adhesive-tape.

Because TiO_2 is formed on Ti surfaces immediately upon anodic polarization in aqueous media (E > 0.0 V; see Fig. 1A), the fact that PbO_2 can be deposited from the NaF - free media seems inconsistent with the general knowledge that TiO_2 is a nonconductor [7]. It is speculated that some Pb(II) might be incorporated into the TiO_2, during formation of the oxide film within the first scan from 0.0 to 1.7 V, to impart semiconductor properties to the otherwise inert oxide. When Ti electrodes are anodically polarized in 1 M $HClO_4$ prior to addition of Pb(II), PbO_2 films cannot be deposited on the TiO_2 film. Ionic doping by various other metal ions has been reported to increase conductivity for oxide films, *e.g.*, Au, Pt, Ir, Ru, V, and Fe [17]. Fluoride has been reported to be an effective doping ion for TiO_2 [17].

Satisfactory adherence cannot be obtained for various doped PbO_2 films doposited directly on the Ti surface from NaF-free media. They are easily removed from the substrate by scraping with a fingernail or rubbing with a tissue. However, doped PbO_2 films deposited onto $F-PbO_2/Ti$ are hard and very adhesive. Furthermore, as described below, they are substantially more active than the PbO_2/Ti surfaces.

Anodic evolution of O_2. - It is believed that the anodic discharge of H_2O to produce adsorbed hydroxyl radicals ($\cdot OH_{ads}$) is essential to support anodic O-transfer reactions [1,2,6,18]. However, formation of $\cdot OH_{ads}$ is also proposed in the anodic evolution of O_2 on metal oxide electrodes [19]. Hence, a major challenge is the optimization of electrode activity for O-transfer reactions without undue increase in the simultaneous background signal for O_2 evolution. The residual voltammetric responses for

several electrodes in 1.0 M $HClO_4$ are compared in Fig. 2 in the potential region for O_2 evolution (*i.e.*, E > 1.4 V). It is quite apparent in Fig. 2 that smaller background currents are obtained in the region E > *ca.* 1.8 V for F-PbO_2/Ti (curve a) and Fe-PbO_2/Ti (curve b) in comparison to PbO_2/Ti (curve c) and Bi-PbO_2/Ti (curve d). Figure 3 shows Tafel plots of log{I/μA} *vs.*η plotted according to Eqn. 2 from the *i-E* data recorded for the positive scan (E $\geq$ 1.4 V, 9 mV s^{-1}). In Eqn. 2, I_o is the exchange current (μA), α_a is the anodic transfer coefficient, and η is the applied overpotential (V). Values of exchange current density (I_o/A, μA cm^{-2}) and α_a are summarized in Table 1 for 1.0 M $HClO_4$ using E° = 0.961 V *vs.* SCE for production of O_2 by a reaction with n = 4 equiv mol^{-1}.

$$\log\{I/\mu A\} = \log\{I_o/\mu A\} + (\alpha_a n/0.059)\eta \tag{2}$$

The values of I_o/A for the PbO_2/Au and F-PbO_2/Ti electrodes (4.0 x 10^{-4} and 4.4 x 10^{-4} μA cm^{-2}, respectively) are small and virtually identical. Values of I_o/A for the Fe-PbO_2/Ti and Bi-PbO_2/Ti electrodes (1.4 x 10^{-2} and 2.0 x 10^{-1} μA cm^{-2}, respectively) are significantly larger than for PbO_2/Au and F-PbO_2/Ti. This evidence supports the research premise that incorporation of sites into the PbO_2 electrode that catalyze anodic O-transfer reaction will increase slightly the rate of anodic discharge of H_2O.

Scanning electrode microscopy. - Micrographs are shown in Fig. 4 for several films generated in this research. Patterns of interlocking crystallites are apparent for the F-PbO_2/Ti surface without postdeposition treatment (Fig. 4A). The Fe-PbO_2 films are more granular (Fig. 4B and D) and there is evidence of intergranular cracking.

Table 1.   Values of exchange current density (I_o/A) and anodic transfer coefficient

(α_a) from Tafel plots for anodic discharge of H_2O at various electrodes in

1.0 $HClO_4$ at 25 °C.

$$2H_2O \rightarrow O_2 + 4H^+ + 4e^-$$
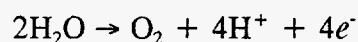
Electrode	I_o/A^a (μA cm^{-2})	α_a^a (eq mol^{-1})
PbO_2/Au	$(4.0 \pm 0.5) \times 10^{-4}$	0.121 ± 0.001
F-PbO_2/Ti	$(4.4 \pm 0.5) \times 10^{-4}$	0.104 ± 0.001
Fe-PbO_2/Ti	$(1.4 \pm 0.3) \times 10^{-2}$	0.092 ± 0.002
Bi-PbO_2/Au	$(2.0 \pm 0.3) \times 10^{-1}$	0.086 ± 0.001

a Standard deviation indicated.

The micrograph of a F-PbO_2/Ti surface following post-deposition treatment by

method B is shown in Fig. 4C. A significant change in morphology is apparent, as a

result of the treatment, with an increase in the size of crystallites. The surface of Fe-

PbO_2/F-PbO_2/Ti without postdeposition treatment is shown in Fig. 4D. The crystallites

are larger than for the Fe-PbO_2/Ti (Fig. 4B) or the posttreated F-PbO_2/Ti (Fig. 4C) and

no fissures are apparent. The use of the F-PbO_2 interlayer is preferred for producing

strongly adherent, relatively crack-free films of Fe-PbO_2 on Ti.

Elemental analysis. - Films of Fe-PbO$_2$ on Ti substrates were analyzed by atomic absorption spectrometry. The mole ratio of Fe/Pb, corrected for the background, was determined to be 0.18 ± 0.01. A value Fe/Pb = 0.053 was reported previously for Fe-PbO$_2$ films on Au [5]. Titanium also was found in the Fe-PbO$_2$ film with the mole ratio Ti/Pb equal to *ca.* 0.7. The presence of Ti in the dissolved sample is suspected to have resulted from dissolution of some TiO$_2$ with the Fe-PbO$_2$ films in the analytical procedure. There is a remote possibility that some Ti(IV) was dissolved during deposition of Fe-PbO$_2$ and was incorporated into the Fe-PbO$_2$/Au film. However, it is not expectd that the catalytic activity observed for the Fe-PbO$_2$ films was the result of incorporated Ti(IV). Evidences supporting this conclusion are: (i) PbO$_2$/Ti and F-PbO$_2$/Ti electrodes were not active in spite of the possible presence of Ti^{IV}, and (ii) Fe-PbO$_2$/Au electrodes exhibited high catalytic activity even there was no possibility for Ti doping [5].

Voltammetric response of dimethyl sulfoxide. - Anodic oxidation of dimethyl sulfoxide to dimethyl sulfone, *i.e.*, (CH$_3$)$_2$SO + H$_2$O → (CH$_3$)$_2$SO$_2$ + 2H$^+$ + 2e$^-$, has been used for intercomparison of electrode activities [3,6,13,18]. There are several reasons for this choice, including: i) (CH$_3$)$_2$SO is unreactive at conventional anode materials (*e.g.*, Au, Pt, GC); ii) the reaction mechanism is assumed to be relatively simple because only one oxygen is transferred; and iii) the reactant and product are uncharged and, therefore,it is presumed that double-layer effects can be ignored in the interpretation of catalytic phenomena. The voltammetric response of (CH$_3$)$_2$SO in 1 M HClO$_4$ is shown in Fig. 5A for F-PbO$_2$/Ti RDE and a Fe-PbO$_2$/F-PbO$_2$/Ti RDE. The

benefit of Fe(III) in the oxide film is obvious in the region $E \geq 1.6$ V. However, the activity is not as great as observed for $Bi-PbO_2/Au$ electrodes [6,16]. The voltammetric response for $(CH_3)_2SO$ at $Ag-Bi-PbO_2/Au$ electrodes is shown in Fig. 6. It is readily apparent from comparison of Fig. 5 and 6 that the activity of $Ag-Bi-PbO_2$ is somewhat greater than that of the $Fe-PbO_2/F-PbO_2$ film electrode and significantly greater than that of the $F-PbO_2$ film electrode. This observation is in agreement with the research premise presented above and the observation that the background signals (I_{bkd}) measured at 1.7 V for anodic discharge of H_2O increase in the order $F-PbO_2 < Fe-PbO_2 < Ag-Bi-PbO_2$.

It is also apparent from Fig. 6 that the response of $(CH_3)_2SO$ at $Ag-Bi-PbO_2$ electrodes is virtually independent of the substrate material.

Voltammetric and kinetic data for $(CH_3)_2SO$ are summarized in Table 2 for various film electrodes. Included are values of $E_{1/2}$, the background current (I_{bkd}), ratios of signal-to-background current (I_{sig}/I_{bkd}), and values of nk_{app} measured at 1.70 V. Previous work [6] established that PbO_2 film electrodes can be activated by anodic electrosorption of Bi(III) as Bi^V to produce an electrode designated as Bi^V/PbO_2 [6,20]. In fact, the activity of these electrodes was determined to be superior to that of $Bi-PbO_2$ film electrodes. Similar activation was observed for $F-PbO_2$ film electrodes exposed to Bi(III) (Table 2, No. 3). The largest value of nk_{app} included in Table 2 (2.1 x 10^{-1} eq cm mol^{-1} s^{-1}) was obtained for a $Ag-Bi-PbO_2$ film electrode deposited directly on a Ti substrate (No. 5). A small sacrifice in activity results when $Bi-Ag-PbO_2$ films are deposited on a Ti substrate with a $F-PbO_2$ interlayer (No. 10); however, an improvement in mechanical

stability is obtained which is considered to offset the undesirability of the small decrease in activity.

Effects of H_2SO_4. - Several oxygen-transfer reactions were determined to proceed more rapidly when H_2SO_4 was used as the supporting electrolyte instead of $HClO_4$ [13]. The *i-E* curves for tetramethylene sulfoxide [$(CH_2)_4SO$] are shown in Fig. 7 as representative evidence of this effect. For a F-PbO$_2$/Ti electrode, reactivity for $(CH_2)_4SO$ oxidation is much greater in 0.50 M H_2SO_4 than in 1.0 M $HClO_4$. After postdeposition treatment of the F-PbO$_2$/Ti electrode in 0.5 M H_2SO_4 by method A, the electrode possesses virtually equal activity for $(CH_2)_4SO$ oxidation, whether tested in 1.0 M $HClO_4$ or 0.50 M H_2SO_4.

These observations inspired the author to apply the same postdeposition treatment to F-PbO$_2$/Ti electrodes to increase electrode activity. The residual *i-E* response of a F-PbO$_2$/Ti RDE in 0.5 M H_2SO_4 is shown in Fig. 8 during repeated cycles of applied potential between the values 0.0 V and 1.8 V. The anodic and cathodic peaks correspond to the conversions $PbO_2 \rightarrow PbSO_4 \rightarrow PbO_2$, respectively. The size of the cathodic and anodic peaks increase with time, probably as a result of increased film porosity, and eventually reach an equilibrium condition after approximately 30 cycles. The resulting PbO$_2$ films are believed to be doped with significant levels of SO_4^{2-} or HSO_4^- [13].

Values of nk_{app} were obtained for $(CH_3)_2SO$ at a thick F-PbO$_2$ film on Ti as a function of cycle number for the voltammetric treatment (methode A) represented in Fig. 8. The reactivity increased to a maximum value within *ca.* 25 to 30 cycles.

Table 2. Summary of response data for oxidation of 10.0 mM DMSO at various film electrodes on Ti substrates in 1.0 M $HClO_4$.

$$DMSO + H_2O \rightarrow DMSO_2 + 2H^+ + 2e^-$$

#	Surface/Substrate	I_{bkd}[a] $(mA\ cm^{-2})$	$E_{1/2}$ (V vs. SCE)	$10^3 nk_{app}$[a] (eq cm $mol^{-1}\ s^{-1}$)	I_{sig}/I_{bkd}[b]
1	PbO_2/Ti	0.5	N.R.[c]	N.R.[c]	1.4
2	$F-PbO_2/Ti$	0.1	N.W.[d]	5.8	47
3	Adsorbed $Bi^V/F-PbO_2/Ti$	0.1	1.60	40	120
4	$Bi-PbO_2/Ti$	3.3	1.52	49	5.4
5	$Ag-Bi-PbO_2-PbO_2/Ti$	1.6	1.54	200	11
6	$Cl-PbO_2/Ti$	0.25	N.W.	2.9	9.6
7	$Cl-PbO_2/F-PbO_2/Ti$	0.45	1.58	9.2	13
8	$Fe-PbO_2/Ti$	0.7	1.56	39	8.5
9	$Fe-PbO_2/F-PbO_2/Ti$	1.2	1.62	10	4.9
10	$Ag-Bi-PbO_2/F-PbO_2/Ti$	2.4	1.57	45	4.9

[a] Measured at 1.70 V.

[b] Measured at 1.70 V with 1600 rev min^{-1}.

[c] Negligible reactivity.

[d] Wave not well developed.

Voltammetric response of thiophene derivatives. - Thiophene, dibenzothiophene, and their derivatives, represent a substantial fraction of "organic sulfur" present in fossil fuels [21]. Consequently, much effort is being directed to the study of hydrodesulfurization of these compounds as useful routes to "cleaner" fuels. The possibility of oxidative desulfurization also has been investigated by Fan *et al* [22] using salts of Fe(III) and Cu(II). They reported that dibenzothiophene is relatively unreactive and only a small fraction is converted to the corresponding sulfone by reaction with Fe^{3+} at 300 °C [22]. Electrolytic oxidations of these compounds might provide a beneficial route to desulfurization.

Work reported here for thiophene derivatives focused on Fe-PbO_2/F-PbO_2/Ti electrodes in 1.0 M $HClO_4$. Typical *i-E* curves are compared in Fig. 9 for 2-thiophene-carboxylic acid and 2-thiophene-malonic acid at PbO_2/Au (Fig. 9A and B) and Fe-PbO_2/F-PbO_2/Ti (Fig. 9A' and B') electrodes. Values of nk_{app} were calculated from the plots of $1/J$ *vs.* $1/\omega^{1/2}$ and, in all cases, the values are approximately five to ten times larger at the Fe-PbO_2/F-PbO_2/Ti electrodes. The voltammetric response of dibenzothiophene (DBT) was obtained in 1:1 mixtures of 1.0 M $HClO_4$ with acetonitrile (ACN). The presence of ACN was necessary to increase the solubility of the nonpolar DBT. Typical *i-E* curves for DBT are shown in Fig. 9C and C' for Au and Fe-PbO_2/F-PbO_2/Ti electrodes, respectively. The kinetic parameters for these and other data are summarized in Table 3 for the Fe-PbO_2/F-PbO_2/Ti electrode.

Values of n for oxidation of several thiophene compounds were determined by exhaustive electrolysis and are given in Table 4. Although no attempt was made to

identify inorganic products of the electrolytic reactions, Table 4 includes the results of a

qualitative test for SO_4^{2-} by addition of several drops of 1 M $Ba(NO_3)_2$. Formation of

white $BaSO_4(s)$ is considered affirmative for the production of at least some SO_4^{2-} by

anodic desulfurization. Dibenzothiophene (No. 1) yields n = 4 eq mol^{-1} without a white

precipitate. This is consistent with the production of the sulfone as illustrated by Eqn. 3.

Electrolysis of a solution of the sulfone of DBT (no. 2) produces very little additional

charge without a white precipitate for a lengthy electrolysis of the solution. For No. 3 to

6 in Table 4, n is significantly larger than the value 4 eq mol^{-1}, and $BaSO_4(s)$ is observed

for all product solutions. Extension of this work is planned to obtain positive

identification of the organic products.

Other reactants. The oxidation of Mn(II) to MnO_4^- is of interest because of the

large number of oxygen atoms transferred. In spite of the presumed complexity of this

multioxygen transfer process, transport-limited signals have been obtained at Bi-PbO_2/Au

electrodes [1,2,18]. The *i-E* response of 1 mM Mn(II) in 1 M $HClO_4$ is shown in Fig. 10

for two electrodes. There is no evidence of activity for Mn(II) at the untreated F-PbO_2/Ti

electrode; however, the activity of this electrode is improved substantially by

postdeposition treatment (methode A). Conversely, the response of the Fe-PbO_2/F-

PbO_2/Ti is quite adequate for Mn(II) oxidation even without postdeposition treatment.

Plots of $1/J$ *vs.* $1/\omega^{1/2}$ for Mn(II) are virtually identical for Fe-PbO_2/Au and Fe-PbO_2/Ti

electrodes indicating no effect of the substrate material on reaction kinetics.

Lead dioxide electrodes have been observed to be very active for oxidation of

ethylenediaminetetra-acetate (EDTA) in acidic media [23,24]. However, there has been disagreement concerning the mechanism of response. Beck [23] reported for $HClO_4$ and H_2SO_4 solutions at 60 °C that EDTA is oxidized by a direct electrochemical process with $n = 6$ eq mol^{-1}. However, Tallant and Huber [24] concluded the oxidation at PbO_2 electrodes to be indirect, involving the redeposition of Pb(II) removed from the oxide film by complexation with EDTA.

Data shown in Fig. 11 indicate a measurable voltammetric response for EDTA at a Au RDE. A mechanism similar to that of Tallant and Huber is highly improbable for this noble metal. Significantly greater anodic signals are obtained for EDTA at PbO_2/Au, $Bi-PbO_2/Au$, and $Fe-PbO_2/F-PbO_2/Ti$ electrodes. The values of n for the anodic reactions at a Au-screen electrode and a $Fe-PbO_2/F-PbO_2/Ti$ coil electrode are *ca.* 6 eq mol^{-1}, as determined by exhaustive electrolysis in 1.0 M $HClO_4$ at 1.6 V. Plots of $1/J$ *vs.* $1/\omega^{1/2}$ for EDTA are linear, and values of nk_{app} are included in Table 5. It is apparent that the activity of the $Fe-PbO_2/F-PbO_2/Ti$ electrode is substantially higher than that of the PbO_2/Au electrode. None of the electrodes is observed to dissolve during a 24 hr period when left under open-circuit conditions in 1.0 M $HClO_4$ containing EDTA. This evidence is contrary to the explanation of Tallant and Huber [24].

For the oxidative degradation of CN^- in alkaline media [4,5,25], when $Fe-PbO_2$ films are applied as anodes in strongly alkaline media, it is necessary to emphasize that the O_2-evolution process can dominate the observed *i-E* response. For example, in 0.1 M NaOH, the residual *i-E* response is very large, and the anodic signals corresponding to oxidation of CN^- cannot be readily distinguished from the background signal.

Table 3.   Summary of response data for oxidation of 1.0 mM thiophene derivatives

at Fe-PbO$_2$/F-PbO$_2$/Ti electrode[a] in 1.0 M HClO$_4$.

#	Compound	I_{bkd}[b] (mA cm^{-2})	$E_{1/2}$ (V vs. SCE)	$10^3 nk_{app}$[b] (eq cm mol^{-1} s^{-1}	I_{sig}/I_{bkd}
1	2-Thiophene-carboxylic acid	1.1	N.W.[c]	16	14
2	3-Thiophene-carboxylic acid	1.0	N.W.[c]	130	5.8
3	2-Thiophene-glyoxylic acid	1.0	1.59	170	17
4	3-Thiophene-malonic acid	1.1	1.46	110	17
5	2-Thiophene-acetic acid	1.2	1.45	370	4
6	2-Thiophene-carbonitrile	0.9	N.R.[d]	N.R.[d]	2
7	2-Thiophene-acetonitrile	1.0	1.49	460	22

[a]   Electrodeposition of F-PbO$_2$ at -2.0 mA for 10 min from 0.1 M HNO$_3$ containing

0.5 M Pb(NO$_3$)$_2$ and 40 mM NaF.

Electrodeposition of Fe-PbO$_2$ at 1.8 V for 10 min from 1.0 M HClO$_4$ containing

5 mM Pb(NO$_3$)$_2$ and 8 mM Fe(NH$_4$)$_2$(SO$_4$)$_2 \cdot$6H$_2$O.

[b]   Values measured at 1.6 V.

[c]   Wave not well developed.

[d]   Negligible reactivity.

Table 4.   Number of electrons passed during oxidation of several thiophene derivatives at $Fe-PbO_2/F-PbO_2/Ti$ electrodes.

#	Compound	n_{net}[a]	Ba^{2+} test for SO_4^{2-}	n_{est}[b] (eq mol^{-1})
1	Dibenzothiophene[d]	4.1	neg.	4.2
2	Dibenzothiophene sulfone	N.R.[e]	neg.	4.4
3	2-Thiophene-carboxylic acid	7.9	pos.	8.4
4	3-Thiophene-malonic acid	15.8	pos.	16
5	2-Thiophene-acetic acid	10.0	pos.	16
6	3-Thiophene-carboxylic acid	10.5	pos.	20

[a]   Exhaustive electrolysis at 1.7 V.

[b]   Values estimated from the slope of $1/J$ vs. $1/\omega^{1/2}$ plots assuming

  $D = 1 \times 10^{-5}$ cm^2 s^{-1}.

[c]   Qualitative test for SO_4^{2-} by addition of $Ba(SO_4)_2$.

[d]   Electrolysis in 1:1 1 M $HClO_4$/ACN.

[e]   Negligible reactivity.

Table 5   Rate constants for anodic response of EDTA at various electrodes in 1.0 M

$HClO_4$.

Electrode	n_{net}[a] (eq mol^{-1})	$10^2 nk_{app}$[b] (eq cm mol^{-1} s^{-1})
Glassy carbon		N.A.[c]
Pt		0.6
Au	6.1	2.5
PbO$_2$/Au		13
F-PbO$_2$/Ti		14
Bi-PbO$_2$/Au		43
Fe-PbO$_2$/F-PbO$_2$/Ti	6.2	46
Fe-PbO$_2$/Ti		116

[a]   Determined by exhaustive electrolysis at 1.7 V.

[b]   Measurements at 1.7 V for 1.0 mM EDTA in 1.0 M $HClO_4$

[c]   Virtually no activity.

The voltammetric response for 5 mM CN^- is shown in Fig. 12 obtained in a

solution buffered at pH 10.0 by 0.014 M $NaHCO_3$/0.011 M Na_2CO_3 (pH 10.0) using F-

Pbo$_2$/Ti and Fe-PbO$_2$/F-PbO$_2$/Ti electrodes. The residual response for the Fe-PbO$_2$/F-

PbO$_2$/Ti electrode is shown for comparison. It is readily apparent that the highest activity

for CN^- is obtained for the Fe-PbO$_2$/F-PbO$_2$/Ti electrode. Values of nk_{app} (eq mol^{-1} cm s^{-1})

determined at 1.3 V are: 1.2 x 10^{-3} for F-PbO$_2$/Ti and 9.4 x 10^{-2} for Fe-PbO$_2$/F-PbO$_2$/Ti.

The value of n is 1.9 $\pm$ 0.01 eq mol^{-1} (N = 3; uncertainty is $\pm$ std. dev.), as determined

by exhaustive electrolysis at 1.3 V at a Fe-PbO$_2$/F-PbO$_2$/Ti coil electrode in NaHCO$_3$/Na$_2$CO$_3$ (pH 10.0). It is concluded that the product is CNO$^-$.

Conclusions

It is concluded from results described here that physically stable F-PbO$_2$ films can be electrodeposited on Ti electrodes from acidic solutions of Pb(II) containing NaF. Furthermore, the resulting films appear ideal as substrates for further electrodeposition of various doped, catalytic PbO$_2$ films. The significant advantage of greater adhesion is sufficient reason to substitute Ti for the noble metals. Obviously, an economic advantage also results from use of Ti, especially for application to large-scale electrolytic processes.

In addition to surface sites for adsorption of ·OH, it is now expected that adsorption of the reactant also can be a prequisite for successful O-transfer reactions [5,25]. As an example, a well-developed anodic wave with a plateau current limited by mass transfer of CN$^-$ is obtained for a Fe-PbO$_2$/Au electrode [5]. The stability of the coordination bond between Fe(III) and CN$^-$ is well known and it is proposed that Fe(III) sites in the Fe-PbO$_2$ surface function to absorb CN$^-$. Apparently, in this instance, the inherent density of sites for ·OH adsorption on PbO$_2$ films is sufficient to support that portion of the reaction mechanism and the undoped electrode is activated merely by generating adsorption sites for the reactant (CN$^-$). The known stability of coordination bonds between Fe(III) and EDTA, as well as the insolubility of Fe(III) sulfide, appears to

give further support to the suggestion that the Fe(III) sites in Fe-PbO$_2$ electrodes also function for adsorption of these reactants.

The validity of the bifunctional-site mechanism is undergoing extensive further testing in this laboratory.
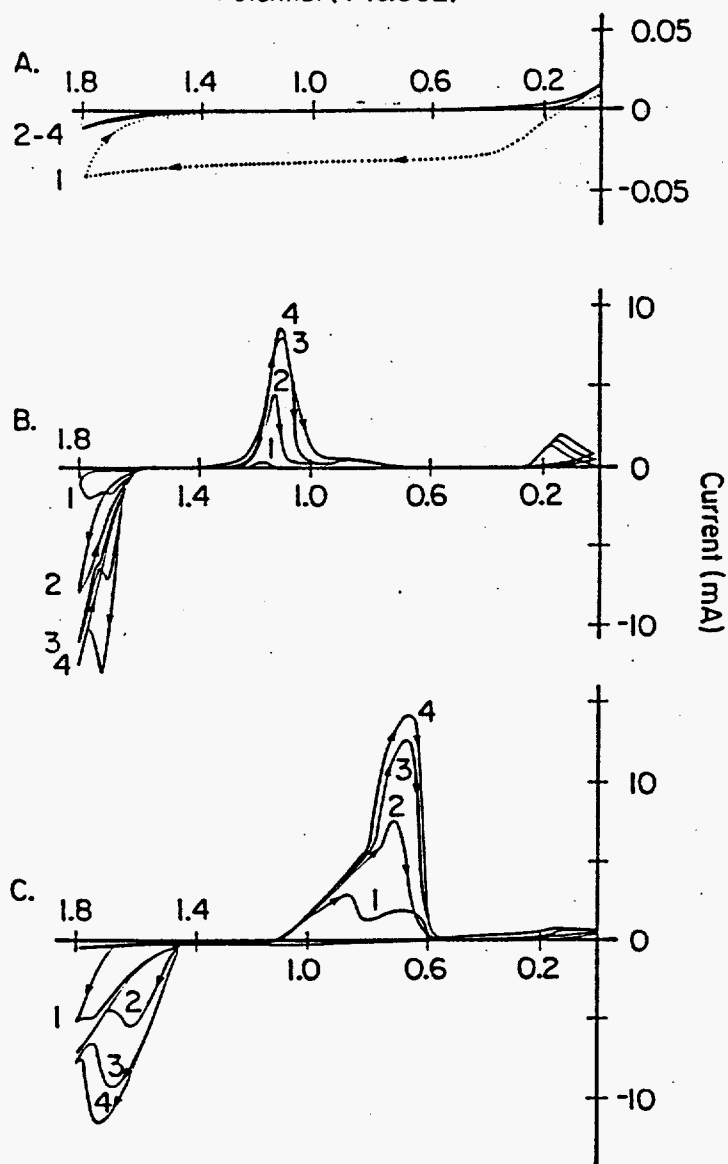
Acknowledgments

Fig. 1.   Voltammetric response for deposition of PbO_2 at a Ti rotated disk electrode.
Rotation speed: 1600 rev min^{-1}. Scan rate: 6 V min^{-1}. (Scan number shown in figure). Solution: (A) 10 mM $Pb(NO_3)_2$ in 1 M $HClO_4$, (B) 0.5 M $Pb(NO_3)_2$ in 1 M $HClO_4$, (C) 0.5 M $Pb(NO_3)_2$ and 40 mM NaF in 0.1 M HNO_3.
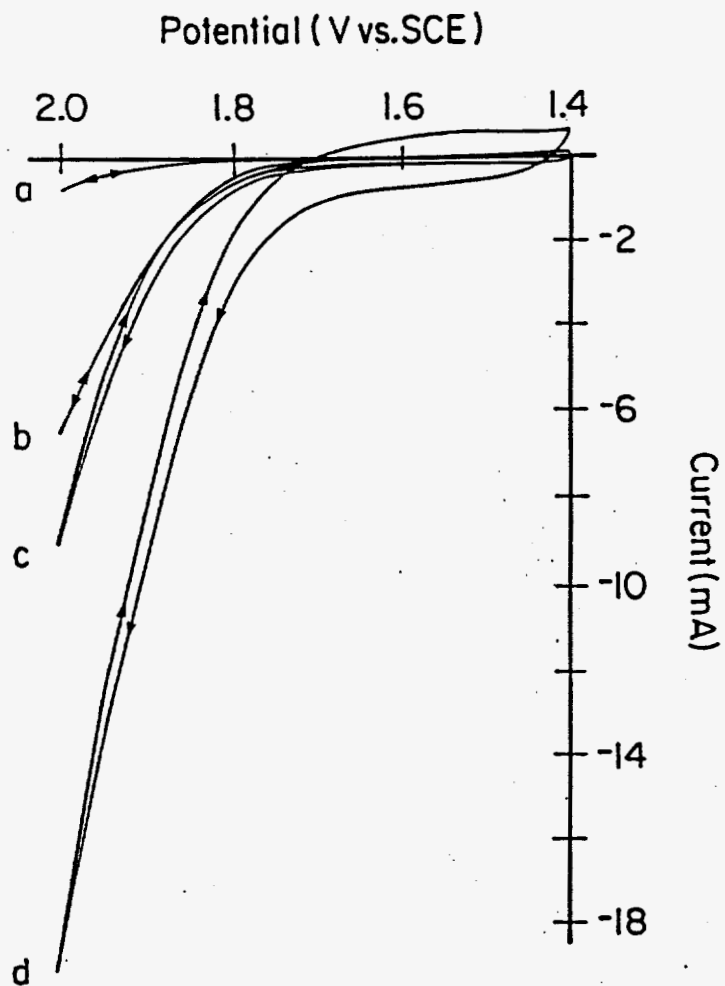
Fig. 2.   Voltammetric response for O_2 evolution at various electrodes in 1.0 M $HClO_4$.
Rotation speed: 1600 rev min^{-1}. Scan rate: 0.6 V min^{-1}; positive scan.
Electrode: (a) F-PbO_2/Ti, (b) Fe-PbO_2/Ti, (c) PbO_2/Au, and (d) Bi-PbO_2/Au.
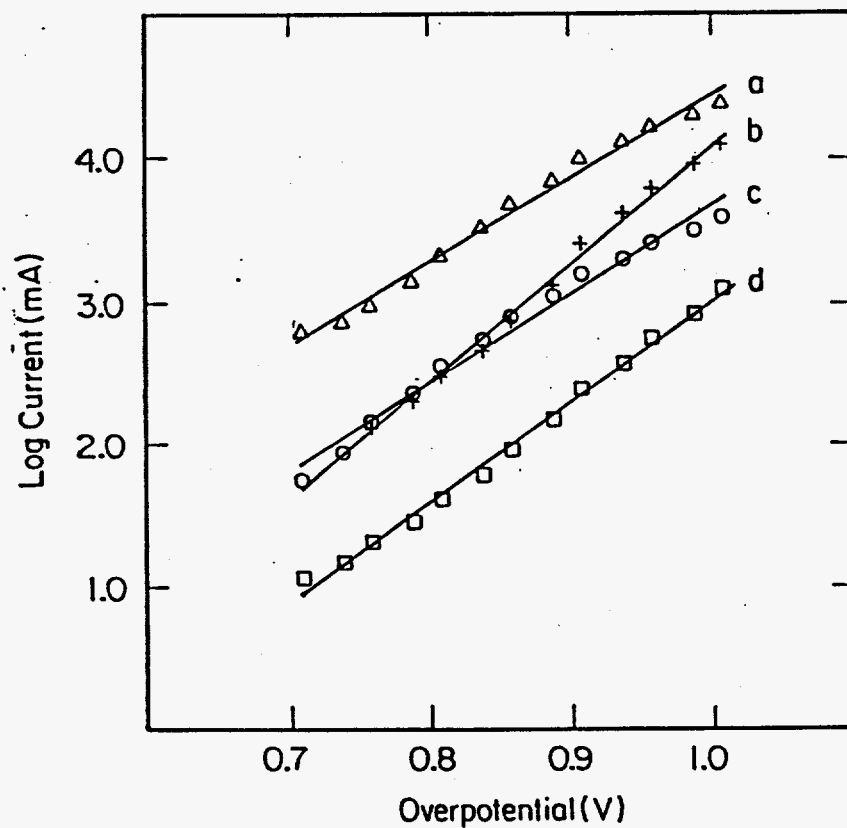
Fig. 3.   Tafel plots of $\log\{I/\mu A\}$ *vs.* η for O_2 evolution corresponding to positve scan at various electrodes in 1.0 M $HClO_4$.
Rotation speed: 1600 rev min^{-1}. Scan rate: 0.54 V min^{-1}.
Electrode: (a) $F\text{-}PbO_2/Ti$, (b) $Fe\text{-}PbO_2/Ti$, (c) PbO_2/Au, and (d) $Bi\text{-}PbO_2/Au$.

A.

B.

20 μM

C.

D.
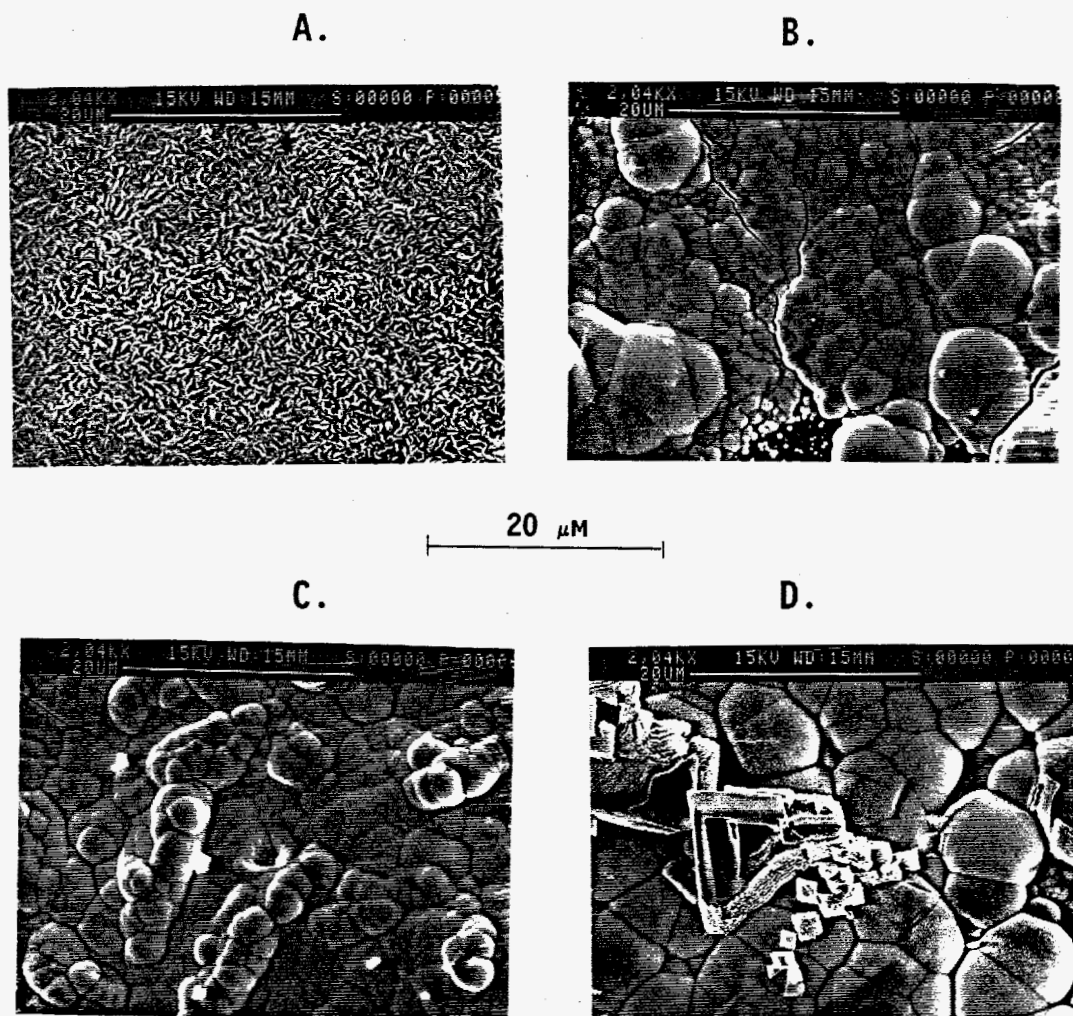
Fig. 4.   Scanning electron micrographs of various film surfaces.
Electrode: (A) F-PbO$_2$/Ti, (B) Fe-PbO$_2$/Ti, (C) F-PbO$_2$/Ti after post-treatment (methode B). (D) Fe-PbO$_2$/F-PbO$_2$/Ti.
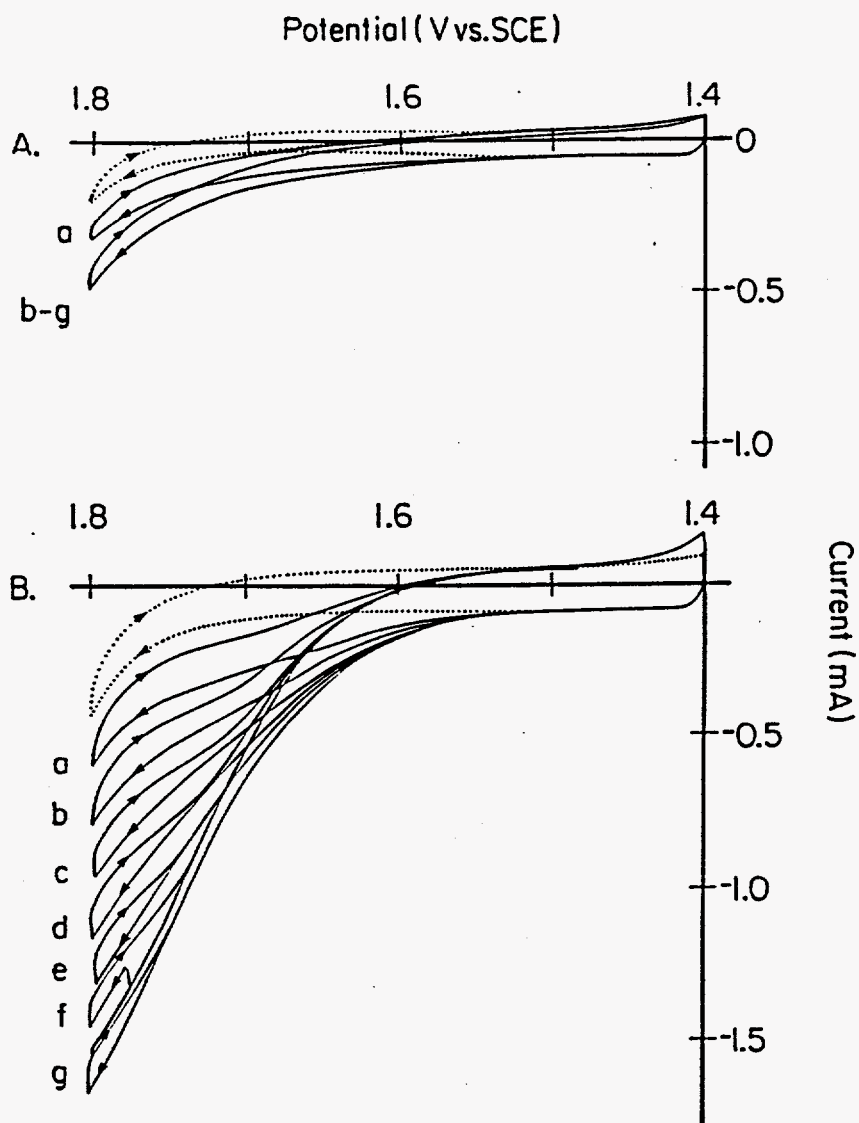
Fig. 5.   Voltammetric response of 10.0 mM DMSO at various films on Ti rotated
disk electrodes in 1.0 M HClO$_4$. Scan rate: 0.6 V min^{-1}. Rotation speed
(rev min^{-1}): (a) 100, (b) 400, (c) 900, (d) 1600, (e) 2500, (f) 3600,
(g) 4900. Curves: (...) residual, (—) DMSO.
Electrode: A - F-PbO$_2$/Ti, B - Fe-PbO$_2$/F-PbO$_2$/Ti.
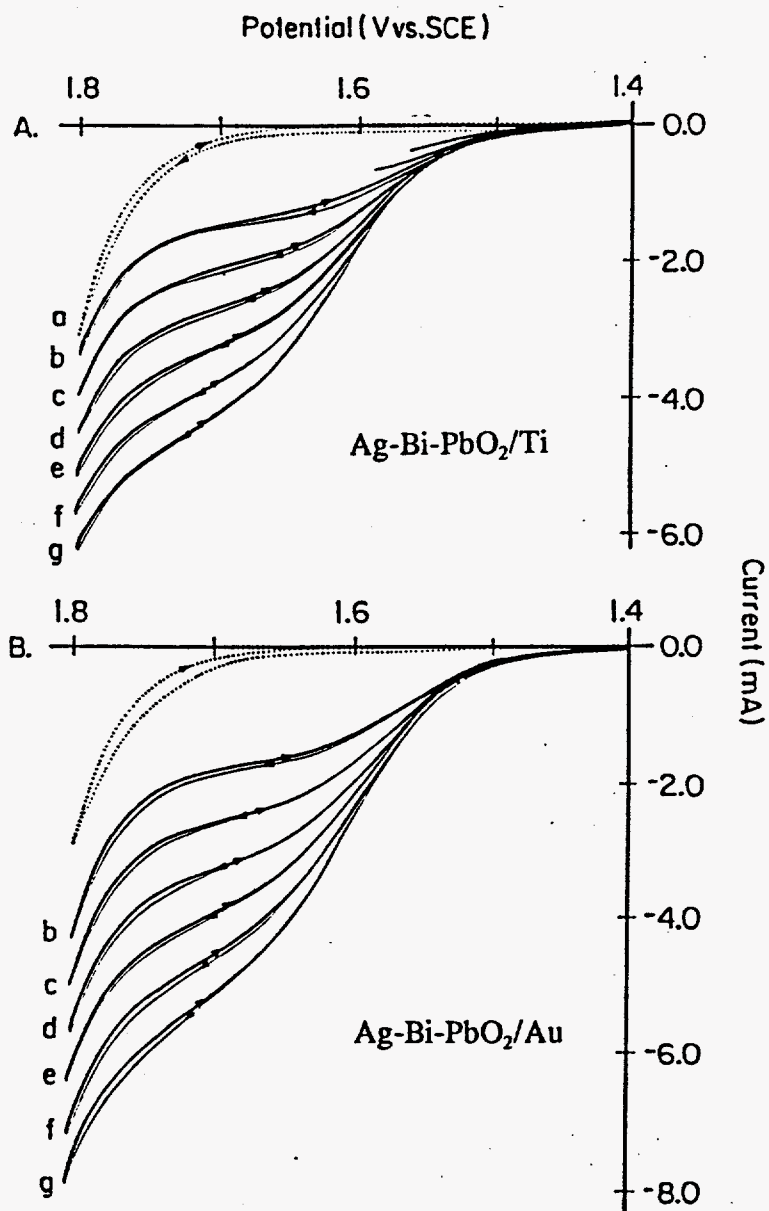
Fig. 6.   Voltammetric response of 10.0 mM DMSO at Ag-Bi-PbO$_2$ films on Ti and
Au rotated disk electrodes in 1 M HClO$_4$.
Deposition: 1.65 V for 10 min at 1600 rev min^{-1} in 1 M HClO$_4$ containing
10 mM Pb(NO$_3$)$_2$, 7 mM Bi(NO$_3$)$_3$·H$_2$O and 15 mM AgNO$_3$. Scan rate
0.6 V min^{-1}.   Rotation speed (rev min^{-1}): (a) 100, (b) 400, (c) 900,
(d) 1600, (e) 2500, (f) 3600, (g) 4900. Curves: (...) residual,
(—) DMSO.
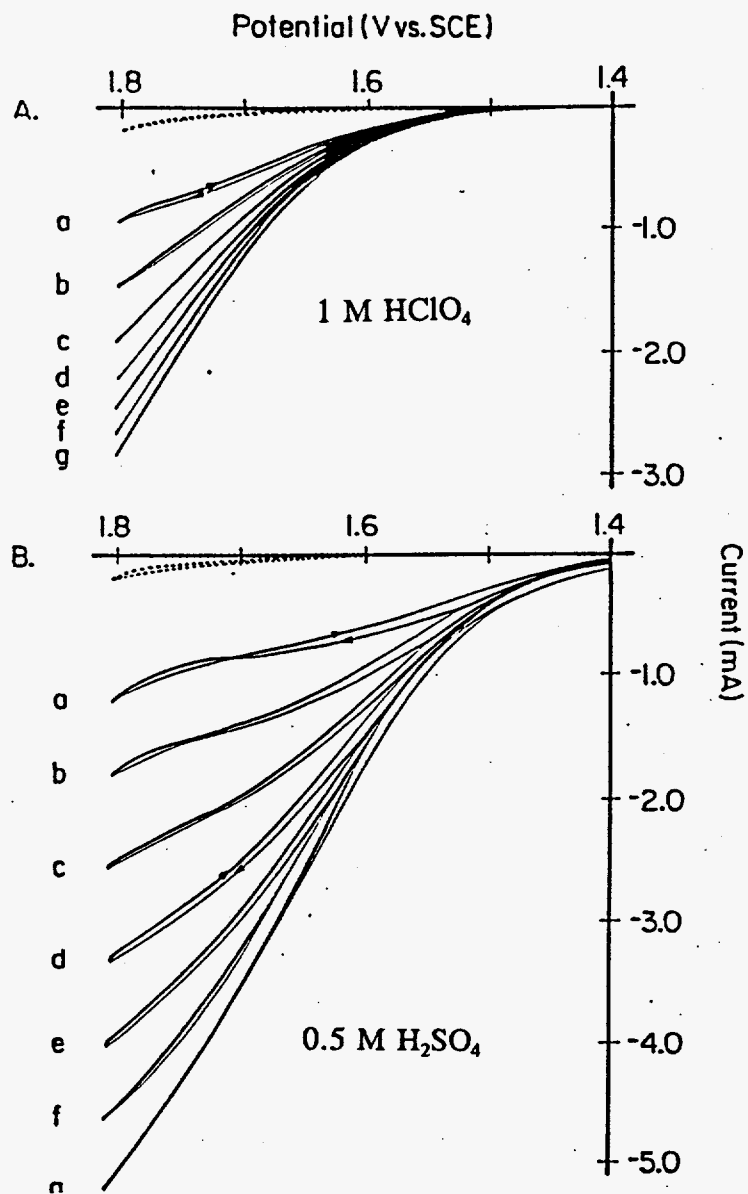
Fig. 7.   Voltammetric response of 10.0 mM TMSO at a F-PbO$_2$/Ti electrode in 1
M HClO$_4$ and 0.5 M H$_2$SO$_4$.
Scan rate: 0.6 V min^{-1}. Rotation speed (rev min^{-1}): (a) 100, (b) 400,
(c) 900, (d) 1600, (e) 2500, (f) 3600, (g) 4900.
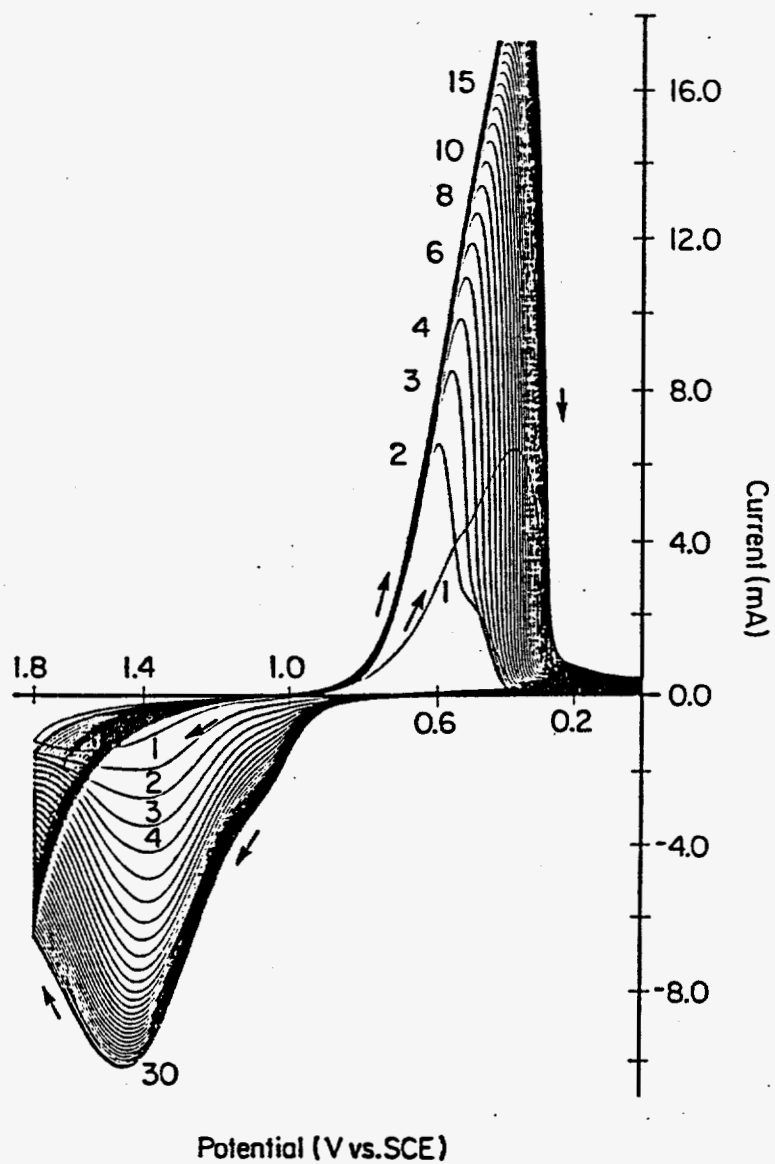
Fig. 8.   Voltammetric response at a F-PbO$_2$/Ti electrode during successive cyclic potential scans in 0.5 M H$_2$SO$_4$.
Rotation speed: 1600 rev min^{-1}. Scan rate: 6.0 V min^{-1}.

Potential (E vs. SCE)
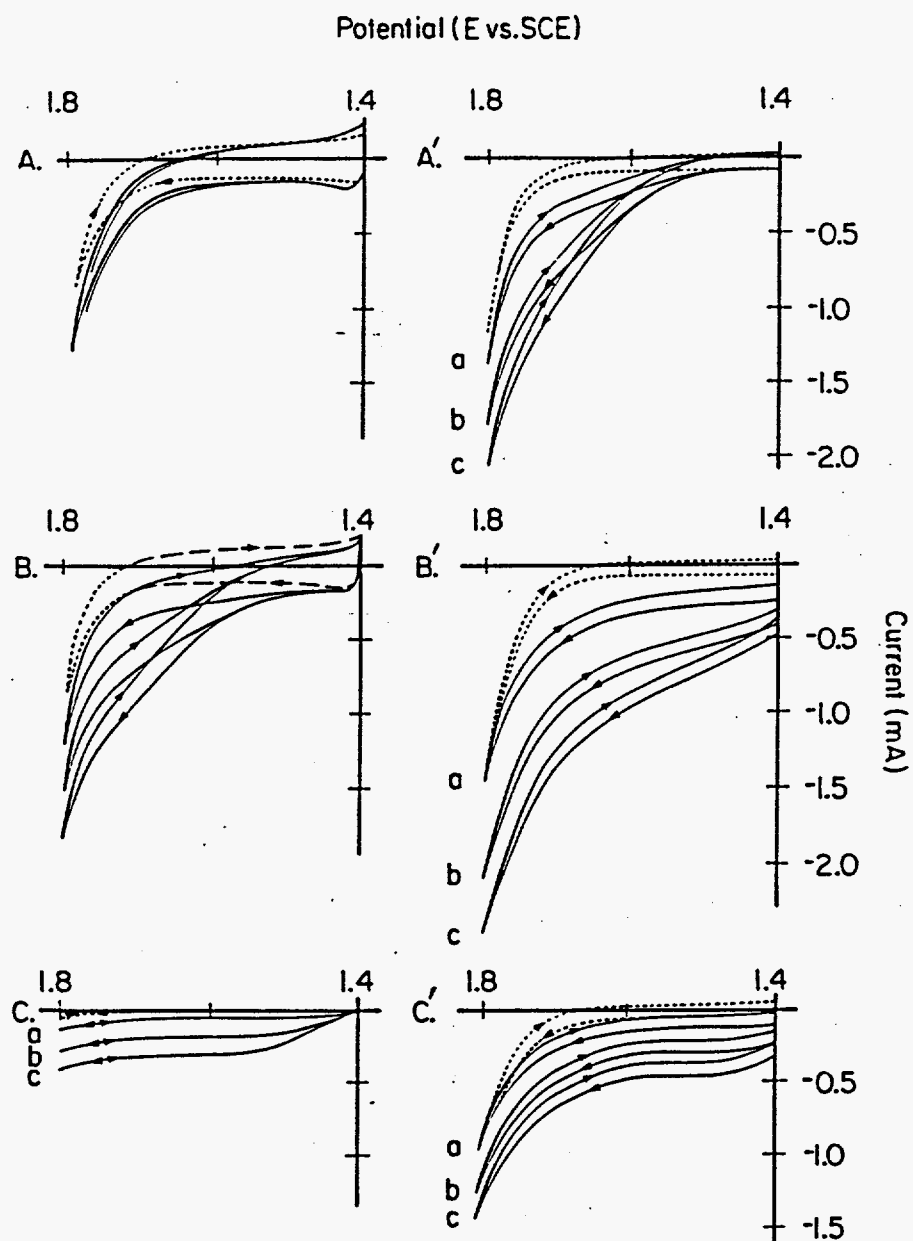
Fig. 9.   Voltammetric response of 1.0 mM thiophene derivatives at various electrodes in a 1:1 mixture of 1 M $HClO_4$ and CH_3CN.
Scan rate: 0.6 V min^{-1}, Rotation speed (rev min^{-1}): (a) 100, (b) 1600, (c) 4900. Curves: (...) residual response. (—) thiophene compound.
Compound: (A,A') 2-thiophenecarboxylic acid, (B,B') 3-thiophenemalonic acid, and (C,C') dibenzothiophene.
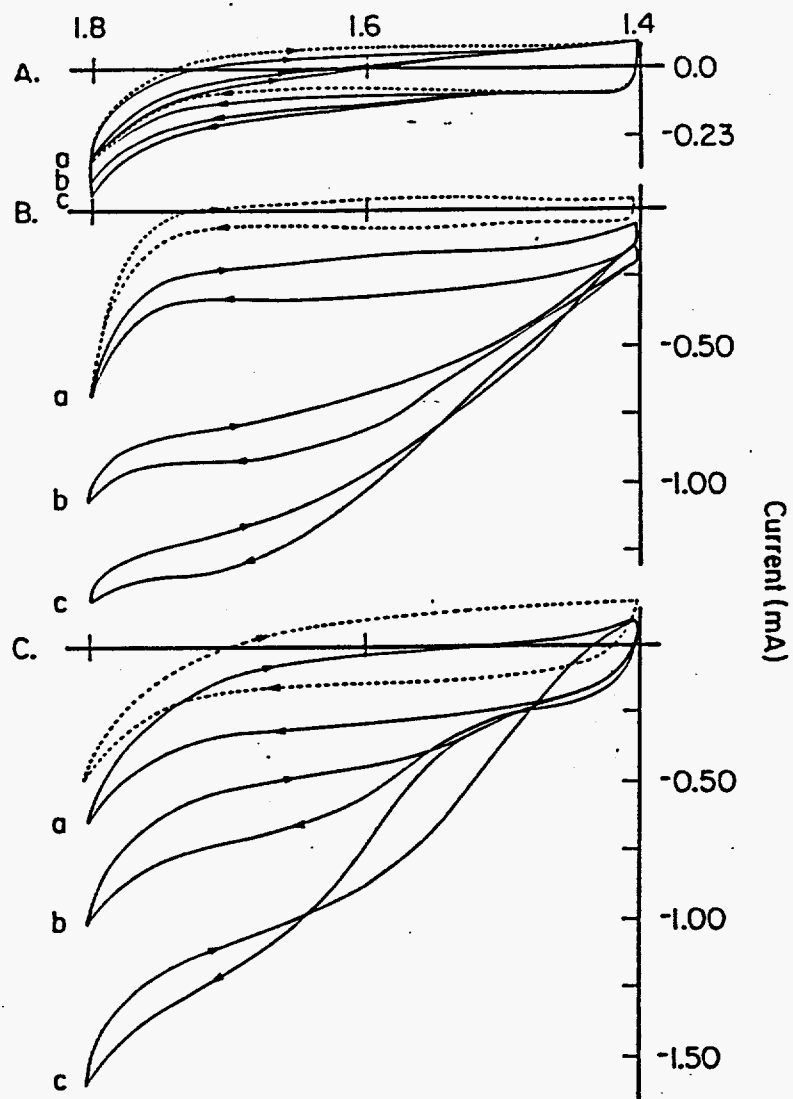
Fig. 10.   Voltammetric response of 1 mM Mn(II) at various electrodes in 1 M
            HClO$_4$.
            Scan rate: 0.6 V min^{-1}. Rotation speed (rev min^{-1}): (a) 100, (b) 1600,
            (c) 4900. Electrode: (A) F-PbO$_2$/Ti, (B) F-PbO$_2$/Ti after post-treatment by
            method A for 30 min in 1 M H$_2$SO$_4$, (C) Fe-PbO$_2$/F-PbO$_2$/Ti.
            Curves: (...) residual response at 1600 rev min^{-1}, (—) presence of Mn(II).
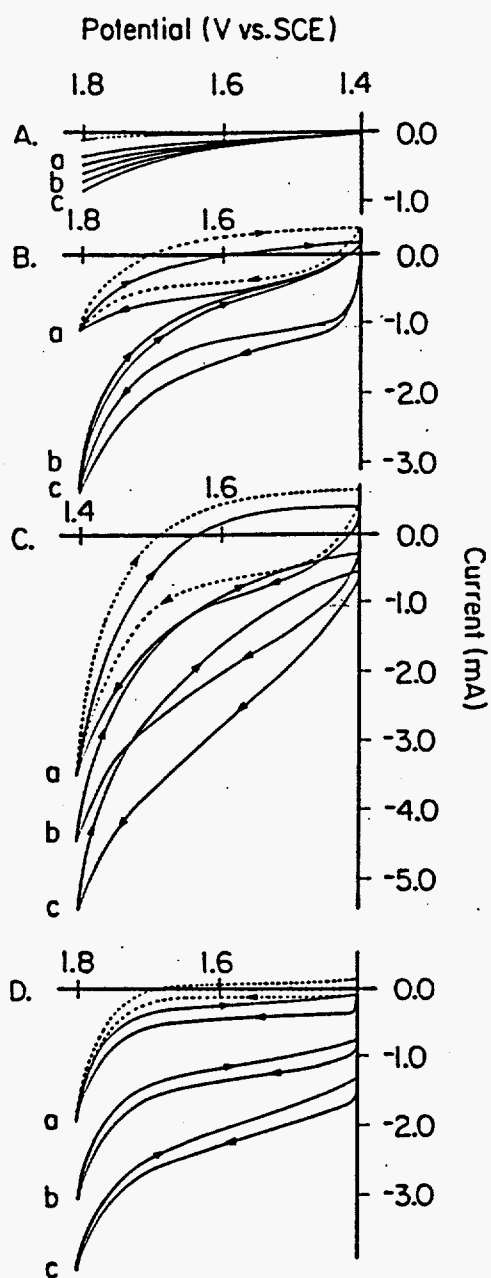
Fig. 11.   Voltammetric response of 1 mM EDTA at various electrodes in 1 M
            HClO$_4$.
            Scan rate: 0.6 V min^{-1}. Rotation speed (rev min^{-1}): (a) 100, (b) 1600,
            (c) - 4900.
            Electrode: A - Au, B - PbO$_2$/Au, C - Bi-PbO$_2$/Au,
            D - Fe-PbO$_2$/F-PbO$_2$/Ti.
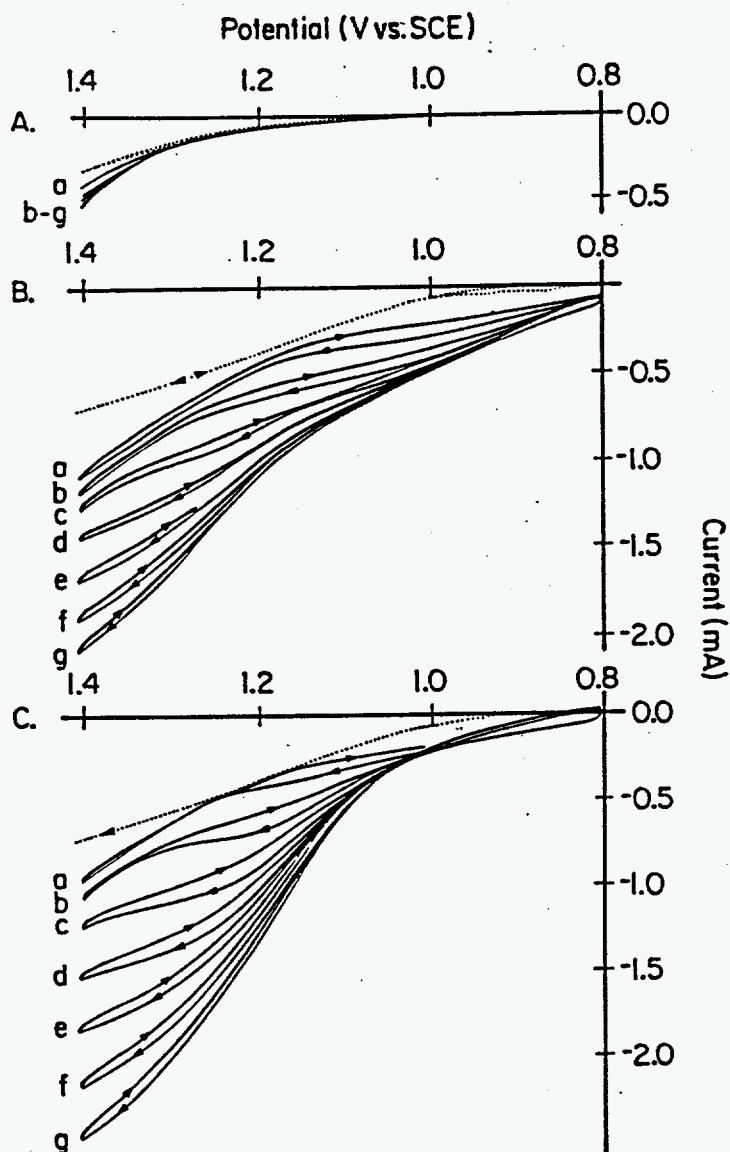
Fig. 12. Comparison of voltammetric response of 5 mM NaCN at F-PbO$_2$/Ti and Fe-PbO$_2$/F-PbO$_2$/Ti disk electrodes in 0.014 M NaHCO$_3$/0.011 M Na$_2$CO$_3$ (pH 10.0).
Scan rate: 0.6 V min^{-1}. Rotation speed (rev min^{-1}): (a) 400, (b) 900, (c) 1600, (d) 2500, (e) 3600. Curves: (A) residual, (B) presence of NaCN.
Electrode: A & C - Fe-PbO$_2$/F-PbO$_2$/Ti, B - F-PbO$_2$/Ti.

REFERENCES

[1]   I-H. Yeo and D. C. Johnson, *J. Electrochem. Soc.*, **134**, 1973 (1983).

[2]   I-H. Yeo, S. Kim, R. Jacobson and D. C. Johnson, *J. Electrochem. Soc.*, **136**, 1398 (1989).

[3]   Y-L. Hsiao and D. C. Johnson, *ibid.*, **136**, 3704 (1989).

[4]   J. Feng and D. C. Johnson, *J. Appl. Electrochem.*, **20**, 116 (1990).

[5]   J. Feng and D. C. Johnson, *J. Electrochem. Soc.*, **137**, 570 (1990).

[6]   H. Chang and D.C. Johnson, *J. Electrochem. Soc.*, **137**, 2452 (1990).

[7]   G. Bewer, H. Debrodt and H. Herbst, "Titanium for Energy and Industrial Application," Daniel Eylon, Editor, pp. 259-75, American Institute of Mining, Metallurgical, and Petroleum Engineers, Inc. New York (1981).

[8]   J. P. Carr and N. A. Hampason, *Chem. Rev.*, **72**, 679 (1972).

[9]   "The Electrochemistry of Lead," A. T. Kuhn, Editor, pp. 288-293, Academic Press, London (1979).

[10]   C . A. Hampel, "Encyclopedia of Electrochemistry," p. 762, Reinhold, New York (1964).

[11]   A. Fukasawa, *Japan Kokai JP* 52-19230[77/19230], p. 4 (Feb. 14, 1977).

[12]   D. Gilroy and R. Stevens, *J. Appl. Electrochem.*, **10**, 511 (1980).

[13]   Y-L. Hsiao, Ph. D. Dissertation, Iowa State University, Ames, IA (1990).

[14]   D. Wabner and H. P. Fritz, *Z. Naturforsch.* **3113**, 39, 45 (1976).

[15]   J. Koutecky and V. G. Levich, *Zh. Fiz. Khim.*, **32**, 1565 (1956).

[16]   H. Chang and D. C. Johnson, *J. Electrochem. Soc.*, **136**, 17 (1989).

[17]   "Semiconductor Electrodes," H. O. Finklea, Editor, p. 60, Elsevier, New York (1988).

[18]   W. R. LaCource, Y-L. Hsiao, D. C. Johnson, *J. Electrochem. Soc.*, **136**, 3714 (1989).

[19]   A. Damjanovic and B. Jovanovic, *ibid.*, **137**, 3071 (1990).

[20]   L. A. Larew, J. S. Gordon, Y-L. Hsiao, D. A. Buttry, and D. C. Johnson, *ibid.*, **137**, 3071 (1990).

[21]   T. D. Wheelock and R. Markuszewski, Paper presented at "Conference on the Chemistry and Physics of Coal Utilization," Iowa State University, Ames, IA, June 1980.

[22]   C. W. Fan, G-W. Dong, R. Markuszewski, and T. D. Wheelock, in "Processing and Utilization of High Sulfur Coals II," Y.P. Chugh and R. D. Caudle, Editors, Elsevier, New York (1987).

[23]   M. T. Beck, *Chemist-Analyst*, **50**, 14 (1961).

[24]   D. R. Tallant and C. O. Huber, *J. Electroanal. Chem.*, **18**, 413, (1968).

[25]   B. Wels and D. C. Johnson, *J. Electrochem. Soc.*, **137**, 2785 (1990).

CHAPTER 4

EVOLUTION OF OZONE

J. Feng, S. N. Lowery[1], J. J. Carey[1] and D. C. Johnson

ABSTRACT

Current efficiencies are compared for the generation of O_3 simultaneously with O_2 during anodic discharge of H_2O at pure and iron(III)-doped β-lead dioxide film electrodes in phosphate buffer (pH 7.5, 10 °C) containing 2.5 mM KF. Also examined is the effects of applied current density. A current efficiency of 14.6% was obtained for the Fe(III)-doped PbO_2 film electrode deposited on an internally cooled (10 °C) tubular titanium substrate at a current density of 200 mA cm^{-2} as compared to only 6.1% at the undoped PbO_2 electrode under the same conditions. This result is tentatively explained on the basis of a mechanism involving the transfer of oxygen from hydroxyl radicals adsorbed on Pb(IV) sites adjacent to Fe(III) sites to O_2 adsorbed at the Fe(III) sites in the surface of the Fe(III)-doped PbO_2 electrodes.

---

[1] Scientists of Kodak Research Laboratories, Rochester.

Introduction

Ozone (O_3) is known to be generated simultaneously with O_2 during anodic

discharge of H_2O at several electrode materials in a variety of aqueous media [1-2]. This

observation has resulted in the suggestion of numerous possibilities for electrolytic

ozonation, including sterilization of water, bleaching of paper, and electrosynthesis. The

electrochemistry of O_3 evolution has been discussed [3-10] and only a brief summary is

given here.

Relevant half-reactions and their corresponding standard potentials are:

$$O_3 + 6H^+ + 6e^- = 3H_2O; \quad E° = 1.51 \text{ V } \textit{vs. NHE} \qquad (1)$$

$$O_2 + 4H^+ + 4e^- = 2H_2O; \quad E° = 1.23 \text{ V } \textit{vs. NHE} \qquad (2)$$
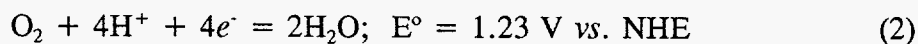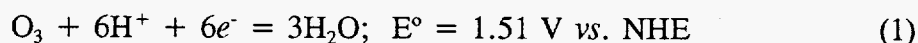
It is apparent from these $E°$ values that anodic generation of O_2 is thermodynamically

favored over that of O_3. Strategies to increase the current efficiency for O_3 generantion

generally include one or more of the following [3-10]: (i) choice of anode materials

characterized by large O_2-evolution overpotential, $\textit{e.g.}$, PbO_2 and glassy carbon (GC); (ii)

application of a large anodic current density to achieve a large positive electrode

potential; (iii) suppression of temperature; and (iv) addition of an absorbate, $\textit{e.g.}$, F^-, BF_4^-

and PF_6^-, to block the O_2-evolution mechanism and, thereby, increase the efficiency for

O_3 evolution.

Representative values reported for O_3-generation efficiency are given in Table 1.

Notable values are: 21% at β-PbO_2 in 2 M HPF_6 (750 mA cm^{-2}, 0 °C) [3], 35% at glassy

carbon (GC) in 7.3 M HBF_4 (600 mA cm^{-2}, 0 °C) [9], and 45% at GC in 62 wt % HBF_4 (200 mA cm^{-2}, -5 °C) [10]. Here we compare the O_3-evolution at Fe(III)-doped and undoped β-PbO_2 film electrodes to determine a possible catalytic benefit from the presence of Fe(III) sites in the β-PbO_2 surfaces.

Table 1.   Reported values of current efficiency for O_3 generation during condtant-current electrolysis at various electrodes in a variety of media.

Anode	Media	Temp. (°C)	Current Density (mA cm^{-2})	current Efficiency (%)	Ref.
Pt	5 M H_2SO_4	0	200	0.15	3
Ru/Ti	5 M H_2SO_4	0	200	0.15	3
β-PbO_2	2 M H_2SO_4	0	120	1.1	3
β-PbO_2	2 M HF	0	750	6	3
β-PbO_2	2 M $H_2PO_4^-$	0	750	3	3
β-PbO_2	2 M $HClO_4$	0	750	12	3
β-PbO_2	2 M HBF_4	0	800	18	3
β-PbO_2	2 M HPF_6	0	400	51	3
β-PbO_2/Eb[a]	0.52 M K_2HPO_4/0.22 M KH_2PO_4/2.5 mM KF (pH 7.5)	0	190	11.7	6
GC	7.3 M HBF_4	0	200	22	9
GC	7.3 M HBF_4	0	600	35	9
GC	62 wt % HBF_4	-5	200	45	10

[a] Eb $\equiv$ Ebonex[R].

Experimental

*Equipments.* - Voltammetric data were obtained with a Au-Au rotated ring-disk electrode (RRDE; A_{disk} = 0.20 cm^2, $\beta^{2/3}$ = 0.52 and N = 0.22; (Pine Instrument Co.). The MSR rotator and RDE4 potentiostat (Pine) were interfaced with a 286/10 microcomputer (Standard) using a DT2801/5716 data acquisition board (Data Translation) and ASYST-2.0 software (Keithley/Asyst). The electrochemical cell (300 ml) was made of Pyrex with a compartment via a Luggin capillary channel. The counter electrode was a Pt-wire coil (*ca.* 10 cm^2) located in a small volume of electrolyte (*ca.* 50 ml) separated from the working compartment by a fritted-glass disk (medium porosity).

Evolution of O_3 for extended periods under galvanostatic conditions was achieved in an undivided Pyrex cell (150 ml) immersed in a refrigerated water bath (Fisher). The cell was constructed to allow continuous and rapid purging with dispersed N_2 so that product mixture of O_3 and O_2 were quantitatively transferred via connecting tubing to aqueous solutions of KI.

Procedures. - Quantitative determinations of O_3 were based on iodometric titrimetry [11]. In this procedure, I_3^- generated according to:

$$O_3 + 3I^- + 2H^+ \rightarrow O_2 + H_2O + I_3^- \tag{3}$$
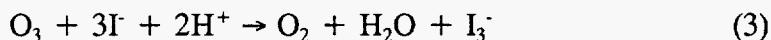
was titrated with standard solutions of $Na_2S_2O_3$ to the starch endpoint:

$$I_3^- + 2 Na_2S_2O_3 \rightarrow 2 Na^+ + 3I^- + Na_2S_4O_6 \tag{4}$$
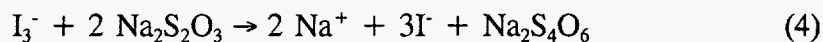
Anode materials. - Some anodes were constructed in the form of flat plates (*ca.* 10 cm^2). Others were constructed from metal U-tubes and thermostated water was passed through the interior of the tubes to achieve temperature control of the electrode surface.

Solid electrode materials included Pt and Au (Johnson Matthey), and ruthenized titanium (designated "Ru/Ti"; Electrosynthesis Co. Inc.). Other electrodes consisted of thin films ($< 10 \, \mu$m) of pure or mixed-metal oxides elecrodeposited on various substrates). These included: β-PbO$_2$ on Ti (designated "β-PbO$_2$/Ti") deposited from 0.1 M HClO$_4$ containing 0.5 M Pb(II) and 40 mM F$^-$ [12]; Fe(III)-doped β-PbO$_2$ on β-PbO$_2$/Ti ("Fe-PbO$_2$/Ti) electrodeposited from 1.0 M HClO$_4$ containing 5 mM Pb(II) and 8 mM Fe(II) [12]; and α-PbO$_2$ on type-304 stainless steel, electrodeposited from 2 M NaOH saturated with PbO(s) [13]. The latter is designated as "Fe-PbO$_2$/SS" because these films have been determined to contain traces of iron presumed to be Fe(III) [13].

Results and Discussion

Ring-disk studies. - The identity of O$_3$ as a product of anodic discharge of H$_2$O was suspected on the basis of odor and confirmed on the basis of voltammetric data obtained with a Au-Au RRDE. Johnson *et al.* demonstrated that O$_3$, generated by electrostatic discharge in a stream of pure O$_2$, can be detected cathodically in 0.1 M HClO$_4$ by the transport-limited reduction to O$_2$ (2 eq mol^{-1}) with E$_{1/2}$ = *ca.* 1.2 V *vs.* SCE (pos. scan) [14]. By comparison, O$_2$ reduction occurs at E < *ca.* 0.5 V *vs.* SCE and, therefore, O$_3$ can be detected voltammetrically at Au electrodes in 0.1 M HClO$_4$ in

the region *ca.* 0.6 to 1.0 V (pos. scan) without interference from dissolved O_2.

Shown in Figure 1 are representative voltammetric data obtained at the Au-ring of the RRDE in 0.1 M $HClO_4$ (25 $\pm$ 3 °C) during evolution of a mixture of O_2 and O_3 under galvanostatic conditions at the disk electrode. The disk surfaces correspond to β-PbO_2/Au in Figure 1A and Fe-PbO_2/Au in Figure 1B. The I_{ring}-E_{ring} curves corresponding to I_{disk} = 0 and 2.0 mA (i.e., I_{disk}/A_{disk} = 0 and 10 mA cm^{-2}) are represented by Curves **a** (---) and **b** (——), respectively. Familiar anodic and cathodic waves are observed for formation of surface oxide (E_{ring} > *ca.* 1.1 V, pos. scan) and oxide reduction (E_{ring} < *ca.* 1.1 V, neg. scan), respectively. The slight changes in these waves observed when I_{disk} is changed from 0 to 2.0 mA are the result of slight increase in acidity at the ring surface from the protons produced during anodic discharge of H_2O.

There is virtually no difference between Curve **a** (---) and Curve **b** (——) in Figure 1A within the region E_{ring} = *ca.* 0.5 to 0.8 V (pos. scan) and it is apparent that virtually no O_3 is evolved at the β-PbO_2/Au disk at I_{disk} = 2.0 mA. In marked contrast, a large signal is apparent in Curve **b** (——) in Figure 1B for I_{disk} = 2.0 mA at the Fe-PbO_2/Au disk. Confirmation that this large cathodic signal originates from reduction of O_3 is based on the close agreement between the value $E_{1/2}$ = *ca.* 1.2 V (pos. scan) with that reported previously for a Au-ring electrode [14].

The percent current efficiency (%CE) for O_3 evolution under the conditions of Figure 1B is estimated from I_{ring} at 0.8 V as demonstrated by:

$$\%CE = 100(I_{ring,0.8V}/NI_{disk}) = 100(0.019 \text{ mA})/(0.22)(2.0 \text{ mA}) = 4.3 \%$$

where $N = 0.22$ is the collection efficiency of the RRDE calculated from the three characteristic radii [15]. Further attempts to apply the RRDE for evaluation of the current efficiency for O_3 evolution using larger disk current densities were not successful because of the formation of gas bubbles (predominately O_2) on the disk surface. These bubbles interfered with transport of O_3 to the ring electrode and, therefore, were the cause of large and irregular fluctuations in I_{ring}. Hence, %CE for O_3 production could not be determined reliably from I_{ring}-E_{ring} data.

Preliminary comparisons of anode materials. - Current efficiencies for O_3 generation were determined on the basis of the iodometric methode for four plate electrodes in 1.0 M $HClO_4$ (25 °C) at a current density of 30 mA cm^{-2}. Whereas highly acidic media are not recommended for O_3 generation at PbO_2 electrodes [3], it is significant that the efficiency of O_3 generation at Fe-PbO_2/Ti (3.2%) is significantly larger than at β-PbO_2/Ti (0.57%) in this electrolyte. No detectable O_3 was generated at the Au and Pt under these conditions.

Current efficiencies for O_3 generation were determined for various plate electrodes in 0.52 M K_2HPO_4/0.22 M KH_2PO_4 buffer containing 2.5 mM KF (pH 7.5, 25 °C) at a current density of 30 mA cm^{-2}. Again, the efficiency at the Fe-PbO_2/Ti electrode (4.2%) was significantly larger than for the β-PbO_2/Ti electrode (1.9%).

Variation of current density. — The current efficiency for O_3 evolution increases as temperature is decreased [3,5]. The current efficiency for O_3 evolution at the Fe-

PbO_2/Ti plate electrode was determined as current densities increased to 100 mA cm^{-2} with the electrolysis cell submerged in a thermostatic bath (25 ° C). The efficiency was determined to increase with increasing current density to a maximum at *ca.* 80 mA cm^{-2} with decreased efficiency for higher current densities. This shows that temperature control of the anode-solution interfacial region is critical for accurate determination of the effect of current density on O_3 evolution at large values of current density for which ohmic heating in the interfacial region can be substantial. Hence, to achieve adequate thermostatic control of our anodes, β-PbO_2 and Fe-PbO_2 films were deposited on U-shaped tubular metal substrates to allow passage of thermostated water through the interior of the electrodes. Furthermore, the bulk temperature of the electrolysis medium also was controlled by placement of the electrolysis cell in the thermostatic bath.

Figure 2 shows values of current efficiency for O_3 generation at a Fe-PbO_2/Ti tubular electrode (10 °C), in 0.52 M K_2HPO_4/0.22 M KH_2PO_4 buffer (pH 7.5, 10 °C) containing 2.5 mM KF, as a function of current density increased to 190 mA cm^{-2}. It is apparent from this figure that the O_3-evolution efficiency increases as a virtually linear function of current density for this electrode to *ca.* 13.7% at 190 mA cm^{-2}.

In a separate experiment, current efficiencies for O_3 evolution were compared for Fe-PbO_2/Ti, β-PbO_2/Ti and Fe-PbO_2/SS tubular electrodes (10 °C) in 0.52 M K_2HPO_4/0.22 M KH_2PO_4 buffer (pH 7.5, 10 °C) containing 2.5 mM KF, at a current density of 200 mA cm^{-2}. These results are given in Table 2. Again, the O_3-evolution efficiency is significantly larger for the Fe(III)-doped PbO_2 films as compared with the undoped β-PbO_2 film.

Table 2.   Current efficiency for O_3 production during constant-current electrolysis

at internally-cooled tubular electrodes in 0.52 M K_2HPO_4/

0.22 M KH_2PO_4 buffer (pH 7.5) containing 2.5 mM KF at 10 °C

in an undivided cell[a].

Electrode	Current Efficiency[b] (%)
β-PbO_2/Ti	6.1 ± 0.4
Fe-PbO_2/Ti	14.6 ± 0.3
Fe-PbO_2/SS	13.5 ± 0.8

[a]   Electrode areas = $ca.$ 10 cm^2;

Anodic current = 2000 mA, $i.e.$,

current density = 200 mA cm^{-2};

Total anodic charge = 180 C.

[b]   Uncertainties represent 90% confidence intervals for five determinations.

Conclusions

Current efficiencies for O_3 generation are significantly larger at Fe(III)-doped PbO_2-film electrodes as compared with pure β-PbO_2 electrodes under all conditions tested. We interpret the apparent electrocatalytic effect of the Fe(III) sites in Fe-PbO_2 anodes as follows: (i) The oxygen stoichiometry for Fe(III) oxides is smaller than for Pb(IV) oxide ($FeO_{1.5}$ vs. PbO_2) and, therfore, substitution of Fe(III) for Pb(IV) in the PbO_2 surface results in destabilization of some oxide ions that normally are situated in highly stable bridging positions between adjacent Pb(IV) sites. (ii) We speculate that the destabilized oxide exist in the form of a hydroxyl species (OH) bound to single Pb(IV) sites adjacent to the Fe(III) sites and the oxygen from these hydroxyl species can be transferred to products of electrochemical oxidations with subsequent regeneration of the hydroxyl species by anodic discharge of H_2O. (iii) Finally, we speculate that oxygen from hydroxyl species on Pb(IV) sites is transferred to O_2 adsorbed at adjacent Fe(III) sites to produce O_3, as illustrated below and in Figure 3.

$$(O_2)_{ads} + (OH)_{abs} \rightarrow O_3 + H^+ + e^- \qquad (5)$$
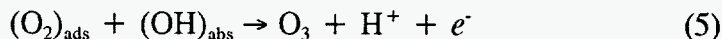
The highest efficiencies for O_3 generation reported in the literature correspond to the use of HPF_6 and HBF_4 (see Table 1). However, we did not make tests in solutions of these electrolytes because of their toxicity. Nevertheless, we are condifent that the distinct advantage of Fe(III)-doped β-PbO_2 electrodes in comparison to undoped β-PbO_2 electrodes observed here will persist for solutions of HPF_6 and HBF_4.

Acknowledgments
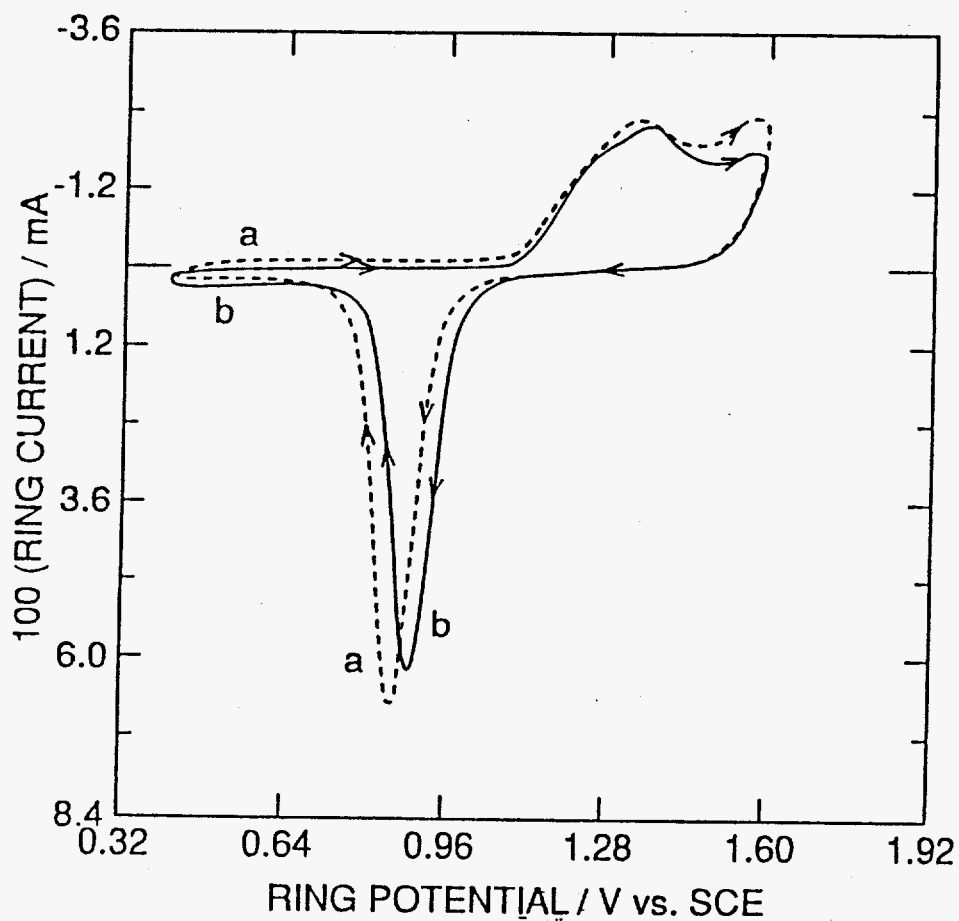
A

Fig. 1.   Voltammetric response at the ring electrode (I_{ring}-E_{ring}) of a Au-Au RRDE
in 1.0 M $HClO_4$ with galvanostatic control of the disk electrode.
Rotation speed: 4900 rev min^{-1}. Scan rate: 6.0 V min^{-1}. Disk electrode
(0.20 cm^2): (A) β-PbO_2/Au and (B) Fe-PbO_2/Au.
Disk current: (a) 0.0 mA, (b) 2.0 mA.
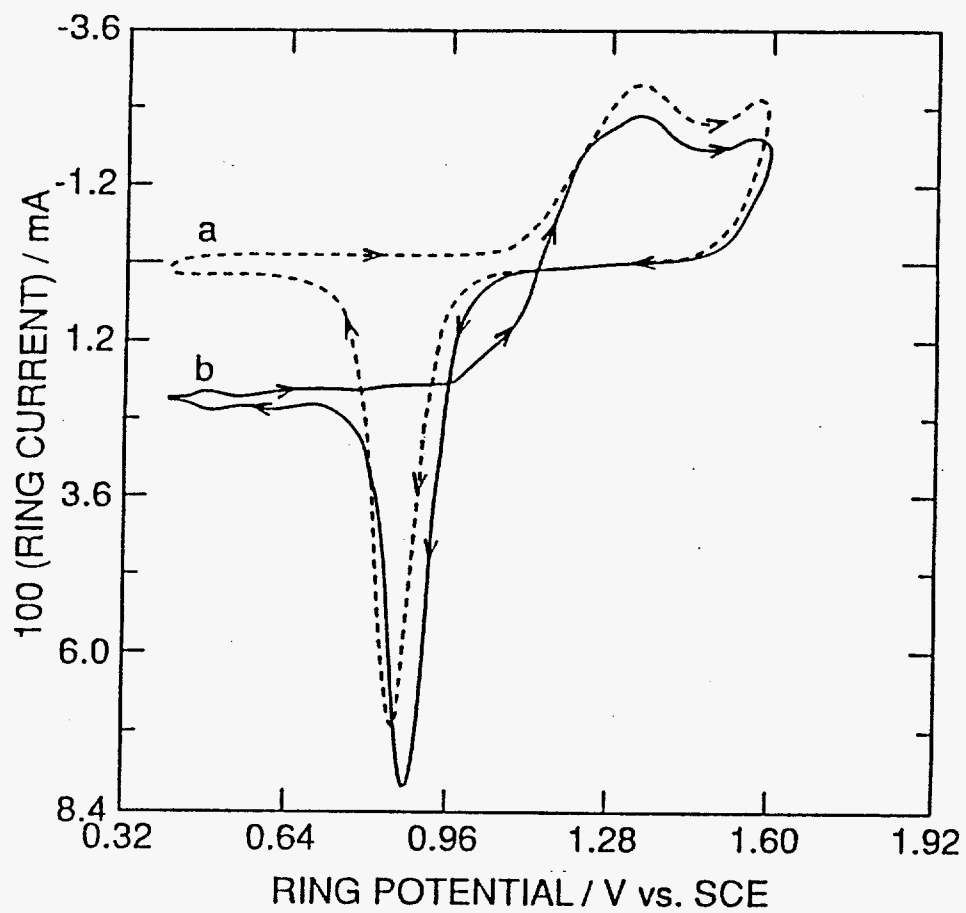
Fig. 1. (continued)
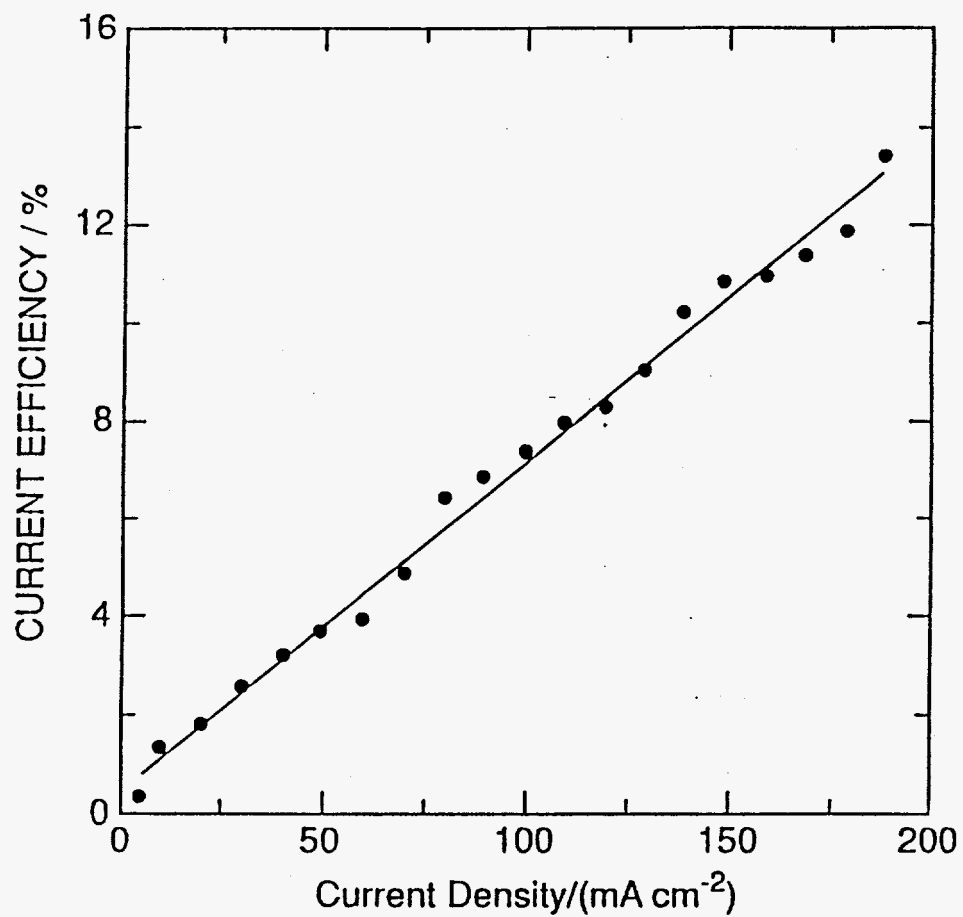
Fig. 2.   Plot of current efficiency for O_3 generation at internally-cooled (10 °C) tubular Fe-PbO$_2$/Ti electrode as a function of current density in 0.52 M K$_2$HPO$_4$/0.22 M KH$_2$PO$_4$ buffer (pH 7.5, 10 °C) containing 2.5 mM KF.
Electrode area: *ca*. 10 cm^2. Total anodic charge: 180 C.

$$H_2O \rightarrow (OH)_{ads} + H^+ + e^-$$

$$(O_2)_{ads} + (OH)_{ads} \rightarrow O_3 + H^+ + e^-$$
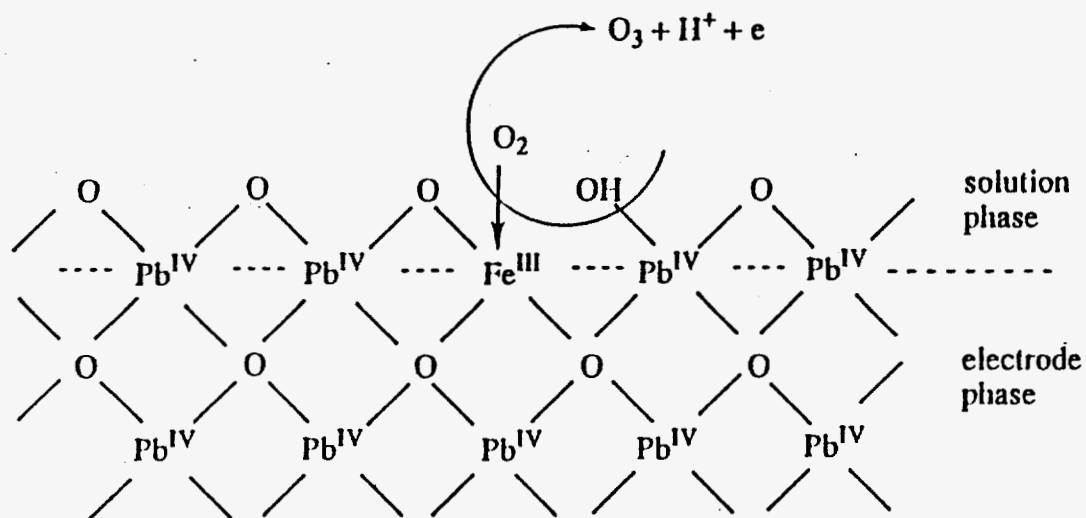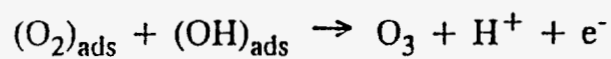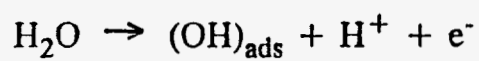
Fig. 4.   Schematic illustration of the anodic transfer of oxygen from surface-bound OH-radical to adsorbed O_2 in the proposed mechanism for anodic generation of O_3 at a Fe-PbO$_2$ electrode surface.

REFERENCES

[1]   J. D. Seader and C. W. Tobias, *Ind. Eng. Chem.*, **44**, 2207 (1952).

[2]   "Encyclopedia of Electrochemistry," C. A. Hampel, Editor, p. 878, Reinhold, New York (1964).

[3]   P. C. Foller and C. W. Tobias, *J. Electrochem. Soc.*, **129**, 506 (1982).

[4]   P.C. Foller and C. W. Tobias, *ibid.*, **129**, 567 (1982).

[5]   J. C. G. Thanos, H. P. Fritz and D. Wabner, *J. Appl. Electrochem.*, **14**, 389 (1984).

[6]   J. E. Graves, D. Pletcher, R. L. Clarke and F. C. Walsh, *J. Appl. Electrochem.*, **22**, 200 (1992)

[7]   P. C. Foller and C. W. Tobias, *J. Phys. Chem.*, **85**, 3238 (1981).

[8]   E. R. Kötz and S. Stucki, *J. Electroanal. Chem.*, **228**, 407 (1987).

[9]   P. C. Foller and M. L. Goowin, *Ozone: Science and Engineering*, **6**, 29 (1984).

[10]   P. C. Foller and G. H. Kelsall, *J. Appl. Electrochem.*, **23**, 996 (1993).

[11]   A. E. Greenberg, J. J. Connors, D. Jenkins and M. A. H. Franson, (Eds.) "Standard Methodes for the Examination of Water and Wastewaster," 15th Ed., p.399, American Public Health Association; Washington D. C. (1980)

[12]   J. Feng and D. C. Johnson, *J. Electrochem. Soc.*, **138**, 3328 (1991).

[13]   J. Feng and D. C. Johnson, *J. Appl. Electrochem.*, **20**, 116 (1990).

[14]   D. C. Johnson, D. T. Napp and S. Bruckenstein, *Anal. Chem.*, **40**, 482 (1968).

[15]   W. J. Albery and M. L. Hitchman, "Ring-Disk Electrodes," Chap. 4., Claredon Press: Oxford, (1971).

CHAPTER 5

ELECTROCHEMICAL INCINERATION OF BENZOQUINONE

J. Feng, S. N. Lowery, J. J. Carey and D. C. Johnson

ABSTRACT

The electrochemical performance of several anode materials is compared for the electrochemical incineration (ECI) of p-benzoquinone (BQ) in aqueous media. The chemical oxygen demand (COD) resulting from BQ in acetate buffered media (pH 5) can be decreased to virtually zero by electrolysis at electrodes comprised of Fe(III)-doped β-PbO_2 films on Ti substrates. The primary electrolysis product is CO_2. Addition of BQ to acetate media is followed by slow formation of a brownish black color concluded to result from the production of at least one humate compound produced by condensation of BQ; however, it cannot concluded whether the condensation reaction is a necessary prerequisite to successful ECI of BQ. Optimal operating conditions suggested for ECI include heating of the anode (*e.g.*, 60 °C) to increase the rate of anodic discharge of H_2O and, thereby, decrease the anodic overpotential. Evidence also is presented that the rate of ECI is enhanced slightly by the presence of a trace of Fe(III) with reduction of dioxygen (O_2) to hydrogen peroxide (H_2O_2) at the cooled stainless steel cathode (*e.g.*, 15 °C) in an undivided cell.

Introduction

The presence of toxic organic compounds in industrial wastewater can offer severe challenges for applications of waste treatment prior to discharge into municipal waste water facilities. Whereas thermal incineration remains the best available techique for disposal of solid toxic wastes, this technology is not practical for degradation of organic compounds dissoved or dispersed in water [1]. Furthermore, the high cost of construction and operation makes thermal incineration an impractical approach for processing small quantities of waste materials. Oxidative degradation using supercritical water has been proposed as an alternative to thermal incineration for organic compounds in wastewater [2]; however, the requirements of high temperature (450 - 500 °C), high pressure (240 - 340 atm), and pure O_2 result in a high cost for this technology.

Research in our laboratories is motivated by the goal of discovering new catalytic electrode materials and appropriate electrolysis conditions for the effective and economical anodic detoxification of organic toxins dissolved in aqueous solutions. These goals can be achieved satisfactorily by conversion of toxic compounds to nontoxic forms; however, in many instances, complete degradation to the respective elemental oxides, *e.g.*, CO_2, etc., might be preferred to achieve zero chemical oxygen demand (COD) of the processed liquids. The obvious similarities between complete electrolytic degradation of organic compounds to CO_2 and thermal incineration has resulted in reference to this electrolytic strategy as *electrochemical incineration* (ECI) [3,4]. Targets of present research activities in our laboratories includes benzene, a carcinogen, as well as various

compounds representing possible intermediate products in the anodic conversion of benzene to CO_2, including phenol and benzoquinone. Anodic oxidation of benzene and phenol to p-benzoquinone (BQ) have been studied extensively [5-9] and some CO_2 has been reported as a product of oxidation of phenol at Pt electrodes [10]. However, relatively little effort appears to have been directed to the total anodic degradation of these compounds to CO_2 [11-13], perhaps because of difficulties encountered as a result of electrode fouling by adherent films. These surface films are produced when the anodic mechanisms are unable to oxidize reactants beyond the state of simple free-radicals which then undergo polymerization on the electrode surfaces. The complete anodic degradations of benzene, phenol, and numerous other aromatic amines, which have been classified as the priority pollutants by the U.S. Environmental Protection Agency, depends upon the discovery of unique anode materials that possess high catalytic activity for the requisite anodic O-transfer mechanisms.

Previous research in this laboratory has demonstrated that electrodes comprised of Fe(III)-doped β-PbO_2 films electrodeposited on Ti substrates ("Fe-PbO_2/Ti") are quite stable in acidic media and offer significantly improved catalytic activity for some O-transfer reactions in comparison to conventional anode materials [14]. Here we describe results obtained in a comparison of Fe-PbO_2/Ti electrodes with other anodes applied for the electrochemical incineration of BQ in acetate media (pH 5).

Experimental

Reagents. - All chemicals were Analytical Reagents and were used without further purification. Water was purified by passage through ion-exchange cartridges (Culligan) and a Milli-Q purification system (Millipore Corp.)

Voltammetry. - Voltammetric and kinetic data were obtained at rotated disk electrodes (RDEs) according to standard procedures using a RDE3 potentiostat (Pine Instrument) [14,15]. Titanium disks (99.9%, Johnson Matthey) were mounted on the ends of stainless steel rods machined to appropriate dimensions for rotation in a MSR rotator (Pine). Films of PbO_2 and $Fe-PbO_2$ were electrodeposited on the Ti disk substrates according to procedures described previously [14]. Only the end-surfaces of Ti disks (*ca.* 0.20 cm^2) contacted solutions used for deposition of films and for kinetic testing. Potentials were controlled with respect to a saturated calomel electrode (SCE, Fisher Scientific) and potentials are reported in V *vs.* SCE.

Electrodes. - Preliminary data for electrolytic degradation of BQ at ambient temperatures utilized electrodes configured in the shape of small plates and wire coils (*ca.* 10 cm^2). Included were a ruthenized titanium plate ("Ru/Ti", 10 cm^2; Electrosynthesis), and a glassy carbon rod ("GC", *ca.* 10 cm^2; Sigri); and Ti plates (99.7%, Johnson Matthey) coated with pure β-PbO_2 films ("PbO_2/Ti") and Fe(III)-doped β-PbO_2 films ("Fe-PbO_2/Ti") electrodeposited according to procedures described previously [14]. Data

obtained for thermostated electrodes utilized a U-shaped Ti tubular anode (6.4-mm o.d., 4.5-mm i.d., 20-cm^2 working area; 99.7%, Sandvik) electroplated with Fe-PbO$_2$ and a U-shaped tubular 316-stainless steel cathode (6.4-mm o.d., 4.5-mm i.d., 20-cm^2 working area; Fry Steel). Thermostated water pumped through these tubular electrodes achieved internal control of electrode temperature.

Voltammetric data were obtained at disk electrodes (0.20 cm^2) rotated in a MSRX rotator with a RDE3 potentiostatic (Pine Instruments).

Electrolysis procedures. - Preliminary data using plate electrodes were obtained in undivided cells corresponding to beakers (50 or 100 mL). The U-shaped tubular electrodes were used in the undivided cell (120 mL) shown in Figure 1. This cell has a double-wall construction to permit circulation of water for controlling the temperature of the electrolysis solution. A Model 90 thermostatic circulating bath (Fisher Scientific) was used for precise temperature control. Alternatively, chilled (*ca.* 15 °C) and heated (*ca.* 60 °C) water from the building supply lines were used for approximate control of temperature.

A model 420X power supply with Model 415 controller (Electrosynthesis) was the source of constant current. All test solutions were buffered with 1.8 M NaOAc/1.0 M HOAc (pH 5).

Chemical Analysis. - The progress of ECI applied to BQ was monitored by determination of chemical oxygen demand (COD) in small aliquots of test solutions. The

standard COD methode based on titration with $K_2Cr_2O_7$ [16] was replaced by titration with $KMnO_4$ (60 °C) because the later procedure was determined not to be responsive to HOAc and NaOAc. Values of COD (mg O_2 L^{-1}) were calculated according to:

$$COD = (5/4)(32)(1000)(M_{titrant})(V_{titrant})/(V_{sample}) \qquad (1)$$

where $M_{titrant}$ (mol L^{-1}) and $V_{titrant}$ (mL) are the molarity and volume, respectively, of the $KMnO_4$ titrant consumed, and V_{sample} is the sample volume (mL).

Electrolytic production of $CO_2(g)$ was confirmed by precipitation as $CaCO_3(s)$ in a solution saturated with $Ca(OH)_2$. Carbon dioxide, purged from the test solution during electrolysis, was quantified by adsorption in standard NaOH solutions followed by back titration with standard HCl solution using a phenolphthalein-methyl red double indicator [17].

In one experiment, progress in the electrolytic degradation of BQ was monitored by liquid chromatography (LC, Waters Chromatography) using a 86-D00-D5 phenyl column (Microsorb-MV™), a mobile phase consisting of a 20:80 mixture of acetonitrile (MeCN) with 1% acetic acid (1.0 mL min^{-1}), photometric detection (240 μm), and injection volumes of 10.0 to 50.0 μL. Chromatograms were recorded on a strip-chart recorder (Beckman).

Analysis of processed solutions for trace metals was achieved by inductively coupled plasma atomic emission spectrometry using a Model 3410 ICP-AES with a Minitorch (Applied Research Laboratory).

Results and Discussion

Voltammetry. - Test solutions prepared by addition of aqueous BQ to 1.8 M

NaOAc/1.0 M HOAc buffer (pH 5) undergo a color change from light yellow to light

brown in *ca.* 10 min with a continuing increase in color intensity to brownish black over

a 10 to 12-hr period. In comparison, solutions prepared by addition of aqueous BQ to 1.8

M HOAc required nearly 2 hr to reach the light brown color. This color transition from

yellow to brownish black is tentatively concluded to correspond to condensation of BQ to

one or more humic products such as represented below [18].
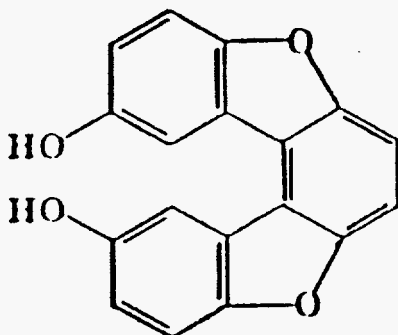
Voltammetric (*i-E*) data shown in Figure 2 are consistent with the conclusion

above. These data correspond to the *i-E* response obtained for a positive potential scan at

a Pt RDE at the designated time intervals following addition of aqueous BQ to the acetate

buffer. The cathodic wave ($E < ca.$ 0.0 V) corresponds to reduction of BQ to the

corresponding hydroquinone (H_2BQ), as indicated by:

$$BQ + 2H^+ + 2e^- \rightarrow H_2BQ \qquad (2)$$

The decrease in limiting cathodic current at *ca.* -0.30 V *vs.* SCE was observed to be correlated with the transition in solution color from light yellow to brownish black. The anodic wave (E > *ca.* 0.1 V) in Figure 2 developed concomitantly with the decrease in cathodic limiting current and the development of the brownish black color. Hence, this anodic wave is speculated to correspond to oxidation of the phenolic groups of the condensation product shown above. The anodic *i-E* response reached a constant value within a 24-hr period (data not shown) corresponding to the total loss of cathodic response for BQ.

The anodic *i-E* response (pos. scan) is shown in Figure 3 for the brownish black condensation product of BQ in the acetate buffer obtained at a $Fe-PbO_2/Ti$ rotated disk electrode (RDE) as a function of rotational velocity. The value of n_{eff} estimated from the slope of the Koutecky-Levich plot (i^{-1} *vs.* $\omega^{-1/2}$) [19] shown in Figure 4 is 2.0 ± 0.2 eq mol^{-1}, calculated for 2.0 mM BQ using the estimates $D = 1 \times 10^{-5}$ cm^2 s^{-1} and $\nu = 0.010$ cm^2 s^{-1}. Hence, it is apparent from this value of n_{eff} that the corresponding anodic process is not sufficient for complete oxidative degradation of the condensation product of BQ in the potential region *ca.* 1.0 to 1.3 V. It is anticipated that oxidation to CO_2 is most likely to accompany rapid generation of adsorbed hydroxyl radicals (OH_{ads}) with simultaneous evolution of O_2 (*i.e.*, E > 1.3 V). Hence, all succeedingly electrolyses of BQ solutions were performed under galvanostatic conditions with a resulting anode potential > 1.4 V.

Preliminary comparison of anode materials. - Various electrode materials configured as small plates (*ca.* 10 cm^2) were compared for their effectiveness in the

anodic degradation of BQ in undivided cells at ambient temperatures under galvanostatic conditions. The results are summarized in Table 1 as values of COD determined by titration with $KMnO_4$ for the product solutions following the specified electrolysis periods. Electrolysis at the glassy carbon (GC) electrode was discontinued after a 10-hr periods because the observation of carbon particles in the test solution indicated severe deterioration of this electrode material under the applied current density (10 mA cm^{-2}). The smalllest COD (7.5 mg O_2 L^{-1}) corresponding to the shortest electrolysis period (10 hr) was obtained for the Fe-PbO_2/Ti electrode. This result is better than the results for the PbO_2/Ti electrode (12 mg O_2 L^{-1}, 24 hr) and the Ru/Ti electrode (28 mg O_2 L^{-1}, 48 hr).

Also included in Table 1 are values of the average current efficiency (CE) calculated for the degradation of BQ to CO_2 (n_{tol} = 24 eq mol^{-1}) according to [10]:

$$CE(\%) = \frac{(COD_{start} - COD_{final})FV100}{8IT_{elect}} \qquad (3)$$

where COD_{start} and COD_{final} are the starting and final values of COD (g O_2 L^{-1}), respectively. F is the faraday constant (96487 C eq^{-1}), V is the volume of test solution (L), I is the constant anodic current (coul s^{-1}), and T is the electrolysis period (s). Based on these CE values, it is apparent that the activity of the Fe-PbO_2/Ti electrode is superior to the other electrodes tested.

Table 1.   Chemical oxygen demand (COD) of 50-mL test solutions of 10 mM p-

benzoquinone in 1.8 M NaOAc/1 M HOAc (pH 5) following electrolysis at

constant current.

Electrode	Current[a] (mA)	Time (hr)	COD[b] (mg/L)	CE[c] (%)	Product solution
None	0	0	1071	n.a.	Dark brownish black color
Au-wire	100	48	582	1.7	Deep yellow color
GC[d]	100	10	-		Presence of carbon particals
Ru/Ti	100	48	28	3.6	Yellow color
PbO$_2$/Ti	100	24	12	7.4	Colorless
Fe-PbO$_2$/Ti	100	10	7.5	23.5	Colorless

[a]   Electrode areas: $ca.$ 10 cm^2. Current density: $ca.$ 10 mA Cm^{-2}.

[b]   COD determined by titration with KMnO$_4$.

[c]   Calculated current efficiency.

[d]   Glassy carbon.

Electrolysis yields. - Determination of COD by titration with $KMnO_4$ confirmed the completenesss of anodic degradations of BQ at $Fe-PbO_2/Ti$ electrodes. Furthermore, production of $CO_2(g)$ during electrolysis was confirmed on the basis of precipitation of $CaCO_3(s)$ in a solution of $Ca(OH)_2$. Attempts to quantify CO_2 yields by adsorption into standard NaOH solutions, followed by titration with standard HCl, consistently gave values in excess of 100%. Undoubtedly, this occurred because of some anodic degradation of OAc^- and/or HOAc to CO_2. Hence, direct determination of CO_2 produced by anodic degradation of BQ was not possible in this study.

Degradation of BQ during electrolysis at a $Fe-PbO_2/Ti$ plate electrode (*ca.* 10 cm^2) at ambient temperature in a 50-mL undivided cell mas monitored using LC. Shown in Figure 5 is a typical plot of peak height for the single chromatographic peak obtained for the brownish black solution during galvanostatic electrolysis. Under these operating conditions, the peak height decreased to 50% of its initial value at *ca.* 2 hr. and to 0.5% of its initial value at *ca.* 14 hr.

Elevation of anodic temperature. - The anodic discharge of H_2O to produce adsorbed hydroxyl radicals (OH_{ads}) is believed to be an requisite step in anodic oxygen-transfer mechanisms to be utilized as the basis of ECI [20-23]. Hence, large anodic overpotentials can be anticipated for galvanostatic operations at high current densities. Therefore, consideration was given to the possible benefit from operating the $Fe-PbO_2/Ti$ anodes at elevated temperature sensitivity for anodic discharge of H_2O at a $Fe-PbO_2/Ti$ RDE is illustrated by data in Figure 6 plotted according to the Tafel equation:

$$\log\{i\} = \log\{i_o\} + (\alpha_a nF/2.3RT)\eta \qquad (4)$$

where i_o is the exchange current ($\mu C\ s^{-1}$), α_a is the anodic transfer coefficient (eq mol^{-1}), and η is the applied overpotential (V) defined by:

$$\eta = E - E^{o'} = E - 0.961 - 0.059pH \qquad (5)$$

for production of O_2 (n = 4 eq mol^{-1}). These data were taken from i-E curves recorded at the Fe-PbO$_2$/Ti RDE using a very slow positive scan (+9 mV s^{-1}) so that double-layer charging currents could be ignored. Values of exchange current density (i_o/A, $\mu A\ cm^{-2}$) obtained by linear regression analysis of the Tafel plots in Figure 6 are given in Table 2.

Table 2.   Values of exchange current density (i_o/A) and anodic transfer coefficient (α_a) from Tafel plots for anodic discharge of H_2O at a Fe-PbO$_2$/Ti in 1.8 M NaOAc/1.0 M HOAc as a function of temperature.

Temperature (°C)	i_o/A ($\mu A\ cm^{-2}$)[a]	α_a (eq mol^{-1})[a]
0	$(7.1 \pm 0.4) \times 10^{-3}$	0.057 ± 0.001
25	$(1.6 \pm 0.1) \times 10^{-2}$	0.059 ± 0.001
40	$(1.7 \pm 0.1) \times 10^{-2}$	0.064 ± 0.001
60	$(2.2 \pm 0.1) \times 10^{-2}$	0.067 ± 0.001

[a]   Uncertainty corresponds to standard deviation.

Clearly, based on these results, an increase in temperature results in a substantial increase in i_o/A for anodic discharge of H_2O at a fixed value of η. Hence under galvanostatic conditions where the applied current density might be in great excess of the faradaic current density for oxidation of the BQ, the overpotential corresponding primarily to anodic evolution of O_2 can be decreased substantially as a benefit of elevated electrode temperature.

The effectiveness of using elevated temperatures on the rate of BQ degradation is illustrated clearly in Figure 7. Shown are values of COD determined for 120-mL samples of 10.0 mM BQ (COD_{start} = 1072 mg L^{-1}) following passage of a constant anodic current (100 mA) for a period of 180 min (*i.e.*, 1080 C) at a $Fe-PbO_2/Ti$ plate electrode (*ca.* 10 cm^2) as a function of solution temperature in the range 20 to 80 °C. As shown, COD is decreased to *ca.* 100 mg L^{-1} after 180 min for a solution temperature of 80 °C as compared to 860 mg L^{-1} after the same time period for 26 °C.

Oxidative degradation of BQ at a stainless steel cathode. - Consideration was given to the possible contribution to oxidative degradation of BQ resulting from generation of H_2O_2 at the cathode by reduction of dissolved O_2 with the presence of Fe(III) catalyst. It is well known that many organic compounds can be oxidized by H_2O_2 in presence of Fe(III), *i.e.*, Fenton's reagent [24-26]. Initial attention was directed to the temperature dependence for cathodic production of H_2O_2. In this study, the limiting anodic current for H_2O_2 in the cathode compartment of a divided cell open to the room atmosphere was determined voltammetrically on the basis of the anodic wave for H_2O_2

obtained at the Pt RDE. The temperature of the tubular 316-SS cathode was controlled by passage of thermostated water through the interior of the tubular electrode. For galvanostatic control of cell current (100 mA) over a 10-min period at *ca.* 0 °C, the limiting current for H_2O_2 was $> 100X$ larger than that resulting from electrolysis at 50 °C for the same time period.

The benefit of using a suppressed cathode temperature (*ca.* 15 °C) in the presence of 2.5 μM $Fe_2(SO_4)_3$ is made apparent by data in Figure 8. The temperature of the tubular anode was not controlled in this comparison. Differences in the rates of degradation with (Curve b) and without (Curve a) the presence of $Fe_2(SO_4)_3$ are apparent in the early stages of the electrolysis (< 0.5 hr). However, the total charge required to achieve $COD_{final} = 0$ mg L^{-1} in this test was decreased by $< 5\%$ when $Fe_2(SO_4)_3$ was present.

Stability of Fe-PbO$_2$/Ti anode. - There is significant concern for the stability of anodes when operated at high current densities. Shown in Table 3 is a comparison of the ruthenium and lead found in separate 100-mL test solutions following 30-hr electrolyses using a Ru/Ti plate anode and a Fe-PbO$_2$/Ti plate anode. These solutions initially contained 10 mM BQ in the acetate buffer. Clearly, the data in Table 3 indicate dissolution of surface oxides from both the Ru/Ti and Fe-PbO$_2$/Ti anodes under these conditions. The instability indicated for the Fe-PbO$_2$/Ti anode is considered to be unacceptable in view of the toxicity of Pb(II).

Table 3.   Current efficiency and metal ion content of product solution for

galvanostatic electrolyses[a] at Ru/Ti and Fe-PbO$_2$/Ti anodes in 100-mL of

1.8 M NaOAc/1.0 M HOAc buffer (pH 5) containing 10 mM BQ.

Electrode	Ru/Ti plate[b]	Fe-PbO$_2$/Ti plate[b]
COD[c] of the solution before electrochemical incineration (mg/L)	1087	1087
COD of the solution after electrochemical incineration (mg/L)	735	0
Current efficiency[d] (%)	5.3	16.4
Metal content in final test solution (ppm)[e]	Ru = 0.7 ± 0.1	Pb = 1.5 ± 0.2

[a]   Anodic current: 200 mA. Electrolysis period: 40 hr.

[b]   Electrode area: *ca.* 20 cm^2.

[c]   Determined by titration with KMnO$_4$.

[d]   Calculated according to Eqn. 5.

[e]   Determined by ICP-AES after 40-hr electrolysis period.

Conclusions

The electrochemical degradation of *p*-benzoquinone (BQ) in acetate buffered media (pH 5) occurs at a significantly faster rate at Fe-PbO$_2$/Ti anodes as compared to Au, GC, Ru/Ti and PbO$_2$/Ti anodes. A change in color for BQ from light yellow to brownish black in acetate media is concluded to result from condensation of BQ to form a humic material. However, it cannot be concluded whether formation of the condensation product is a prerequisite to successful anodic degradation of BQ at the Fe-PbO$_2$/Ti anodes.

A significant increase in the rate of anodic degradation of BQ is observed as a result of elevation of the temperature of Fe-PbO$_2$/Ti anodes under galvanostatic control. This corresponds to an advantageous increase in the current efficiency for the corresponding degradation reaction which has significance for improved economic efficiency in possible commercial applications of electrochemical incineration. Also of economic significance is the concomitant decrease in anodic overpotential resulting from increased anode temperature.

Preliminary data indicate a small benefit in the overall rate of degradation of BQ as a result of the generation of H$_2$O$_2$ by reduction of O$_2$ at the chilled stainless steel cathode with the presence of Fe(III). This effect is concluded to correspond to a so-called *Fenton's* reaction in which oxidation of BQ, and/or its various intermediate oxidation products, by H$_2$O$_2$ is mediated by Fe(III). The benefit of this mediated reaction deserves more attention.

Some deterioration of Fe-PbO$_2$/Ti is observed to occur during electrolyses even at

moderation current density (*e.g.* 10 mA cm^{-2}). The stability of Fe-PbO$_2$/Ti electrodes must be improved before possible commercial application of this anode material can be considered seriously.
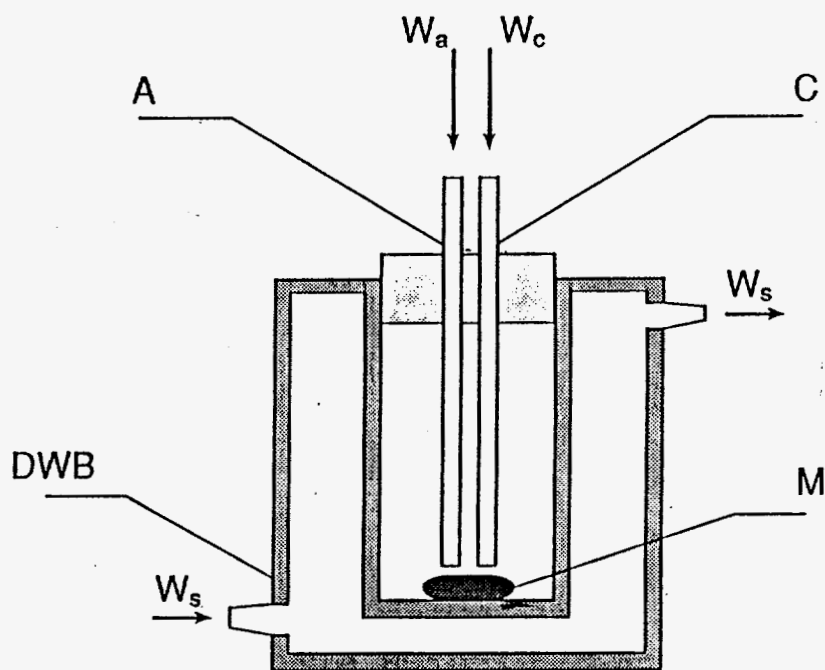
Acknowledgment

Fig. 1.   An undivided two electrodes cell used in constant current electrolysis.
(A) - Edge-view of U-shaped, tubular, Fe-PbO$_2$/Ti anode.
(C) - Edge-view of U-shaped, tubular, 316-stainless steel cathode.
(M) - Magnetic stirring bar.
(W$_a$) - Heated water pumped through the anode (*e.g.*, *ca.* 60 °C).
(W$_c$) - Chilled water pumped through the cathode (*e.g.*, *ca.* 15 °C).
(W$_s$) - Chilled water pumped through the double-wall compartment of
            DWB for control of solution temperature (*ca.* 15 °C).
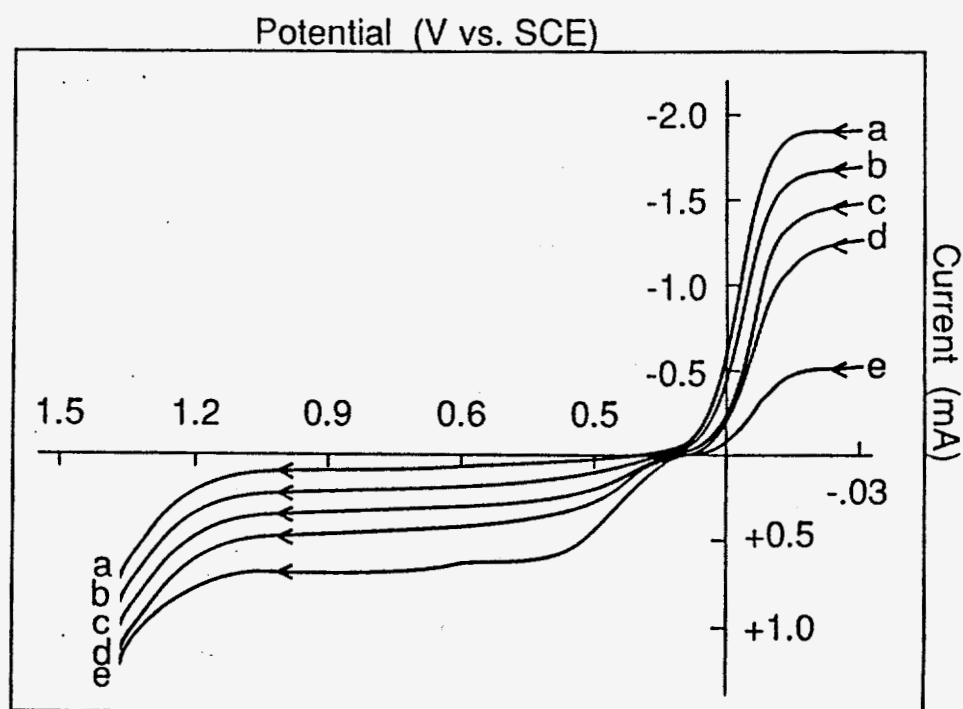(DWB) - Doubl-wall beaker.

Fig. 2.   Voltammetric response (pos. scan) for 10.0 mM BQ at a Pt RDE
(0.20 cm²) in 1.8 M NaOAc/1.0 M HOAc.
Rotation: 168 rad s⁻¹. Scan rate: 6.0 V min⁻¹.
Time (hr): (a) 0, (b) 1, (c) 2, (d) 3, (e) 7.
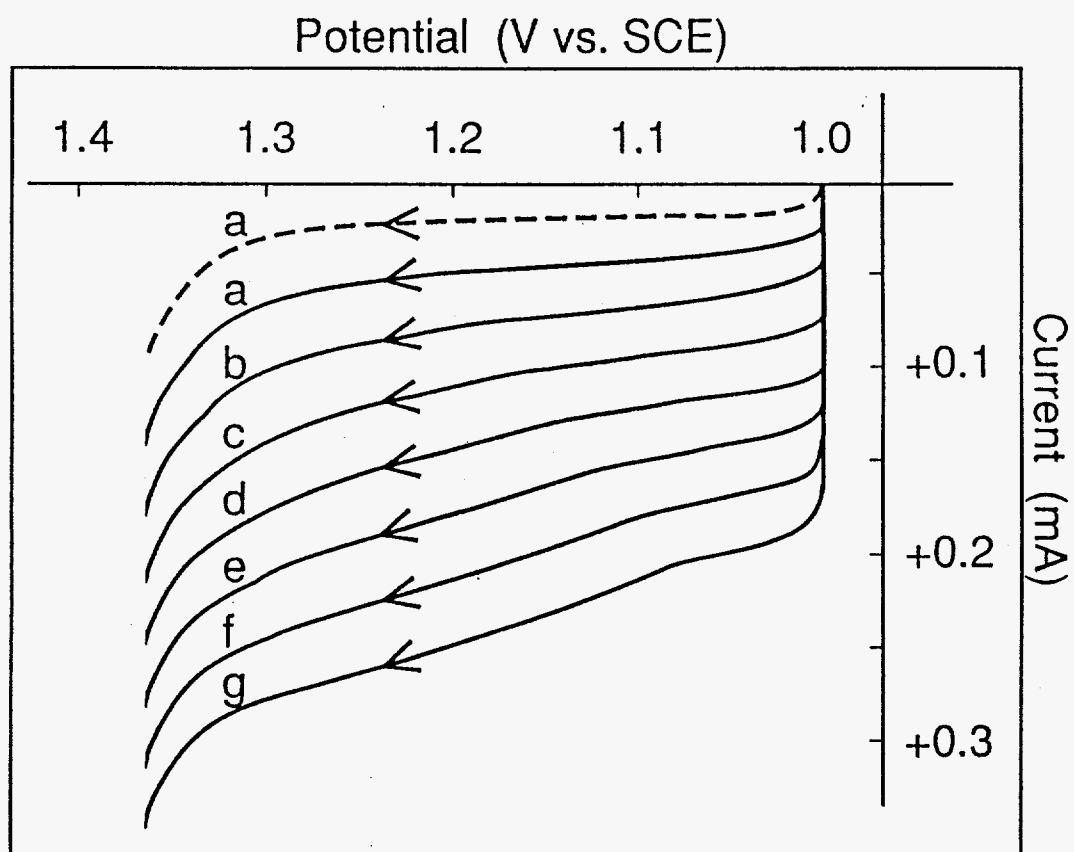
Fig. 3.   Voltammetric response (pos. scan) for brownish black condensation
            product(s) of 2.0 mM BQ at a Fe-PbO$_2$/Ti RDE in 1.8 M NaOAc/1 M
            HOAc.
            Scan rate: 1.8 V min^{-1}. Rotation (rad s^{-1}): (a) 10.5, (b) 41.9, (c) 94.2
            (d) 168, (e) 377, (g) 513. Curves: (···) - residual, (—) - condensation
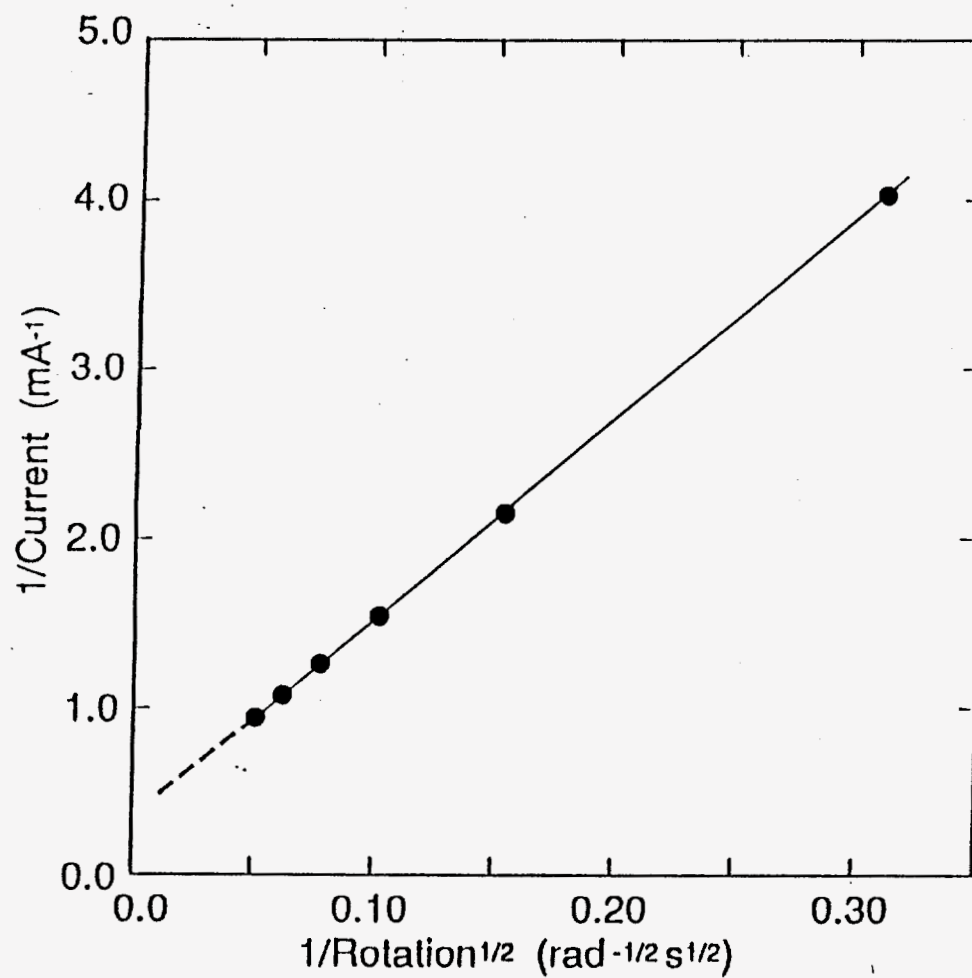   product(s).

Fig. 4.   Koutecky-Levich plots for limiting anodic current observed for
             condensation product(s) at a Fe-PbO$_2$/Ti RDE (0.20 cm^2).
             Test conditions: 10.0 mM BQ in 1.8 M NaOAc/1.0 M HOAc.
             Potential: 1.2 V *vs*. SCE.
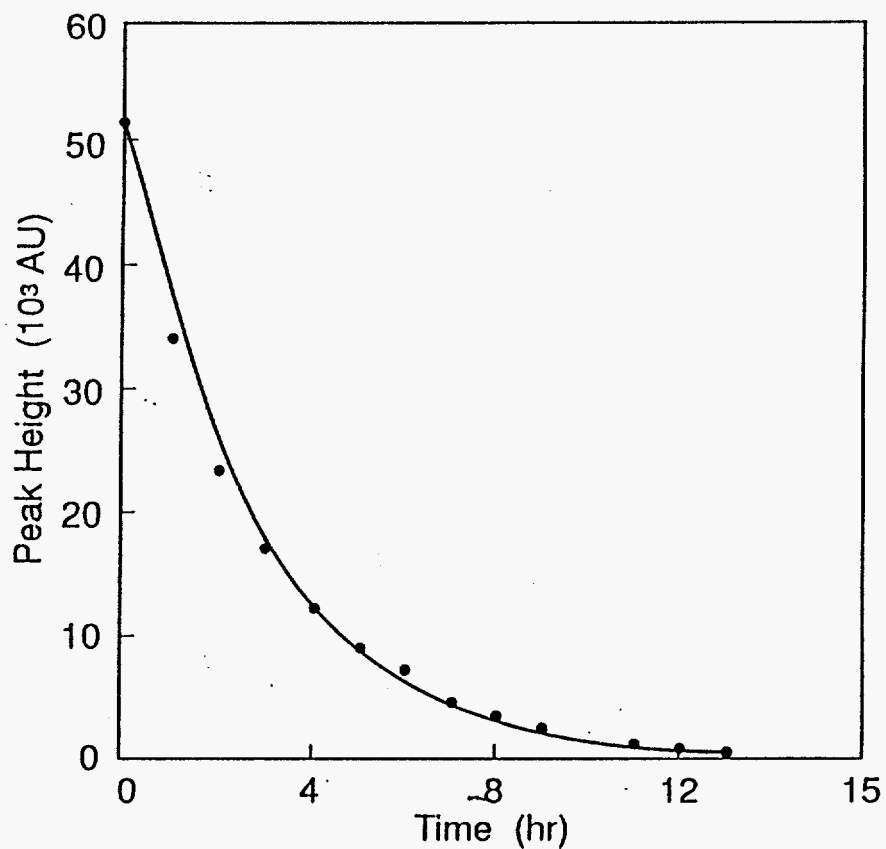
Fig. 5.   Plot of chromatogrphic peak height corresponding to condensation product from BQ as a function of electrolysis time at a Fe-PbO$_2$/Ti plate electrode in 1.8 M NaOAc/1.0 M HOAc containing 10.0 mM BQ.
Electrode area: *ca.* 10 cm^2. Anodic current: 100 mA. Solution temperature: 25 °C.
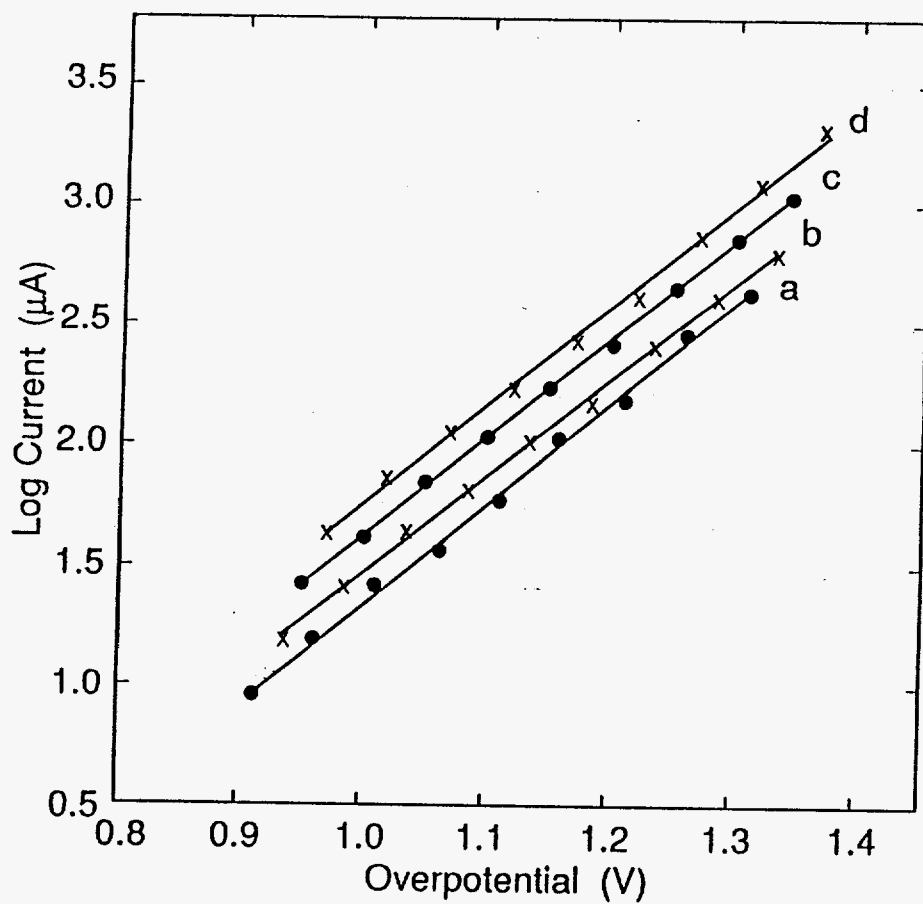
Fig. 6.   Tafel plots for anodic evolution of O_2 during the positive scan at a Fe-
PbO$_2$/Ti RDE as a function of solution temperature.
Rotation speed: 1600 rev min^{-1}. Scan rate: +9.0 mV s^{-1}.
Temperature (°C): (a) 0, (b) 25, (c) 40, (d) 60.
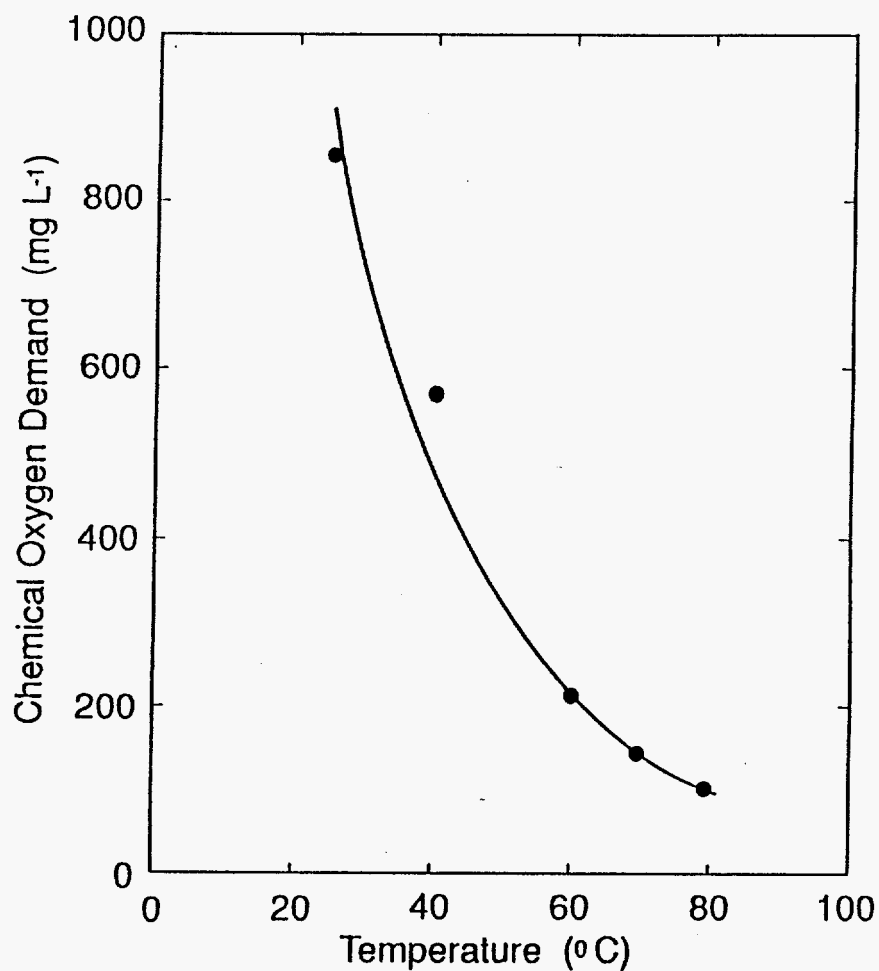
Fig. 7.   Temperature dependence of COD measured following passage of 1080 C
            (*i.e.*, 100 mA for 180 min) in the galvanostatic electrolysis of 10.0 mM
            BQ in 1.8 M NaOAc/1.0 M HOAc (pH 5) using an Fe-PbO$_2$/Ti tubular
            anode (10 cm^2) and a 316-stainless steel tubular cathode (10 cm^2) in an
            undivided cell (120 mL).
            Temperatures (°C): $T_{sol'n}$ = variable, T_{anode} = ambient, $T_{cathode}$ =
            ambient.

Fig. 8.   Effect of the presence of $Fe_2(SO_4)_3$ on the plot of COD *vs.* coulombic
charge during galvanostatic electrolysis (2.0 A) of 10 mM BQ in 1.8 M
NaOAc/1.0 M HOAc (pH 5) using a $Fe-PbO_2$/Ti plate anode and a 316-
stainless steel tubular cathode in an undivided cell (120 mL).
Temperatures (°C): $T_{sol'n}$ = ambient, $T_{cathode}$ = *ca.* 15.
Conc. of $Fe_2(SO_4)_3$ (μM): (a) 0, (b) 2.5.

REFERENCES

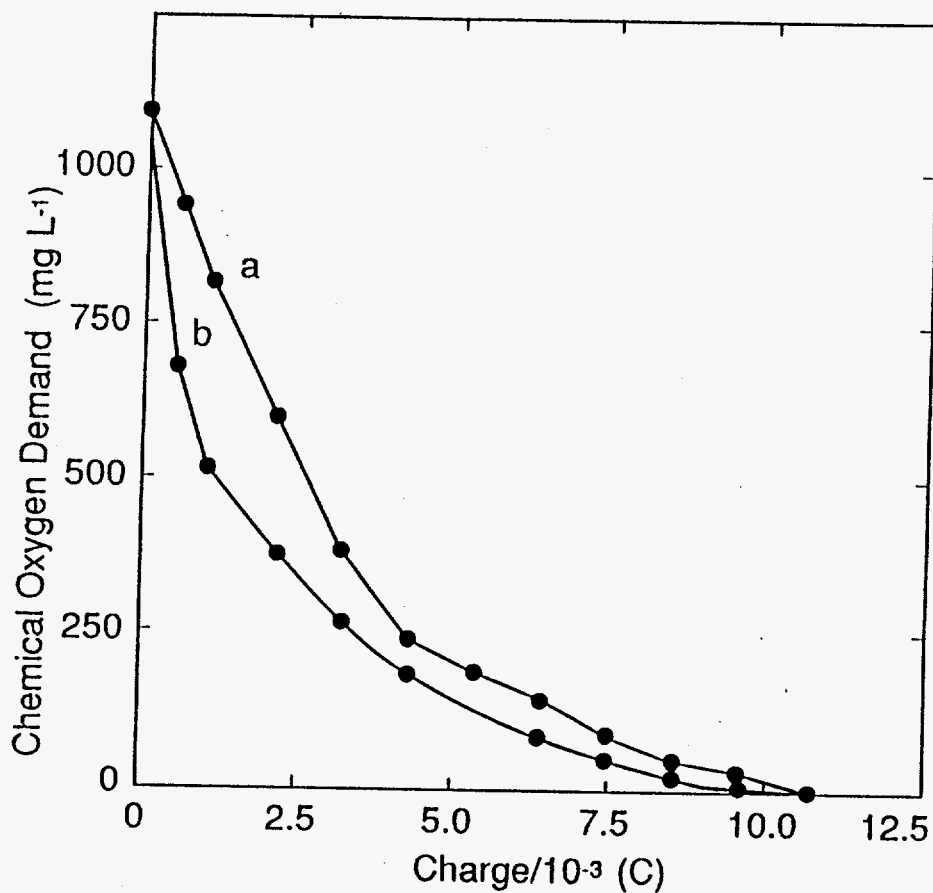[1]   "Incineration," W. J. Myers *et al.* (Eds), pp. 48 -116, Water Pollution Control Federation: Alexandria, VA (1988).

[2]   "Supercritical Water Oxidation Model Development for Selected EPA Priority Pollutants," E. F. Gloyna and L. Li, p. 7, Center for Research in Water Resources: Austin, TX (1993).

[3]   L. Kaba, G. D. Hitchens and J. O'M. Bockris, *J. Electrochem. Soc.*, **137**, 1341 (1990).

[4]   D. C. Johnson, H. Chang, J. Feng and W. Wang, in J. D. Genders and N. L. Weinberg (Eds), "Electrochemistry for a Cleaner Environment," The Electrosynthesis Company Inc.: East Amherst, NY (1992).

[5]   J. S. Clarke, R. E. Ehigamusoe and A. T. Kuhn, *J. Electroanal. Chem.*, **70**, 333 (1976).

[6]   C. Oloman, in "Tutorial Lectures in Electrochemical Engineering and Technology," R. Alkire and T. Beck (Eds.), American Institute of Chemical Engineers: New York, NY (1981).

[7]   A. J. Bard, W. M. Flarsheim and K. P. Johnson, *J. Electrochem. Soc.*, **138**, 1939 (1988).

[8]   M. Gattrell and D. W. Kirk, *Can. J. Chem. Eng.*, **68**, 997 (1990).

[9]   B. Fleszar and J. Ploszynska, *Electrochem. Acta*, **30**, 31 (1985).

[10]   Ch. Comninellis and C. Pulgarin, *J. Appl. Electrochem.*, **23**, 108 (1993).

[11]   V. S. De Sucre and A. P. Watkinson, *Can. J. Chem. Eng.*, **59**, 52 (1981).

[12]   R. Kötz, S. Stucki and B. Carcer, *J. Appl. Electrochem.*, **15**, 285 (1985).

[13]   D. W. Kirk, H. Sharifian and F. R. Foulkes, *J. Appl. Electrochem.*, **15**, 285 (1985).

[14]   J. Feng and D. C. Johnson, *J. Electrochem. Soc.*, **138**, 3328 (1991).

[15]   J. Feng and D. C. Johnson, *J. Electrochem. Soc.*, **137**, 507 (1990).

[16]   "Water Analysis Handbook," p. 461, Hach Co.: Loveland, CO (1989).

[17]   "Laboratory Manual for the Course in Quantitative Analysis," H. Diehl *et al.*, p. 6-1, Oakland Street Science Press: Ames, IA (1985).

[18]   "Advanced Organic Chemistry," L. F. Feiser and M. Fieser, p. 846, Reinhold Publishing Co.: New York, NY (1961).

[19]   J. Koutecky and V. G. Levich, *Dokl. Akad. Nauk. SSSR*, **117**, 441 (1957); *Zh. Fiz. Khim.*, **32**, 1565 (1958).

[20]   I.-H. Yeo and D. C. Johnson, *J. Electrochem. Soc.*, **134**, 1973 (1987).

[21]   I.-H. Yeo, S. Kim, R. A. Jacobson and D. C. Johnson, *ibid.*, **136**, 1398 (1989).

[22]   H. Chang and D. C. Johnson, *ibid.*, **137**, 2452 (1990).

[23]   W. R. LaCourse, Y.-L. Hsiao, D. C. Johnson and W. H. Weber, *ibid.*, **136**, 3714 (1984).

[24]   T. Tzedakis, A. Sovall and M. J. Clifton, *J. Appl. Electrochem.*, **19**, 911 (1989).

[25]   N. Al-Hayex and M. Dore, *Env. Tech. Lett.*, **6**, 37 (1985).

[26]   E. E. Kalu and C. Oloman, *J. Appl. Electrochem.*, **20**, 932 (1990).

CHAPTER 6

GENERAL CONCLUSIONS

The consequential discoveries related to my research are recapitulated as follows:

1) The Fe(III)-PbO$_2$ electrodes has good activity for many anodic O-transfer reactions. Some of these reactions, *e.g.*, degradation of cyanide, electroincineration of benzoquinone and anodic evolution of ozone, are of great significance in environmental chemistry.

2) The oxygen stoichiometry for Fe(III) oxides is smaller than for Pb(IV) oxide (FeO$_{1.5}$ *vs.* PbO$_2$). And therefore, substitution of Fe(III) for Pb(IV) in the PbO$_2$ surface results in creation of defects in the PbO$_2$ lattice. It is concluded tentatively that Fe(III) can offer unfilled p- and/or d- orbitals which function for adsorption of ·OH and the reactants such as CN$^-$, oxygen, EDTA, etc., thus promoting the anodic O-transfer reactions relevant to these species.

3) Catalytic Fe-PbO$_2$ film electrodes have been sucessfully electrodeposited on less expensive Ti substrates with the presence of an physically stable interlayer of F-PbO$_2$. The significant advantage of greater adhesion for electrodeposited film on Ti, as compared to Au and Pt, is a sufficient reason to substitute Ti for the noble metals in large scale electrolytic processes.

4) The chemical oxygen demand from the presence of BQ and/or its condensation product(s) can be decreased effectively to zero by anodic degradation at Fe-PbO$_2$ film

electrodes. Current efficiency for electrochemical incineration of BQ can be increase vigorously by thermostatic control of anodes at elevated temperatures. It is speculated that this is a direct benefit of the decrease in anode potential resulting from increased rates of the anodic discharge for H_2O at elevated temperature.

106

REFERENCES

[1]   D. C. Johnson, H. Chang, J. Feng and W. Wang, in "Electrochemistry for a Cleaner Environment," J. D. Genders and N. L. Weinberg (Editors), pp.331-345. The Electrosynthesis Company Inc., East Amherst (1992).

[2]   I-Y. Yeo and D. C. Johnson, *ibid.*, **134**, 1973 (1987).

[3]   H. Chang and D. C. Johnsn, *J. Electrochem. Soc.*, **136**, 17 (1989).

        137, 3071 (1990)

[4]   W. R. LaCourse, Y-L. Hsiao, D. C. Johnson and W. H. Weber, *J. Electrochem. Soc.*, **136**, 3714 (1989).

[5]   I-H. Yeo, S. Kim, R. Jacobson and D. C. Johnson, *ibid.*, **136**, 1398 (1989).

[6]   H. Chang and D. C. Johnson, *ibid.*, **137**, 2852 (1990).

[7]   L. A. Larew, J. S. Gordon, Y-L. Hsiao, D. A. Buttry and D. C. Johnson, *ibid.*,

[8]   Y-L. Hsiao and D. C. Johnson, *J. Electrochem. Soc.*, **136**, 3704 (1989).

[9]   J. Feng and D. C. Johnson, *J. Appl. Electrochem.*, **20**, 116 (1990).

[10]   J. Feng and D. C. Johnson, *J. Electrochem. Soc.*, **137**, 507 (1990).

[11]   J. E. Vitt, L. A. Larew and D. C. Johnson, *Electroanalysis*, **2**, 21 (1990).

[12]   J. Feng and D. C. Johnson, *J. Electrochem. Soc.*, **138**, 3328 (1991).

[13]   A. Damjanovic and B. Jovanovic, *ibid.*, **123**, 374 (1976).

[14]   B. Wels and D. C. Johnson, *J. Electrochem. Soc.*, **137**, 2785 (1990).

APPENDIX

ELECTROCATALYSIS OF ANODIC OXYGEN-TRANSFER REACTIONS:

α-LEAD DIOXIDE ELECTRODEPOSITED ON STAINLESS STEEL SUBSTRATES

J. Feng and D. C. Johnson[2]

ABSTRACT

Dense and uniform films of α-PbO_2 were electrodeposited on the surfaces of various types of stainless steel. In strongly alkaline media, these films were found to be very stable and exhibited significant electrocatalytic activity for the oxidation of Cr(III) and CN$^-$. In acidic media, α-PbO_2 films deposited on type-416 stainless steel, which had been passivated by anodization in a phosphate solution, were relatively stable and exhibited catalytic activity for oxidation of Mn(II). Rate constants for the anodic oxygen-transfer reactions of Cr(III), CN$^-$ and Mn(II) were estimated from data obtained at rotated disk electrodes.

---

[2] Author for correspondence.

Introduction

Electrolytically deposited PbO_2 can exist in two polymorphic forms. The β-form, deposited from acidic solutions of Pb(II), has a slightly distorted rutile structure. The α-form, deposited from neutral and slightly alkaline solutions, has the columbite form [1,2]. Deposition of α-PbO_2 from 2 M NaOH saturated with PbO(s) has also been described [3].

Electrodes consisting of films of both α-PbO_2 formed by electrodeposition on inert substrates have been applied successfully for numerous anodic electrosynthetic reactions [2,4]. Noble metal substrates, while receiving much attention in the laboratory, are too expensive to be practical as substrates for PbO_2-film electrodes of large area intended for industrial applications. Alternately, more economical materials receiving attention have included Pb, Pb alloys, graphite, Ti, and plastics [5-10]. Matantsev [11] tested Ni, Al, Cr, Fe, Armoiron[R], ferrosilicon, and stainless steel, and concluded that these materials are not appropriate as substrates.

Research to improve the performance of lead-acid batteries has considered the effects of metal impurities (for example, Ag, As, Co, Mn, Ni, Se, Sn, Te, V and Ti) on structure, oxygen stoichiometry, crystal morphology and self-discharge rates [12]. Recently, films of Bi-doped β-PbO_2 electrodeposited on Au and Pt rotated disk electrodes (RDEs) were demonstrated to have increased electrocatalytic activity for several anodic oxygen-transfer reactions, as compared to pure β-PbO_2 films on the same substrates [13]. We also have preliminary data indicating that PbO_2 films doped with Fe(III) exhibit a

moderately increased activity for oxidation of several compounds [14].

Research summarised here was based on the premise that iron and/or stainless steel (SS) can be useful as inexpensive substrates for pure and modified PbO_2-film electrodes. The manufacture of passive "iron black" films (Fe_3O_4), and phosphate-containing films on Fe and Fe-alloys, has become a mature technology [15] and these coatings can protect the substrates during exposure to highly corrosive conditions. It is well known, for example, that iron tanks are used successfully for storage and shipment of concentrated nitric and sulphuric acids. The corrosion resistance of stainless steels (SS) is provided by very thin surface films of passive oxides which are self-healing in a wide variety of corrosive environments. It has been reported [15] that SS can be highly resistant to 50% boiling caustic soda and some austenitic steels can withstand strong acid. Furthermore, PbO_2 films might offer additional protection to SS substrates because of their stability in stronly acidic and alkaline media. These facts inspired us to test various passivated SS substrates for use in the preparation of PbO_2-film anodes.

Passive oxide films can be formed at the surfaces of Fe and Fe-alloys. Furthermore, passive phosphate-containing films can be formed anodically in phosphate media. Beneficial modification of the electrodeposited films was expected to result from incorporation of one or more of the components of the stainless steels into the deposited PbO_2 films (*i.e.*, Fe) > Two basic questions pervaded this research: (i) Can PbO_2 films on stainless steel substrates function satisfactorily at large positive values of applied potential in various aqueous media? (ii) Do these electrodes exhibit improved catalytic activity for O-transfer reactions in comparison with pure PbO_2 films on noble metal

substrates?

Experimental

Reagents. - All chemicals were AR Grade from Fisher Scientific, Alfa Products, or Aldrich Chemicals. Water was purified in a NANOpure II system (SYBRON/Barnstead). Supporting electrolytes were 1.0 M $HClO_4$, 0.50 M H_2SO_4, 0.014 M $NaHCO_3$/0.011 M Na_2CO_3 (pH 10.0), 0.30 M HOAc/0.50 M NaOAc (pH 5.0) and 2.0 M NaOH. Anodic passivation of SS surfaces was performed in 1 M Na_3PO_4/4 M H_3PO_4 (pH 0.7). Other reagents included $Cr(NO_3)_3 \cdot 9H_2O$, NaCN, and $Mn(NO_3)_2$.

Instrumentation. - Noble metal disk electrodes included Au (0.196 cm^2) and Pt (0.159 cm^2) (Pine Instrument Co.). Stainless steel (SS) disks were constructed from the SS alloys 416 (0.196 cm$_2$), and 302, 304, 317, and 321 (0.349 cm^2) (Fry Steel Co.). Disk electrodes were mounted in a Model MSR Rotator (Pine Instrument Co.). Exhaustive electrolysis was performed at films deposited on cylindrical electrodes made from Pt-screen and 304-SS screen (Johnson-Matthey).

Electronic instrumentation included a Model RDE4 potentiostat (Pine Instrument Co.), a Model 551 potentiostat (ECO, Inc.), a Model 7035B X-Y recorder (Hewlett Packard), a Series 5500 stripchart recorder (Houston Instruments Co.), a Research Coulometer (U.K. Thompson Electrochem Ltd), a Zeromatic SS-3 pH meter (Beckman Co.), and a Model 197 digital multimeter (Keithley Instruments).

Procedures. - The surfaces of S disk electroes were polished with 320-grit

Carbimet paper strips followed by 1 μm diamond paste. Some SS substrates were

passivated by anodic polarization (5 min at -192 mA) in the phosphate solution described

previously. Dissolution of components of the SS surfaces was initially very rapid, as

indicated by a slow initial rate for O_2 bubble formation. Passivation increased, as noted

by the increased rate of O_2 formation, until reaching an apparent steady-state value after

3-4 min. The resulting electrode surfaces had a uniformly dark gray appearance.

In some cases, thin Au films were anodically deposited at constant current on SS

substrates (1.0 mA cm^{-2} for 20 min) from solutions containing 4.0 mg ml^{-1}

$HAuCl_4 \cdot 3H_2O$, 6.4 mg ml^{-1} KCN and 4.0 mg ml^{-1} $Na_2HPO_4 \cdot 7H_2O$. α-PbO_2 films were

deposited anodically for 3.0 min at 0.35-0.40 V from 2.0 M NaOH saturated with

PbO(s). Bismuth-doped β-PbO_2 films were deposited anodically at + 1.60 V for 20 min

from solutions containing 1.0 mM Pb(II) plus 0.70 mM Bi(III) in 1.0 M $HClO_4$.

Positive and negative scan limits in voltammetric studies were chosen on the basis

of onset of anodic evolution of O_2 and cathodic dissolution of the oxide films,

respectively. All potentials were recorded and are reported as volts measured with respect

to a saturated calomel electrode (V *vs.* SCE).

Electrocatalytic comparisons. - To facilitate intercomparison of the electrocatalytic

activities of various electrodes, apparent heterogeneous rate constants (k_{app}, cm s^{-1}) were

estimated from plots of the reciprocal of the anodic current (i), normalized for area (A) and bulk concentration of reactant (C^b), according to Equation 1,

$$\frac{1}{J} = \frac{1}{i/AC^b} = \frac{1}{nFk_{app}} + \frac{3.091}{0.62n_{eff}FD^{2/3}v^{1/6}}(\frac{1}{\omega^{1/2}})$$

In Equation 1, J is the normalized current density (mA mM^{-1} cm^{-2}), n_{eff} is the effective number of electrons in the reaction (eq mol^{-1}), γ is the solution kinematic viscosity (cm^2 s^{-1}). ω is the rotation speed (rev min^{-1}), 3.091 is the constant for interconversion of the square roots of ω and rotational velocity (rad s^{-1}), and F and D have thir conventional electrochemical significance. The value of n_{eff} for kinetically coupled reactions can be smaller than the total number (n_{tot}) of electrons determined by exhaustive electrolysis. Values of electrode current (i) were measured at a constant applied electrode potential and were corrected for the background.

Results and Discussion

Deposition of α-PbO$_2$ films. - Several types of stainless steels were considered as substrates for anodic deposition of α-PbO$_2$. Members of the 300-series contain high levels of Cr and Ni, and are called "austenitic" stainless steels. These are considered to have high corrosion resistance. Members of the 400-series have a high iron content and have good mechanical properties, but with some sacrifice in corrosion resistance.

The voltammetric responses (i-E) for several bright (*i.e.*, untreated) and passivated

stainless steel (SS) rotated disk electrodes (RDEs) were obtained in 2.0 M NaOH after

saturation with Pb(II) by addition of excess PbO(s) powder. The data are typified by *i-E*

curves shown in Fig. 1. The background response obtained for the absence of PbO(s)

(dashed lines) contains peaks and waves which are attributed to anodic dissolution of

components in the SS substrates, as well as anodic formation and cathodic dissolution of

surface oxide. It is obvious that the overpotential for O_2 evolution is larger at SS surfaces

which had been anodically passivated (*e.g.*, Curves A and C) in comparison to the bright

surfaces (*e.g.*, Curves B and D). With PbO(s) present (solid lines), significantly larger

anodic currents were observed near +0.4 V which correspond to the anodic deposition of

α-PbO$_2$. The broad cathodic waves observed at approximately 0.0 V on the negative

potential scan result from cathodic dissolution of PbO$_2$ deposited during the previous

positive scan (see especially Curve C). The anodic currents for the deposition process are

significantly less than the mass transport limited value and, therefore, are probably

proportional to the true surface area. Accordingly, the deposition current is significantly

larger at SS surfaces which have been passivated, because this anodic process results in a

significant increase in surface roughness (see Curve C for 416-SS).

The colors of the deposited oxide films were observed to differ significantly on

the various substrates. The film was green on bright 321-SS, yellow on 302-SS, brown

on 304-SS and purple on 416-SS. Whereas differences in color intensity are expected to

be the result of variations in film thickness, differences in hue are interpreted to result

from differences in oxide composition and/or structure. We conclude tentatively that α-

PbO$_2$ was formed by the anodic deposition from the highly alkaline media and that Fe(III)

stripped from the SS substrate simultaneously with the deposition process was present as a doping agent in the PbO_2 film.

A strongly adherent PbO_2 film is highly desirable for industrial applicaitons. A simple test for film adherence was applied. A piece of conventional, transparent adhesive tape (Scotch, 3M) was pressed onto the deposited films and then removed by a swift pull. No α-PbO_2 was observed to be removed from the films deposited on passivated 416-SS substrates. The same test applied to α-PbO_2 films on Au and Au-plated SS substrates resulted in obvious removal of small portions of PbO_2.

Corrosion resistance of α-PbO_2 films. - The resistance to anodic corrosion of electrodes consisting of α-PbO_2 films on 304- and 416- SS substrates was tested by determination of the weight loss which occurred during a 24 hr period of anodic polarization under galvanostatic conditions in solutions of 0.10 M Cr(III) in 2.0 M NaOH and 1.0 M H_2SO_4. The results, summarised in Table 1, indicate that the electrodes tested can withstand anodic polarization in alkaline media with virtually no loss of mass. In acidic media, the electrodes experienced considerable weight loss over a 24 hr period. This loss is concluded to have occured primarily by dissolution of the substrate in regions exposed to the electrolyte solution through small pinholes or fissures in the α-PbO_2 films.

Scanning Electron Microscopy. - Micrographs obtained by Scanning Electron Microscopy (SEM) are shown in Fig. 2 for passivated 416-SS, and for α-PbO_2 films on Au and on passsivated and bright 416-SS. The surface morphology of the films is similar,

although tiny holes are apparent in the film on the Au substrate. We conclude, on the basis of Fig. 2, that the α-PbO_2 films on SS substrates were more dense, uniform and relatively free of holes and fissures. Furthermore, since both α- and β-PbO_2 films exhibited excellent stability in acidic media, we conclude that the continuous, hole-free films of PbO_2 can contribute to increased corrosion resistance of SS substrates.

Table 1.   Weight loss of anodes during 24 hr of galvanic polarization in alkaline and acidic media.

Media[a]	Anode	Initial Weight (g)	Final Weight (g)	Weight Change (mg)
0.10 M Cr(III) in 1.0 M NaOH	α-PbO_2 on 304-SS	46.5315	46.5310	-0.5
0.10 M Cr(III) in 1.0 M NaOH	α-PbO_2 on 416-SS	42.3209	42.3208	-0.1
0.10 M Cr(III) in 1.0 M H_2SO_4	β-PbO_2 on Au	46.4288	46.4256	-3.2
0.10 M Cr(III) in 1.0 M H_2SO_4	α-PbO_2 on 416-SS	42.3397	42.3110	-28.7
0.10 M Cr(III) in 1.0 M H_2SO_4	β-PbO_2 On 416-SS[b]	50.2062	50.2022	-4.0

[a]   Current density: -50 mA cm^{-2}.

[b]   SS substrate passivated by anodic treatment in phosphate solution.

Anodic oxidation of Cr(III). - The electrolytic oxidation of Cr(III) is of major importance in a wide range of electrochemical applications [11,16,17] and PbO_2 has been considered widely as a practical anode material in those processes. The usual conditions for Cr(III) oxidation are highly corrosive because of both the high acidity and the large anodic potential required. The anodic evolution of O_2 always is observed to occur simultaneously with Cr(III) oxidation and this side reaction decreases the current efficiency for the desired process. It is highly desirable to identify anode materials which have high stability and which can selectively catalyse the oxidation of Cr(III) without a significant increase in the rate of O_2 evolution.

Voltammetric curves shown in Fig. 3 provide the basis for estimating the catalytic activities of the various α-PbO_2 film electrodes for oxidation of Cr(III). It is readily apparent that the residual response for the α-PbO_2 films on SS is virtually the same as for this film on noble metals in the range of potential values tested (compare dashed lines in Curves A and C). However, this evidence is only a tentative indicator of long term stability of the PbO_2-substrate interface.

As anticipate on the basis of balanced half reaction for conversion of Cr(III) to Cr(VI), the activity of electrodes for Cr(III) oxidation is sensitive to changes in solution pH. There was virtually no anodic reaction of Cr(III) for the electrodes in highly acidic media (Curves A-C), and only slight reactivity at pH 2.3 (Curves D and E) and pH 5.0 (Curves F and G). In 2.0 M NaOH, the oxidation of Cr(III) occured at the α-PbO_2 film on SS electrode (Curve I) to yeild a current plateau over an extended potential range (0.3 to +0.6 V), whereas little activity was observed for Bi-doped β-PbO_2 on Au (Curve H)

or α-PbO$_2$ on Pt (data not shown).

The catalytic activities of the various deposited films for Cr(III) oxidation were compared based on rate constants estimated from the intercepts of plots of 1/J *vs.* 1/ω (see eqn. 1). Since the intercept of a 1/J - 1/ω plot is related to the reciprocal of the apparent rate constant (k$_{app}$), these plots provide easy visual comparison of the catalytic activities of the various electrodes. The plots of experimental data are shown in Figs. 4 to 6 for three different pH values, and the kinetic results are summarised in Table 2. It is apparent from Table 2 that the α-PbO$_2$ films on SS substrates exhibited the highest catalytic activity for oxidation of Cr(III) in 2.0 M NaOH. Furthermore, activity was greatest for the case of bright rather than passivated 416-SS with the reaction being virtually mass transport controlled (*i.e.*, 1/nFk$_{app}$ = 0). Pure α-PbO$_2$ films on Pt exhibited moderate activity in the strongly alkaline media but very low activity in acidic media. The activity of Bi-doped β-PbO$_2$ films on Au was very low. The higher activity for α-PbO$_2$ films on SS is concluded to be the result of incorporation into the oxide of Fe(III) which was produced by anodic dissolution of the SS substrate simultaneously with the deposition process. Since the anodic passivation of SS in the phosphate solution protects the SS substrate from anodic dissolution during the subsequent electrodeposition of PbO$_2$, the electrodes comprised of α-PbO$_2$ films on passivated SS were more stable but less active than the films on the untreated bright SS surfaces. It is speculated that deposition of α-PbO$_2$ from a solution containing Fe(II and/or III) will produce an anode with optimum stability and reactivity. Further testing of this assumption will be presented later [14].

Values of $n_{tot} = 3.0 \pm 0.2$ eq mol^{-1} for Cr(III) were determined by exhaustive electrocatalysis at cylindrical-screen SS and Pt electrodes which had been plated with α-PbO_2 films (see Table 2) and the product was concluded to be Cr(VI).

Anodic oxidation of cyanide. - The fact and efficient electrolytic degradation of CN⁻ by direct anodic reaction could have environmental significance for clean-up of wastes from metal plating industries [18,19]. It is preferable that this degradation process be applied in alkaline media to minimize the volatility of HCN. Hence, α-PbO_2 films electrodeposited on SS substrated could be significant because of their electrochemical stability, provided they exhibit sufficient electrocatalytic activity for the desired oxygen-transfer reaction.

The voltammetric response of CN⁻ is compared in Fig. 7 for various electrodes in alkaline solutions. It is evident that the catalytic activity of the α-PbO_2 films on SS substrates was greater than that of the β-PbO_2 film on Au. The greatest activity was for the bright 304-SS substrate (Curve E) and incorporation of Fe(III) into the α-PbO_2 films during deposition is concluded tentatively to have been responsible for the high electrocatalytic reactivity. The available potential range for CN⁻ oxidation was quite extensive, approximately $+0.8$ to $+1.1$ V *vs.* SCE. For $E > +1.1$ V, evolution of O_2 occured simultaneously with CN⁻ oxidation. As observed for Cr(III) oxidation, the PbO_2 films on the bright SS substrates exhibited higher catalytic activity but lower stability than for the passivated SS substrates.

Table 2.   Rate constants for oxidation of Cr(III)[a].

Anode	Media	n_{tot}[b] (eq mol^{-1})	$10^3 k_{app}$ (cm s^{-1})
α-PbO$_2$ on bright 416-SS	2 M NaOH	3.0 $\pm$ 0.02	97 $\pm$ 1
same	HOAc/NaOAc (pH 5.0)	3.0 $\pm$ 0.09	19 $\pm$ 1
same	0.5 M Na$_2$SO$_4$ (pH 2.3)	NA[c]	
same	0.5 M H$_2$SO$_4$	NA[c]	
α-PbO$_2$ on 416-SS after passivation	2 M NaOH	3.0 $\pm$ 0.07	67 $\pm$ 1
same	HOAc/NaOAc (pH 5.0)	3.0 $\pm$ 0.1	38 $\pm$ 1
same	0.5 M Na$_2$SO$_4$ (pH 2.3)	3.0 $\pm$ 0.05	46 $\pm$ 1
same	0.5 M H$_2$SO$_4$	NA[c]	
Bi-doped β-PbO$_2$ on Au	2 M NaOH	3.0 $\pm$ 0.03	59 $\pm$ 1
same	HOAc/NaOAc (pH 5.0)	3.0 $\pm$ 0.3	13 $\pm$ 2
same	Na$_2$SO$_4$ (pH 2.3)	3.0 $\pm$ 0.2	33 $\pm$ 1
same	0.5 M H$_2$SO$_4$	NA[c]	
α-PbO$_2$ on Pt	2 M NaOH	3.0 $\pm$ 0.2	11 $\pm$ 1
same	HOAc/NaOAc (pH 5.0)	3.0 $\pm$ 0.2	30 $\pm$ 1
same	0.5 M Na$_2$SO$_4$ (pH 2.3)	NA[c]	
same	0.5 M H$_2$SO$_4$	NA[c]	

[a]   Experimental conditions for kinetic measurements are same in Fig. 4A-C.

[b]   Value of n_{tot} determined by controlled-potential exhaustive electrolysis.

[c]   No activity observed.

The large activity of the α-PbO_2 film on the 304-SS substrate for oxidation of CN^- is readily apparent from plots of $1/J$ *vs.* $1/\omega^{1/2}$ shown in Fig. 8. Values of k_{app} calculated from the intercepts are 0.020 cm s^{-1} at α-PbO_2 on 304-SS and 0.0063 cm s^{-1} at α-PbO_2 on passivated 416-SS. Only very small anodic signals were obtained for CN^- at α-PbO_2 on Au and Bi-doped β-PbO_2 on Au, which is indicative of low catalytic activity. Furthermore, these anodic signals did not change with variation of the rotation velocity, which is further support of the conclusion of kinetic control. The oxidation of CN^- in alkaline media was determined by exhaustive electrolysis to occur with $n_{tot} = 2.0 \pm 0.1$ eq mol^{-1} at α-PbO_2 films deposited on the cylindrical Pt and 304-SS screen electrodes. We conclude the anodic reaction produces cyanate, as shown by equation 2.

$$CN^- + 2OH^- \rightarrow CNO^- + H_2O + 2e^- \qquad (2)$$
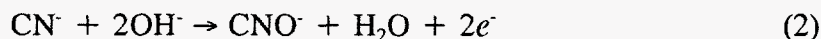
Catalytic activity for CN^- oxidation was investigated for α-PbO_2 on bright 304-SS as a function of variation in the film thickness, deposition potential and solution pH. The maximum anodic response was obtained for a 30 min deposition. On the basis of the measured deposition current (-2.0 mA), $n_{tot} = 2.0$ eq mol^{-1} and the density of α-PbO_2 (9.38 g cm^{-3}), we estimate the film thickness to be 30 μm for the optimum film. The catalytic activity was only a slight function of the deposition potential. For $E_{dep} = +0.35$ V, a higher activity was obtained than for $E_{dep} \geqslant 0.35$ V corresponds to the maximum rate of Fe(III) production at the 304-SS electrode during film deposition. Oxidation of CNO^- to CO_2 is favored thermodynamically at extremely high pH, as indicated by Equation 3. However, only a small increase in anodic current was observed at 0.85 V for a pH change from 9.5 to 10.6 and we conclude that CNO^- is the product of CN^- oxidation

under these conditions.

$$2CNO^- + 8OH^- \rightarrow 2CO_3^{2-} + N_2 + 4H_2O + 6e^- \tag{3}$$
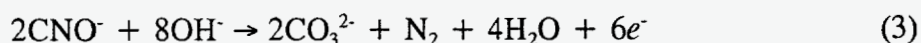
Anodic Oxidation of Mn(II). - The catalytic activity of the various electrode surfaces for anodic oxidation of Mn(II) in 1.0 M $HClO_4$ was of interest because of the large number of oxygen atoms assumed to be transferred in the conversion to MnO_4^-. Furthermore, the rate for Mn(II) oxidation is slow at pure PbO_2 films deposited at noble-metal substrates. The Bi-doped β-PbO_2 on Au has been determined to have a high catalytic activity for the reaction and the anodic signals are limited virtually by mass transport of the Mn(II). The voltammetric response of Mn(II) is summarised in Fig. 9 for Mn(II) in 1.0 M $HClO_4$. The background current at the α-PbO_2 film on the passivated 416-SS substrate is comparable to that for PbO_2 on the noble metal substrates. Without the passive coating formed during the phosphate treatment, the PbO_2 films failed to protect the SS substrates and rapid dissolution of the SS occurred with ultimate detachment of the PbO_2 films. Type-416 SS was very inert after anodic passivation in phosphate media and the roughened surface produced by the anodic process (see Fig. 2A) allowed for a strong attachment of the α-PbO_2 films. There was no evidence of removal of any portion of the deposited film onto a piece of transparent tape pressed against the film and then pulled away.

As was the observation for oxidation of Cr(III) and CN⁻, catalytic activity for Mn(II) oxidation is greater for α-PbO_2 on SS rather than noble-metal substrates. Quantitative information to support this conclusion is shown in Fig. 10 as plots of 1/J *vs.*

$1/\omega^{1/2}$. The rate constants determined from the intercepts of the plots were 0.0011 cm s^{-1} at the Bi-doped PbO$_2$ film on Au, 0.0022 cm s^{-1} at the α-PbO$_2$ on a Au-coated 416-SS, and 0.0024 cm s^{-1} at the α-PbO$_2$ film on 416-SS. There was no advantage in using a Au inter-layer on the SS substrate either for higher catalytic activity or greater adherence of α-PbO$_2$ films.

Conclusions

A passive and roughened durface is produced on 416-SS by anodization in phosphate medium. The passivating layer is concluded to be conductive and the roughened surface allows for the strong adherence of electrodeposited α-PbO$_2$ films. Anodes consisting of α-PbO$_2$ on passivated 416-SS can be used in alkaline, neutral and slightly acidic media at large positive applied potenial values without apparent decomposition.

Amperometric data support the conclusion that α-PbO$_2$ films on SS possess greater activity than observed for pure α-PbO$_2$ and Bi-doped β-PbO$_2$ films on Au for the anodic O-transfer reactions of CN$^-$ and Cr(III) in alkaline media, Cr(III) at pH $\geq$ 5, and Mn (II) in acidic media. The high catalytic activity is concluded tentatively to be the result of Fe(III), produced by anodic corrosion of the SS substrate simultaneously with deposition, which is incorporated into the PbO$_2$ films. We speculate that Fe(II and/or III) added to solutions of Pb(II) used for deposition of PbO$_2$ films will result in a significant increase in catalytic activity for the doped films.
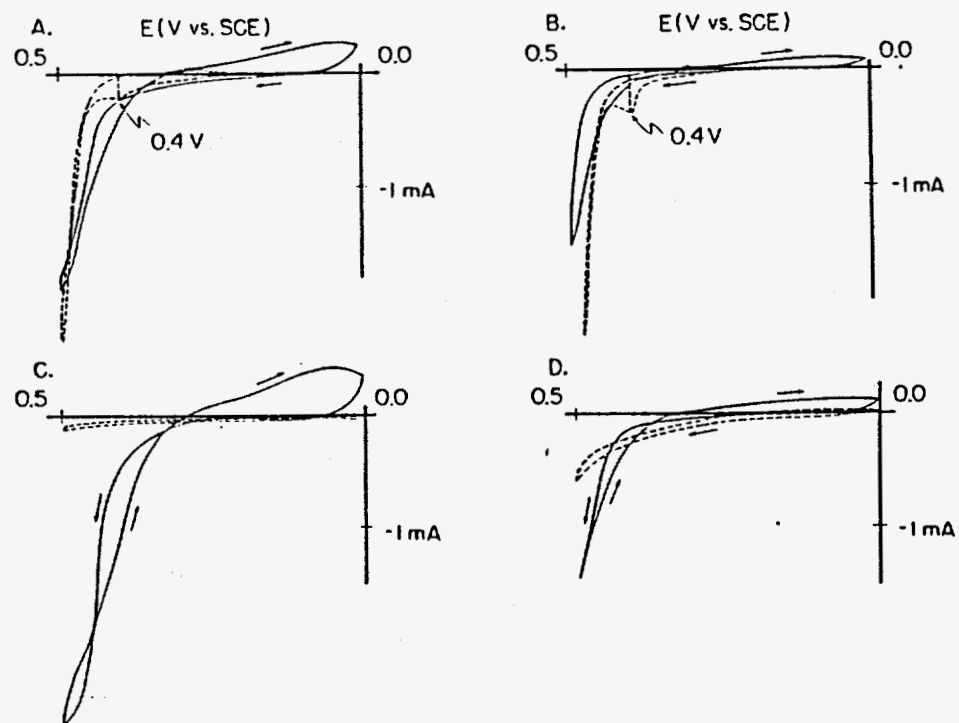
Fig. 1.   Voltammetric response of various SS rotated disk electrodes in PbO(s)-saturated 2.0 M NaOH.
Conditions: 0.6 V min^{-1}. Curves: (...) residual, (—) PbO(s)-saturated solution.
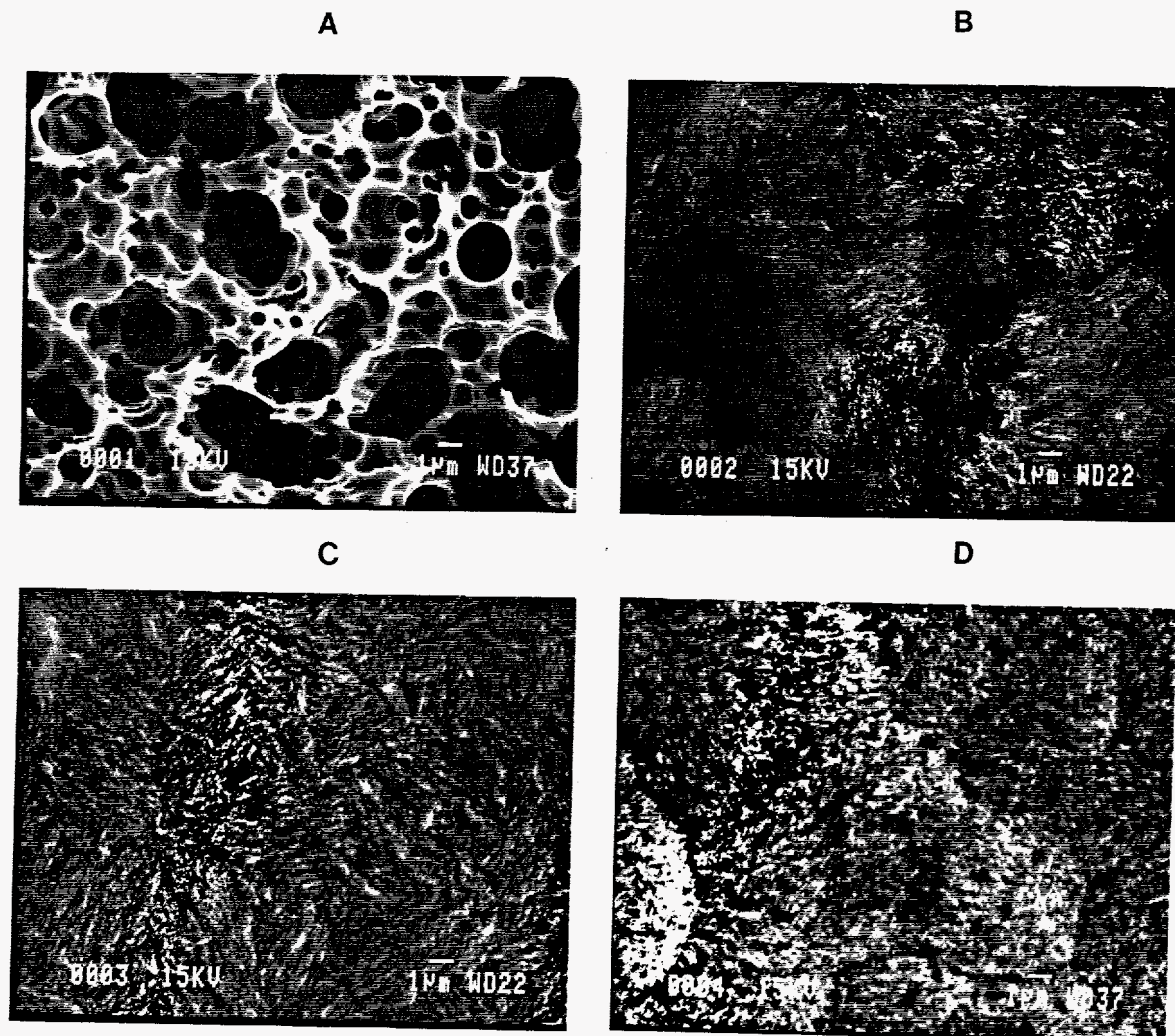
Fig. 2.   Micrographs of substrates and PbO$_2$ films.
(A) Passivated 416-SS, (B) α-PbO$_2$ on Au, (C) α-PbO$_2$ on bright 416-SS,
(D) α-PbO$_2$ on passivated 416-SS.

E (V vs. SCE)
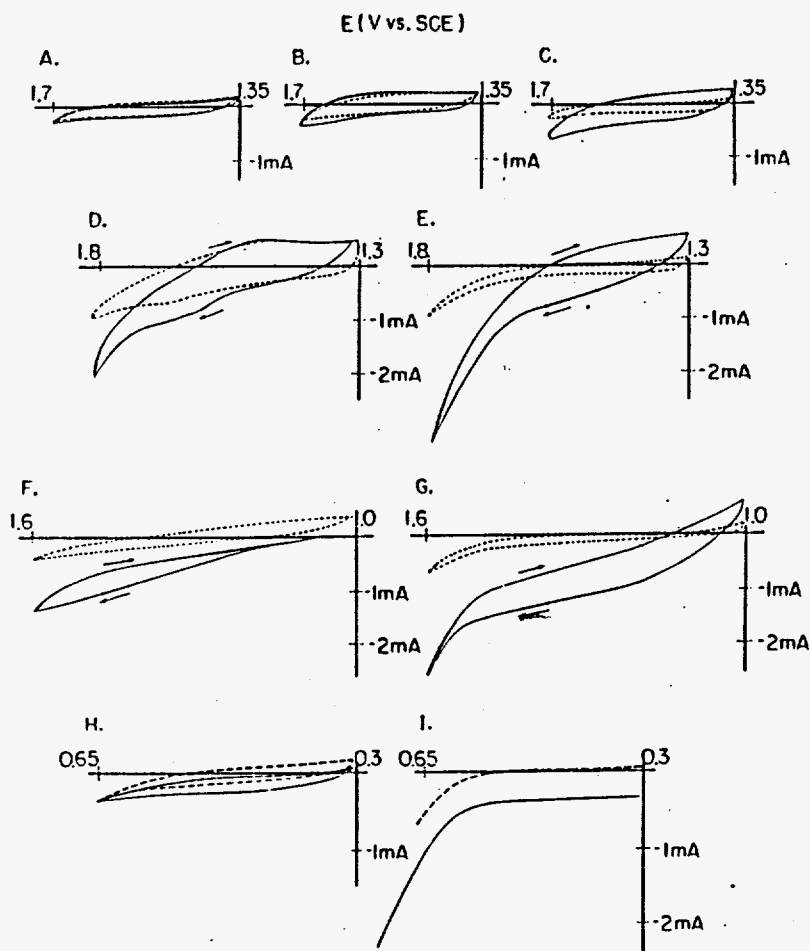

Fig. 3.   Voltammetric response for Cr(III) at a rotated disk electrode.
Conditions: 0.60 V min^{-1}, 1600 rev min^{-1}. Curves: (...) residual,
(—) response for Cr(III). Solutions: (A-C) 1.0 mM Cr(III)/0.50 M H$_2$SO$_4$,
(D-E) 5.0 mM Cr(III)/0.50 M Na$_2$SO$_4$ (pH 2.3),
(F-G) 5.0 mM Cr(III)/1.0M HOAc/NaOAc (pH 5.0),
(H-I) 1.0 mM Cr(III)/2.0 M NaOH. Electrodes: (A) α-PbO$_2$ on Pt,
(B,D,F,H) Bi-doped β-PbO$_2$ on Au, (C,E,G,I) α-PbO$_2$ on passivated
416 SS.
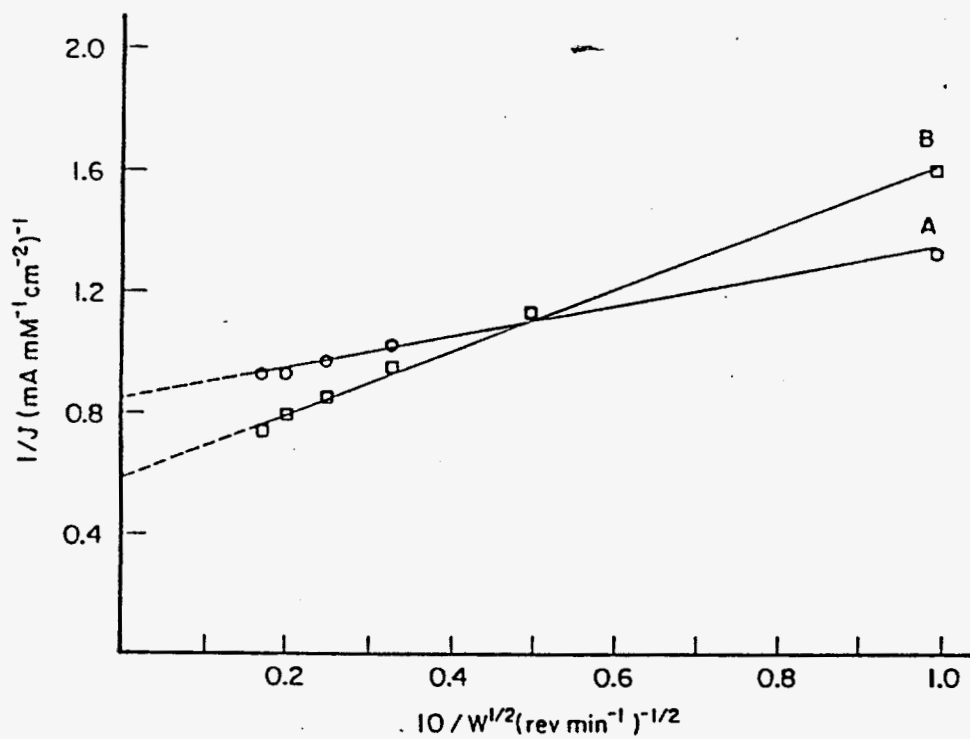
Fig. 4.   Plots of 1/J *vs.* $1/\omega^{1/2}$ for oxidation of 5.0 mM Cr(III) at 1.6 V in 0.5 M Na_2SO_4 (pH 2.3). Electrodes: (A) Bi-doped β-PbO_2 on Au, (B) α-PbO_2 on passivated 416 SS.
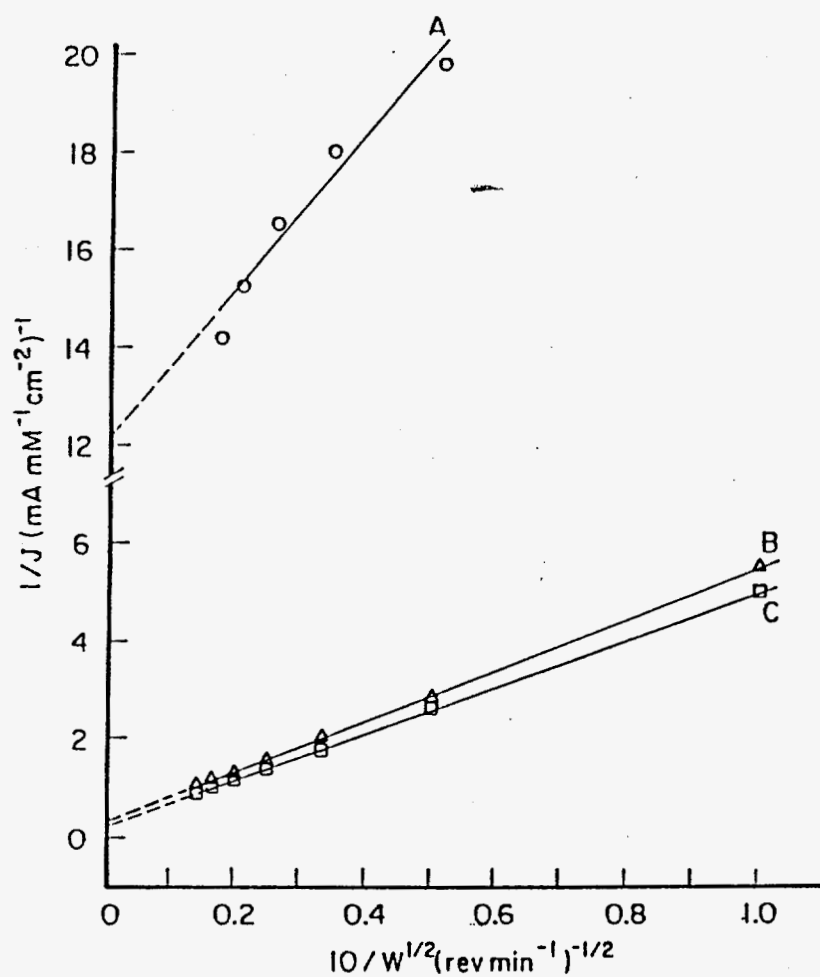
Fig. 5.   Plots of 1/J *vs.* $1/\omega^{1/2}$ for oxidation of 5.0 mM Cr(III) at 1.4 V in 1.0 M HOAc/NaOAc (pH 5.0).
Electrodes: (A) α-PbO$_2$ on Pt, (B) Bi-doped β-PbO$_2$ on Au, (C) α-PbO$_2$ on passivated 416-SS.
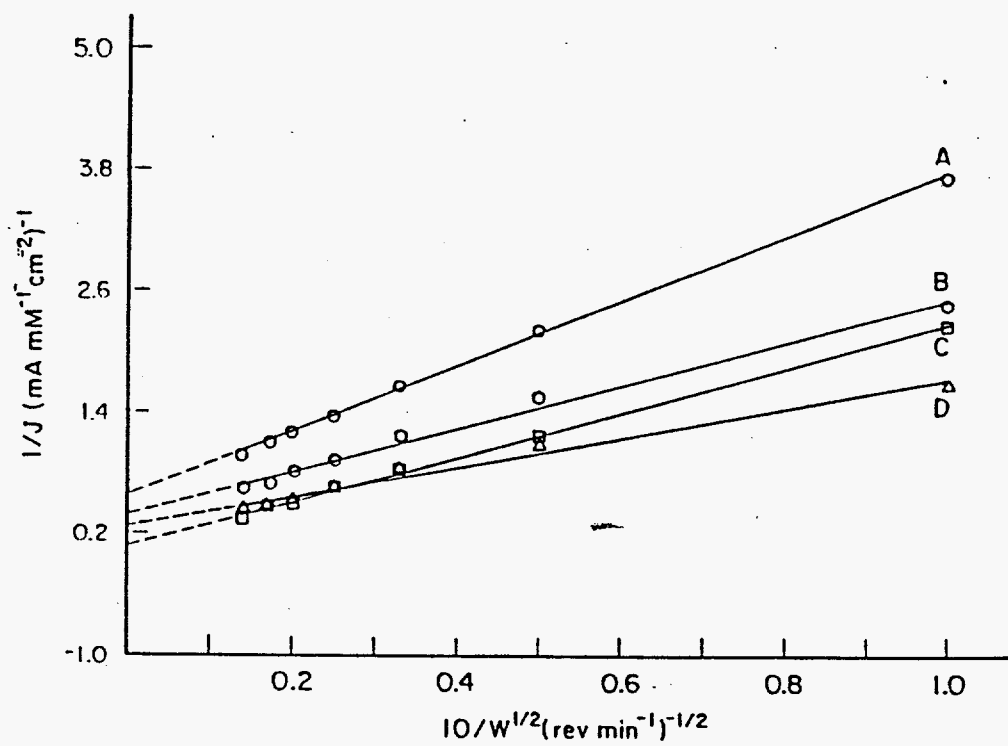
Fig. 6.   Plots of 1/J *vs.* 1/$\omega^{1/2}$ for oxidation of 5.0 mM Cr(III) at 0.50 V in 2.0 M NaOH. Electrodes: (A) Bi-doped β-PbO$_2$ on Au, (B) α-PbO$_2$ on Pt, (C) α-PbO$_2$ on bright 416-SS, (D) α-PbO$_2$ on passivated 416-SS.
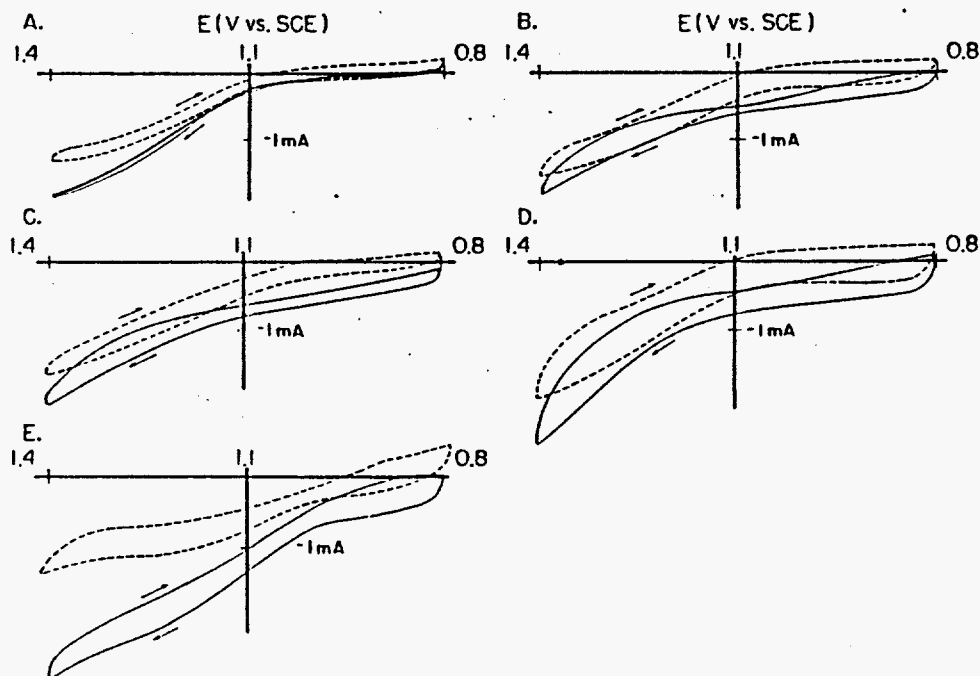
Fig. 7.   Voltammetric response for 5.0 mM NaCN in 0.014 M NaHCO₃/0.011 M
Na₂CO₃ (pH 10.0). Conditions: 0.6 V min⁻¹, 1600 rev min⁻¹.
Curves: (...) residual, (—) NaCN. Electrodes: (A) Bi-doped β-PbO₂
on Au, (B) α-PbO₂ on Au, (C) α-PbO₂ on passivated 416 SS, (D) α-PbO₂
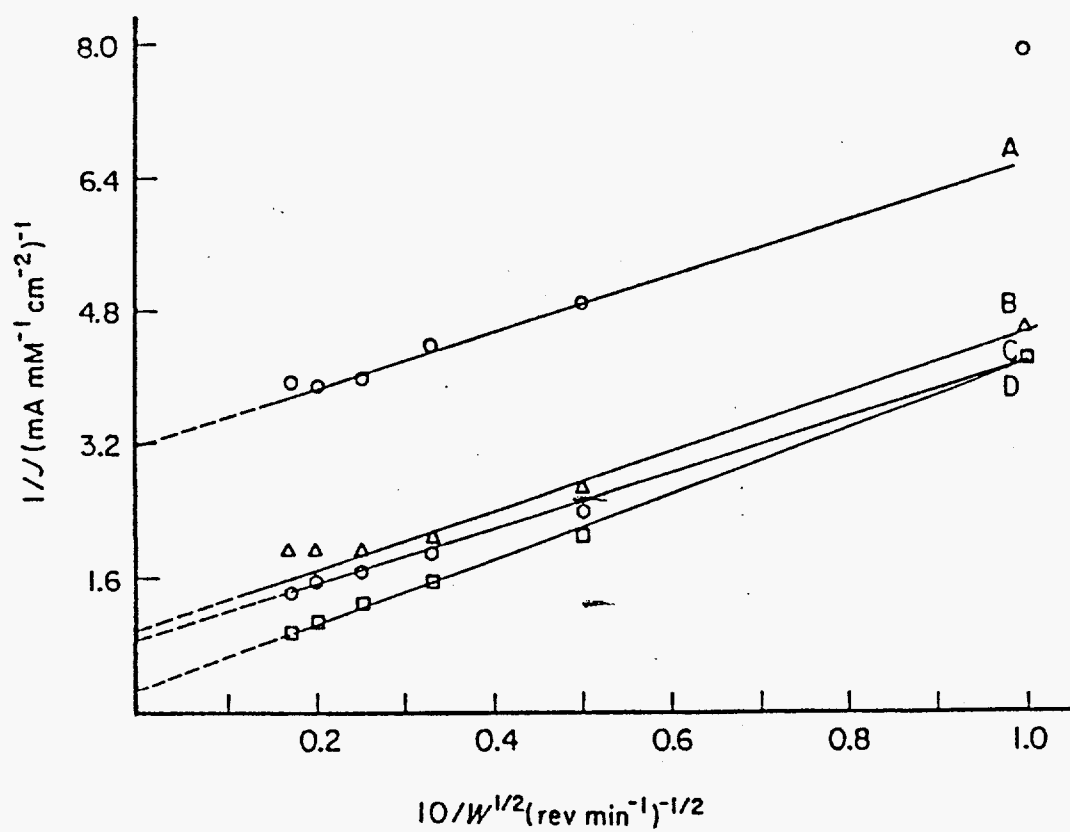on bright 416 SS, (E) α-PbO₂ on bright 304-SS.

Fig. 8.   Plots of $1/J$ *vs.* $1/\omega^{1/2}$ for oxidation of 5.0 mM NaCN at 1.10 V in 0.014 M NaHCO$_3$/0.011 M Na$_2$CO$_3$ (pH 10.0). Electrodes: (A) Bi-doped β-PbO$_2$ on Au, (B) α-PbO$_2$ on Au, (C) α-PbO$_2$ on passivated 416-SS, (D) α-PbO$_2$ on bright 304-SS.

A.   E (V vs. SCE)

1.65   1.45

                                        -1 mA

B.
65   1.45

                                        -1 mA

C.
1.65   1.45

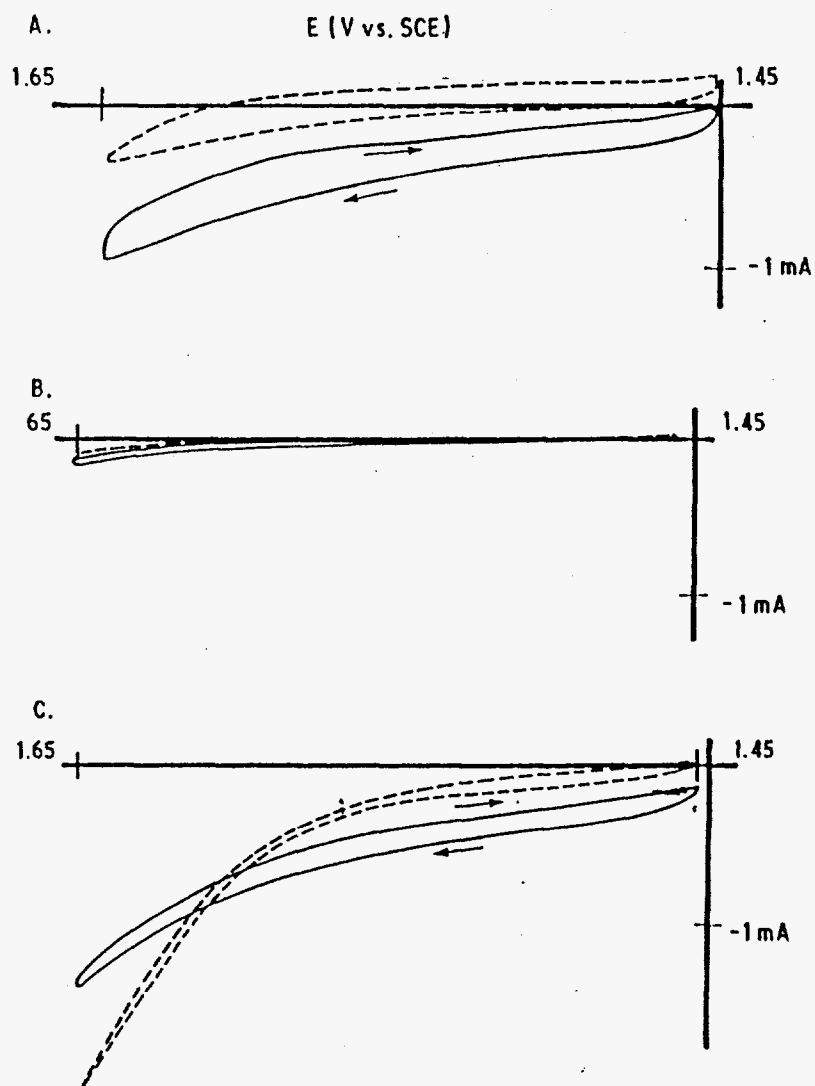   -1 mA

Fig. 9.   Voltammetric response for 1.0 mM Mn(II) in 1.0 M HClO$_4$.
Conditions: 0.6 V min^{-1}, 1600 rev min^{-1}. Curves: (...) residual,
(—) Mn(II). Electrodes: (A) Bi-doped β-PbO$_2$ on Au, (B) α-PbO$_2$ on Au,
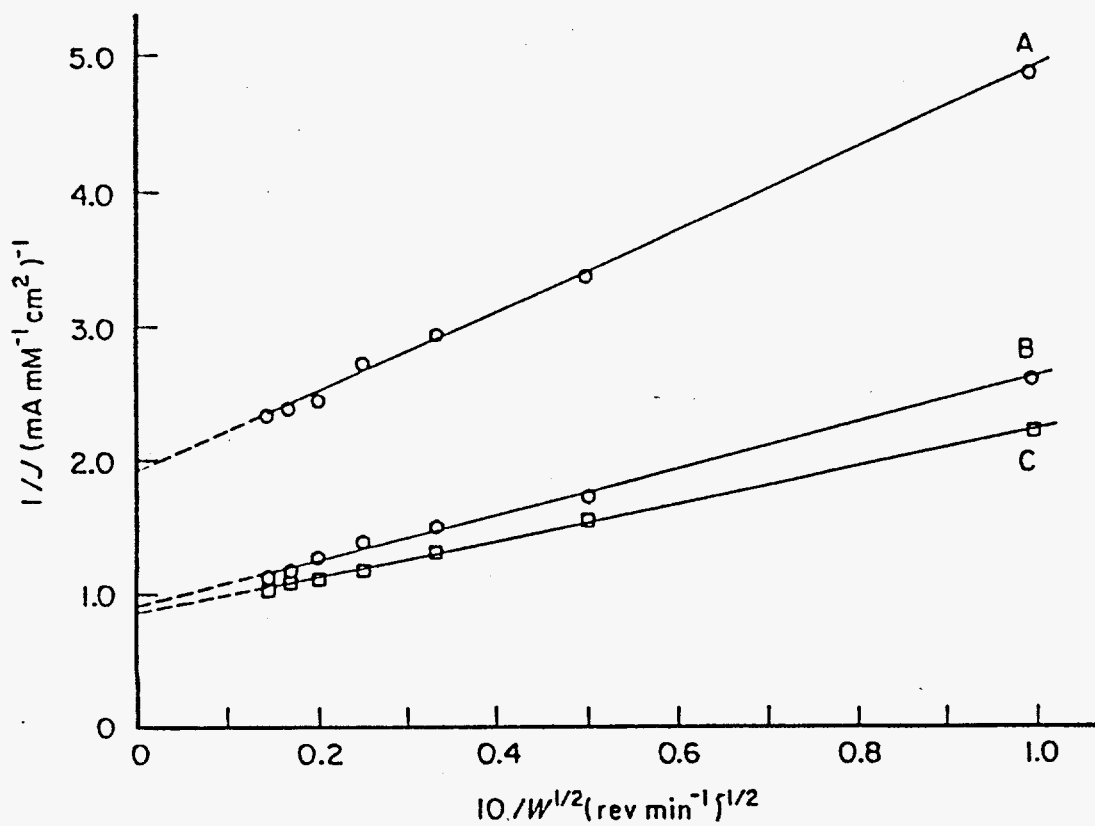(C) α-PbO$_2$ on passivated 416-SS.

Fig. 10.   Plots of 1/J *vs.* $1/\omega^{1/2}$ for oxidation of 1.0 mM Mn(II) at 1.45 V in 1.0 M HClO$_4$. Electrodes: (A) Bi-doped β-PbO$_2$ on Au, (B) α-PbO$_2$ on passivated 416-SS, (C) α-PbO$_2$ on Au-coated, passivated 416-SS.

REFERENCES

[1] R. W. Wyckoff, "Crystal Structure," Vol. 1, 2nd Ed., p.259, Interscience, New York (1963).

[2] "The Electrochemistry of Lead," (edited by A. T. Kuhn), pp. 53-63, 217-51, Academic Press, London (1979).

[3] A. Fukasawa, *Japan Kokai JP 52/19230 [77/19230]*, Feb. 14 (1977), p.4.

[4] Inam-UI-Haque and A. Mohammad, *Pak. J. Sci.*, **31**, 237 (1979).

[5] Electrochemistry Group of Guizhou Institute of Metallurgy, *Youse Jinshu*, **34**, 51 (1982).

[6] K. C. Narasimham and H. V. K. Udupa, *J. Electrochem. Soc.*, **123**, 1284 (1976).

[7] C. Comminellis and E. Plattner, *J. Appl. Electrochem.*, **12**, 399 (1982).

[8] W. Q. Zhou and X. Chen., *Huaxue Xuebao*, **43**, 819 (1981).

[9] R. G. Barradas and A. Q. Contractor, *J. Electroanal. Chem.*, **138**, 425 (1982).

[10] D. Gilroy and R. Stevens, *J. Appl. Electrochem.*, **10**, 511 (1980).

[11] A. I. Matantsev and A. J. Falicheva, *Zh. Priklad. Khim.*, **37**, 2426 (1964); cited by: A. T. Kuhn and R. Clarke, *J. Appl. Chem. Biotechnol.*, **26**, 407 (1975).

[12] A. Boggio, M. Maja and N. Penazzi, *J. Power Source*, **9**, 221 (1983).

[13] I.H. Yeo and D. C. Johnson, *J. Electrochem. Soc.*, **134**, 1973 (1987).

[14] J. Feng and D. C. Johnson, *J. Electrochem. Soc.*, **137**, 507 (1990).

[15] A. J. Sedriks, "Corrosion of Stainless Steel," pp. 213-5, Wiley Interscience, New York (1979).

[16] T. Fukinaga and T. Yoshimura, *Fres. Z. Anal. Chem.*, **306**, 20 (1981).

[17] D. Pletcher and S. J. D. Tait, *J. Appl. Electrochem.*, **11**, 493 (1981).

[18] G. W. Dawson and B. N. Mercer, "Hazardous Waste Management," pp.331,

New York (1984).

[19]   J. W. Patterson, "Wastewater Treatment Technology," pp. 92-6, Ann Arbor Science Publishers, Ann Arbor (1975).